DEVELOPMENT OF A SOFT LINEAR ACTUATOR TO USE IN WEARABLE ASSISTIVE EXOSUITS

A.L. Kulasekera

178036T

Doctor of Philosophy

Department of Mechanical Engineering
Faculty of Engineering

University of Moratuwa
Sri Lanka

February 2023

DEVELOPMENT OF A SOFT LINEAR ACTUATOR TO USE IN WEARABLE ASSISTIVE EXOSUITS

A.L. Kulasekera

178036T

Thesis submitted in partial fulfillment of the requirements for the degree
Doctor of Philosophy

Department of Mechanical Engineering
Faculty of Engineering

University of Moratuwa
Sri Lanka

February 2023

DECLARATION

I declare that this is my own work and this Thesis does not incorporate without acknowledgement any material previously submitted for a Degree or Diploma in any other University or Institute of higher learning and to the best of my knowledge and belief it does not contain any material previously published or written by another person except where the acknowledgement is made in the text. I retain the right to use this content in whole or part in future works (such as articles or books).

Signature: UOM Verified Signature Date: 24/02/2023

The supervisors should certify the Thesis with the following declaration.

The above candidate has carried out research for the Doctor of Philosophy Thesis under our supervision. We confirm that the declaration made above by the student is true and correct.

Name of Supervisor: Dr. K.V.D.S. Chathuranga

Signature of the Supervisor: UOM Verified Signature Date: 27/02/2023

Name of Supervisor: Prof. R.A.R.C. Gopura

Signature of the Supervisor: UOM Verified Signature Date: 24/02/2023

Name of Supervisor: Dr. S.W.H.M.T.D. Lalitharatne

Signature of the Supervisor: UOM Verified Signature Date: 24/02/2023

DEDICATION

To

Vidhun,

Mihiru,

and

Minuki.

ACKNOWLEDGEMENT

I am wholeheartedly grateful to all those who supported me in completing this research and thesis. First, I would like to thank Dr. Damith Chathuranga for always being there, understanding, and motivating me to achieve my best no matter the circumstances. I thank him for providing me with invaluable opportunities to develop myself, learn to lead a research lab, and be part of an exceptional research team. I want to thank Prof. Ruwan Gopura, who has always been a great mentor throughout my research and academic life and an excellent beacon for my academic, professional, and personal growth. His constant guidance, insight, and support were vital in completing my research. I also thank Dr. Thilina Lalitharathne for his continuous support and intuitive guidance. I am sincerely grateful to all three of my research supervisors for the exceptional support, guidance, critical mentoring, and friendship provided throughout.

My progress review panel's generous feedback and guidance were instrumental in this research. I thank Prof. Buddhika Jayasekera and Dr. Palitha Dassanayake for their valuable input and critical feedback in developing and honing my research.

I want to thank the fantastic support I had from fellow laboratory colleagues in every aspect of my research. I thank Mr. Rancimal Arumathanthri, Mr. Chanaka Premachandra, and Mr. Chanuka Lihini for enriching my research and the company that made this a joyous journey. Next, I need to thank the colleagues from the Bionics laboratory, Mr. Pubudu Ranaweera, for his constant aid at a minute's notice and the critical analysis whenever needed, and Mr. Sanka Chandrasiri for his assistance in human subject testing. Next, I would like to extend my gratitude to the past and present heads of the Department of Mechanical Engineering, Prof. Gopura, and Dr. Himan Punchihewa, the past and current research coordinators, Dr. Damith and Dr. Nalaka Samaraweera, for the continued administrative support.

Next, I would like to thank the AOTULE program for allowing me to conduct part of my research at the Tokyo Institute of Technology, Tokyo, Japan. I want to thank Prof. Yasuke Sugahara and Prof. Yukio Takeda for their kind and helpful guidance during my time at Tokyo Tech. I also want to thank my Mechanical Systems Design Lab colleagues, Mr. Andres Osorio and Mr. Jyuon Yamakazi, for their collaborative contributions and friendship. Further, it would be amiss if I did not thank Sam, Yathest, and Salika for their inspiration and camaraderie during my stay in Japan.

I express my gratitude to the National Research Council of Sri Lanka (17-018) and the University of Moratuwa-Senate Research Committee (SRC/TP/ 2017/10) for their financial support in completing this research. I again thank the University of Moratuwa-Senate Research Committee for the publication aid provided via the conference and publication support scheme.

Finally, I would like to thank my loving wife, Dr. Himanga Benaragama, for her constant support, without which this research would not have been possible, and Vidhun, Mihiru, and Minuki, for understanding my absence during their play times.

ABSTRACT

Wearable exosuits require flexible, linearly contractile, and lightweight actuators to provide sufficient force to move the respective limb. This thesis presents the concept, design, fabrication, experimental performance characterization, and numerical modeling of two types of respectively thin and low-profile vacuum-driven, soft, linearly contractile actuators. The proposed soft actuators are made of an inextensible yet flexible thin-skinned pouch supported by a collapsible skeleton that orients the collapse of the actuator in the longitudinal axis upon the evacuation of the air within the pouch. The proposed novel soft, lightweight, contractile actuators are thin (ThinVAc) and low-profile (LPVAc). Both these actuators are lightweight (ThinVAc: 0.75 g; LPVAc: 14 g), provide high maximum blocked forces (ThinVAc: 5.2 N; LPVAc: 39 N), provide maximum stresses similar to that expected from biological muscles (ThinVAc: 184 kPa; LPVAc: 117 kPa) and have high force-to-weight ratios (ThinVAc: 477; LPVAc: 285). The ThinVAc can combine to create multifilament actuators for force scaling. Combining 15 units of 500 mm ThinVAcs generates a maximum blocked force of 54 N (Max. stress: 62 kPa), 290 times the self-weight. The LPVAc integrates a position sensor based on an inductive sensor allowing closed-loop control with minimal error at 0.25 Hz. Numerical models for the contraction and blocked force of mono- and multifilament actuators allow for predicting their behavior independent of external sensors. The proposed actuators are tested in wearable applications to check their suitability. The ThinVAc is integrated into a knee rehabilitation assist device, and the LPVAc is incorporated into a novel mono-articular sit-to-stand transition (StSt) assist exosuit, helping to reduce muscle activity by 45%. These actuators have the potential to be integrated into a wide range of assistive devices and orthoses, such as knee or ankle braces, exoskeletons, and prosthetics, to provide the necessary support for people with mobility impairments.

Keywords: Linear soft actuators, contractile vacuum actuators, Exosuits, Soft robotics, Soft sensors

TABLE OF CONTENTS

Declaration of the Candidate & Supervisor i

Dedication iii

Acknowledgement v

Abstract vii

Table of Contents ix

List of Figures xiii

List of Tables xv

List of Appendices xvii

1 Introduction 1

1.1 Introduction and motivation 1

1.2 Research problem 2

1.3 Thesis outline 2

1.4 Main contributions 3

2 Literature review 5

2.1 Soft fluidic actuators 5

2.2 Pneumatic artificial muscles 7

2.3 Vacuum-driven soft actuators 8

2.4 Vacuum-driven contractile actuators 9

2.5 Sensing in soft actuators 12

2.6 Assessment of PAM performance 12

2.7 Soft exosuits 13

2.7.1 Advantages and disadvantages over rigid exoskeletons 15

2.7.2 Knee rehabilitation assist devices 16

2.7.3 Sit-to-stand-transition assist exosuits 17

2.8 Summary 17

3 Development of soft linear actuators 23

3.1 Introduction 23

3.2 Conceptual Design 23

3.3 Thin Vacuum Actuator (ThinVAc) 24
3.3.1 LDPE-ThinVAc 25
3.3.2 LDPE-ThinVAc Multi-filament actuators 26
3.3.3 TPU-ThinVAc 27
3.3.4 TPU-ThinVAc multi-filament actuator 28
3.4 Low-profile Vacuum Actuator (LPVAc) 29
3.4.1 Integrated sensing for the LPVAc 32
3.5 Summary 34
4 Actuator Performance evaluation 37
4.1 Performance evaluation of the ThinVAc 37
4.1.1 Contraction performance of the ThinVAc 38
4.1.2 Force-displacement characteristics of the ThinVAc 38
4.1.3 Blocked force performance of the ThinVAc 39
4.1.4 Applications of the proposed ThinVAc 40
4.1.5 Blocked force performance of multi-filament ThinVAc 42
4.2 Performance evaluation of the LPVAc 44
4.2.1 Spring properties 44
4.2.2 Contraction performance of the LPVAc 45
4.2.3 Force-displacement characteristics of the LPVAc 46
4.2.4 Blocked force performance of the LPVAc 46
4.2.5 Blocked force performance with varying width-to-height ratio 47
4.2.6 Integrated displacement sensor calibration 50
4.2.7 Characterization of the integrated sensor 52
4.2.8 Using the integrated sensor for feedback control of the LPVAc 54
4.3 Summary 55
5 Numerical models for contraction and force 59
5.1 LDPE-ThinVAc contraction model 59
5.2 TPU-ThinVAc contraction model 61
5.3 LDPE-ThinVAc blocked force model 62
5.4 TPU-ThinVAc blocked force model 63
5.5 Summary 65

6 Exosuit development and testing 67
6.1 Knee rehabilitation assist device 67
6.1.1 Introduction 67
6.1.2 Knee extension assist system 67
6.2 Sit-to-stand-transition assist exosuit 69
6.2.1 Introduction 69
6.2.2 Exosuit design 71
6.2.3 Performance evaluation of the exosuit 72
6.2.4 EMG capture test setup 72
6.2.5 EMG analysis 74
6.3 Summary 75
7 Conclusions and Future work 77
7.1 Conclusions 77
7.2 Future directions 78
8 List of publications 79
References 81
Appendix A Plane and motion notations used in anatomy 95
Appendix B Muscle recruitment in Lower limb motions 97
Appendix C Types of lower limb orthoses 99
Appendix D Regression models used for LDPE-ThinVAc 101

LIST OF FIGURES

Figure	Description	Page
Figure 2.1	Classification of EIAs based on motion path.	6
Figure 2.2	Contemporary contractile vacuum actuators.	10
Figure 2.3	The concept of origami-inspired vacuum actuators.	11
Figure 2.4	Soft sensors used in PAMs.	12
Figure 2.5	Static characterization of PAMs.	13
Figure 2.6	The Wehner soft exosuit design.	14
Figure 2.7	Bowden cable driven exosuits.	19
Figure 2.8	Other contemporary exosuits.	20
Figure 2.9	Knee rehabilitation assist devices found in literature.	21
Figure 2.10	Sit-to-Stand-transition assist exosuits.	21
Figure 3.1	The potential design paths.	24
Figure 3.2	Concept of the proposed thin vacuum actuator (ThinVAc).	25
Figure 3.3	The proposed thin vacuum actuator (ThinVAc).	26
Figure 3.4	The proposed multi-filament actuator design and fabricated actuators.	27
Figure 3.5	TPU-ThinVAc: main components and fabricated actuators	28
Figure 3.6	Multi-filament TPU-ThinVAcs: 3- and 5-filament.	29
Figure 3.7	Concept of the proposed low-profile vacuum actuator (LPVAc).	30
Figure 3.8	Conceptual design of the LPVAc and the fabricated actuator.	31
Figure 3.9	The main steps of fabricating the proposed LPVAc.	31
Figure 3.10	A parallel LC tank circuit.	33
Figure 3.11	LDC1614 functional block diagram and module.	33
Figure 3.12	LPVAc with the integrated inductive displacement sensing module.	34
Figure 4.1	The general experimental setup.	37
Figure 4.2	ThinVAc experimental test setups.	38
Figure 4.3	ThinVAc no-load contraction.	39
Figure 4.4	ThinVAc force-displacement characteristics.	40
Figure 4.5	LDPE-ThinVAc force-displacement characteristics (CR).	40
Figure 4.6	ThinVAc force-displacement characteristics (CR).	41
Figure 4.7	ThinVAc maximum blocked force.	42
Figure 4.8	Actuation of a soft toy using a 100 mm LDPE-ThinVAc.	43
Figure 4.9	Actuation of a compliant gripper by the ThinVAc.	43
Figure 4.10	Time domain response of the compliant gripper tip motion.	44
Figure 4.11	LDPE-ThinVAc multi-filament actuator blocked force characteristics.	45
Figure 4.12	LDPE-ThinVAc multi-filament actuator operating while deformed.	46
Figure 4.13	LDPE-ThinVAc multi-filament lifting 10.6 N.	47
Figure 4.14	TPU-ThinVAc multi-filament maximum blocked force performance.	48
Figure 4.15	MS and GI obround spring coefficients.	48
Figure 4.16	LPVAc experimental test setups.	49
Figure 4.17	LPVAc isotonic performance (load:200g).	49
Figure 4.18	LPVAc maximum strain (65% at 20 kPa(abs.)).	50

Figure 4.19	LPVAc load-displacement characteristics.	50
Figure 4.20	LPVAc blocked force performance.	51
Figure 4.21	LPVAc blocked force variation with W/H ratio.	51
Figure 4.22	Inductive sensor calibration.	52
Figure 4.23	Hysteresis performance of the integrated sensor.	53
Figure 4.24	Repeatability performance of the integrated sensor.	53
Figure 4.25	Measurement error of the LPVAc over its working range.	54
Figure 4.26	LPVAc feedback control test setup.	55
Figure 4.27	LPVAc feedback control block diagram.	55
Figure 4.28	LPVAc sensor response.	56
Figure 4.29	Comparison of the actuators with literature.	58
Figure 5.1	Multi-parameter regression contraction model for the LDPE-ThinVAc.	60
Figure 5.2	Multi-parameter regression contraction model for the LDPE-ThinVAc	61
Figure 5.3	The multiplicative blocked force model for the LDPE-ThinVAc multi-filamant actuators.	63
Figure 5.4	The blocked force model for the TPU-ThinVAc multi-filamant actuators.	64
Figure 6.1	CAD model of Knee extension assist setup.	68
Figure 6.2	Knee extension with 15 x 100 mm LDPE-ThinVAc multi-filament.	69
Figure 6.3	Knee extension with 10 x 200 mm LDPE-ThinVAc multi-filament.	69
Figure 6.4	Time response of shank angle: 15 x 100 mm LDPE-ThinVAc multi-filament.	70
Figure 6.5	Time response of shank angle: 10 x 200 mm LDPE-ThinVAc multi-filament.	70
Figure 6.6	The proposed novel mono-articular StSt-assist soft exosuit.	71
Figure 6.7	The test protocol used for StSt assist performance evaluation.	73
Figure 6.8	The Bagnoli EMG capture system.	73
Figure 6.9	The EMG capture test setup.	74
Figure 6.10	EMG reduction observed in the test subjects.	75
Figure A.1	Body plane notions used in anatomy	95
Figure A.2	Limb motion definitions	95
Figure B.1	Classification of the muscles used for lower limb motions	97
Figure C.1	Types of lower limb orthoses.	99
Figure D.1	Model 1: CR	101
Figure D.2	LDPE-ThinVAc isobaric CR	103

LIST OF TABLES

Table	Description	Page
Table 2.1	Comparison of biological muscles and PAMs	8
Table 3.1	Characteristics of the SS spring used in the ThinVAc	25
Table 3.2	Weight of each Multifilament actuator combination	27
Table 3.3	The main parameters of the fabricated LPVAcs	32
Table 3.4	The main features available on the LDC1614 module.	34
Table 3.5	A comparison of the developed actuators.	35
Table 4.1	ThinVAc no-load contraction performance at 20 kPA (abs.)	39
Table 4.2	A summary of characteristics of the monofilament ThinVAcs.	41
Table 4.3	A summary of LDPE-ThinVAc multi-filament actuator performance	44
Table 4.4	LPVAc blocked force performance with varying W/H ratio	49
Table 4.5	Performance measures for repeatability of the integrated sensor	52
Table 4.6	ThinVAc force performance in comparison to literature.	57
Table 5.1	The goodness of fit parameters for the multi-parameter LDPE-ThinVAc monofilament contraction model.	60
Table 5.2	RMSE of contraction ratio (%) : LDPE-ThinVAc	61
Table 5.3	RMSE of contraction ratio (%): LDPE-ThinVAc	61
Table 5.4	Regression fits for the LDPE-ThinVAc blocked force performance	62
Table 5.5	RMSE values for the initial and correction fit for the multiplicative model for the LDPE-ThinVAc multi-filament actuators	63
Table 5.6	Comparison of predicted and experimental values for blocked force for the LDPE-ThinVAc	64
Table 5.7	TPU-ThinVAc multi-filament blocked force model evaluation	65
Table 6.1	Shank response with ThinVAc actuation.	68
Table 6.2	Test subject details and observed sEMG signal reduction	72
Table D.1	Linear regression fit: ThinVAc length and pressure level (model I).	102
Table D.2	Isobaric comparison of RMSE for contraction and contraction ratio linear regression models.	103

LIST OF APPENDICES

Appendix	Description	Page
Appendix -A	Plane and motion notations used in anatomy	95
Appendix -B	Muscle recruitment in Lower limb motions	97
Appendix -C	Types of lower limb orthoses	99
Appendix -D	Regression models used for LDPE-ThinVAc	101

CHAPTER 1

INTRODUCTION

1.1 Introduction and motivation

Soft robotics is a novel and disruptive field of research in modern robotics [1]. Robotic systems made of soft and compliant materials compared to their environment are classified as soft robotic systems [2]. Industries have traditionally favored rigid robots made of steel, metal, and rigid plastics due to their accuracy, precision, and efficiency. In contrast, soft robotics promise inherent safety and compliance with biological structures. With the recent interest in safer human-robot interactions and wearable technologies, where safety is emphasized over accuracy and power, soft robotics is poised to replace conventional rigid systems [3].

A crucial part of any soft robotic system is the soft actuator. The effectiveness of a soft robotic system relies heavily on the performance of its actuators. Recent research presents a boom in soft actuator development over the last decade. Many materials and actuation methods have been employed in developing modern soft actuators for applications ranging from micro to macro-scale. Among these developments, we can find the following standard features; shape-adaptability/compliance, back-drivability, passive-force control, stress dispersion, gentle touch, low self-weight, and inherent safety [4–6].

Diseases, trauma, obesity, and age can reduce a person's mobility either temporarily or permanently. In such cases, promoting continued attempts at independent motion is helpful in recovery/management [7]. Robotic systems have come to aid in such applications in supplying mobility aid in activities of daily living (ADL) and robot-assisted rehabilitation. Rigid exoskeleton-based wearable systems have been the preferred assistance solution in many assistive applications [8, 9]. These rigid systems carry several drawbacks, such as deviations from natural motion, increased metabolic cost due to the additional inertial loads, and subsequent axial misalignments leading to wearer discomfort [10–12]. The soft exosuit is a solution to overcome these limitations. An exosuit is a soft, wearable garment-based device that may be worn under regular clothes and provides assistive or augmentative forces to the wearer's limbs [7, 13, 14]. Unlike rigid exoskeletons, which transmit torque across limb joints, the exosuit aims to imitate muscular actuation by applying forces parallel to the muscles.

Soft exosuits hold great promise for improving wearable assistive solutions, with a foremost advantage being their ability to feel and seem transparent to the wearer, providing discretion, increased comfort, and ultimately prolonged wear time. The ideal soft actuators for such exosuits must be lightweight, have low-volume and low cross-sectional dimensions, and be flexible enough to attach along body contours while delivering adequate contractile forces similar to biological muscles. As a result, there has been growing interest in developing thin, low-profile, and lightweight contractile soft actuators with high force-to-weight ratios [15, 16]. However, current limitations exist in the lack of suitable soft actuators for optimal integration, highlighting the need for continued research and development. This thesis will present the development of soft linear actuators for wearable exosuits to cater to this demand.

1.2 Research problem

Soft wearable assist devices require soft low-profile, compliant linear actuators to match body contours for effective exosuit integration and have a high force-to-weight ratio for effective performance. The work presented in this thesis describes the development of soft linear actuators that successfully address the above primary problems of exosuit integration.

1.3 Thesis outline

This thesis is divided into eight chapters. Chapter 2 is presented next with a thorough overview of relevant recent literature. The recent breakthroughs in soft linear contractile actuator development in techniques, materials, and evaluation are discussed there. The importance of the work provided in this thesis is justified as well. The third chapter addresses the design of two thin, low-profile soft linear contractile actuators. A description of their design concepts and the relevant manufacturing processes are presented. The experimental assessment of the proposed actuators to characterize their performance and experimental evaluation of controlling the actuators are presented in chapter 4. The next chapter describes the mathematical models developed for the proposed thin vacuum actuators. The sixth chapter discusses using the new actuators created in exosuit applications. Evaluations based on testbeds as well as human participants are provided here. Chapter 7 summarizes the key findings in the conclusion and presents areas for further research. Chapter 8, lists the publications arising from this research.

1.4 Main contributions

The research work presented in this thesis provides several novel contributions in the field of soft robotic actuators for use in wearable exosuit applications.

- Two different variants of soft low-profile contractile actuators are proposed. Their design, fabrication, and experimental performance characterization are presented. Numerical models are developed to describe and predict their displacement and force.
- First, a novel, thin (6 mm OD), lightweight ($< 1.25\,g$), contractile, monofilament, soft actuator (ThinVAc) that delivers a high force-to-weight ratio (477 times self-weight) is developed. The ThinVAc presents a maximum contraction ratio of 60 % at no load condition and a maximum isometric blocked force of 5.2 N. A scalable, multi-filament design combines thin-walled actuators; their design, fabrication, and performance characterization are presented. An 18 g multi-filament actuator bundling 15, 100 mm ThinVAcs can produce a maximum blocked force of 54 N at a force-to-weight ratio of 291.
- Second, a novel low-profile vacuum actuator (LPVAc) with an integrated inductive displacement sensor that is lightweight (14 g) and can provide high strain (65%), a maximum blocked force of 39 N, and a high force-to-weight ratio (285 times self-weight).
- An integrated sensor feedback system is developed for the proposed LPVAc and is experimentally characterized. This proposed sensor uses inductive displacement sensing in a vacuum-driven soft actuator for the first time.
- The performance of the ThinVAc and LPVAc are experimentally evaluated in a lower limb model and human subjects. Further, the ThinVAc is used in case studies to show its applicability in soft robotics and wearable applications.
- A novel hip and knee flexion-assist mono-articular exosuit is developed to evaluate the applicability of the developed LPVAc in sit-to-stand transition assistance. Human experiments demonstrate that the suit with actuation condition successfully reduces mean muscle activity by more than 45 percent compared to the no suit condition.

Other research contributions:

- A novel casting method based on a 2D-layered approach and thermal programming of pneumatic tubing for simplification of fluidic soft robotic structure prototyping was developed [17].
- A scalable multi-thread SMA actuator using thermally conductive fluid was developed, and its blocked force performance was characterized. It showed that the force of an SMA actuator could be scaled without significant changes in the power source and without insulation between single wires [18].

CHAPTER 2

LITERATURE REVIEW

The development of soft robots compared to their working environment has become of recent interest in robotics [4]. For several reasons, the novel concept of 'soft' robotic systems has been a point of interest among contemporary robotic researchers. Firstly, conventional rigid robots are limited in their capability for safe operation in real-world environments, especially close to biological systems. Secondly, there has been an omnipresent influence from nature driving robotic researchers to provide the same compliance seen in animals and plants. Last but not least, the identification of the role taken up by biological bodies in movement control and intelligence (Embodied intelligence/morphological computation [19]) has fascinated researchers to try to embed control and intelligence into the mechanical structure itself [20].

The soft actuator is a critical component in any soft robotic application. The commonly used actuation methods in soft actuators [21] are; electrical charges [22–24], chemical reactions [25], shape-memory alloys [22, 23], and fluids [26–28].

Among the soft actuation methods mentioned in the literature, soft actuators driven by fluids have become an attractive option [21] due to their ease of fabrication, the safety of operation, high power-to-weight ratio, and low cost [29–31]. These soft fluidic actuators are inflatable bladders made of soft material, with some method of deformation control stimulated by air pressure.

The literature review presented in the chapter is organized as follows. First, a review of soft fluidic actuators in the literature is presented. Next, pneumatic artificial muscles are described, with a comparison with organic muscles. Then, the novel area of vacuum-driven soft actuators is given, including the details of vacuum actuation. Next, the particular area of vacuum-driven contractile actuators is discussed. This section is followed by a discussion of sensing methods used in soft actuators. Next, the methods used to assess soft actuator performance are presented. Finally, the concept and examples of soft exosuits are given.

2.1 Soft fluidic actuators

Soft fluidic actuators (SFAs) made of soft deformable material have been identified in the literature as elastic inflatable actuators (EIAs), pneumatic artificial muscles (PAMs), Pneumatic muscle actuators (PMA), soft pneumatic actuators (SPA), flexible fluidic actuators (FFA), Biomimetic Actuator, Fluidic Muscle. SFAs can be primarily categorized by their fabrication method [21], such as; those made from a single molding step [32, 33], pneumatic muscles (McKibben type [34–37] and fiber-reinforced type [32, 38–43]), or those with multiple air chambers with connecting passages [26, 44–49].

The advantage of soft fluidic actuation include the availability of large strokes, minimal friction, and distributed force generation [50]. Compared to other contemporary soft actuator technologies, it does not require large electric or magnetic fields (*i.e.* electrostatic, piezoelectric actuators and electroactive polymers) or increased temper-

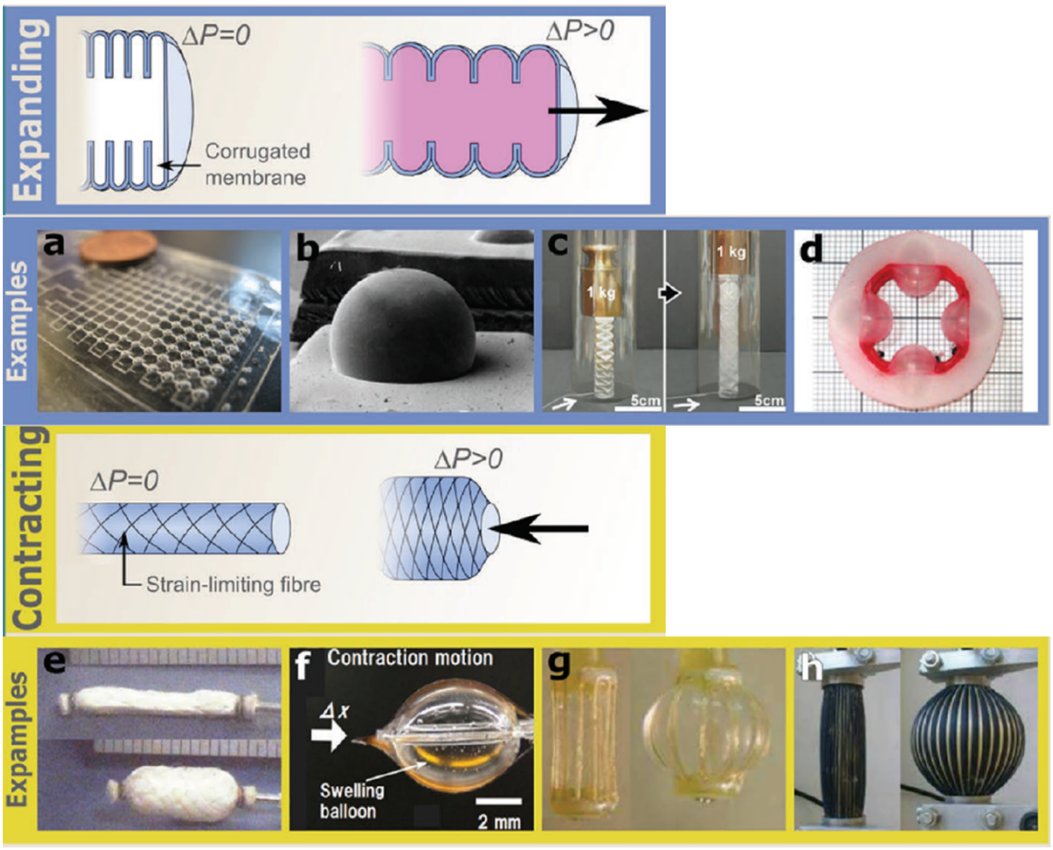

Fig. 2.1: Classification of EIAs based on motion path (extracted from [52]). a) an array of Braille actuators [56], b) Osmotic micro-actuator [57], c) Origami extension actuator [58], d) Stator for pneumatic rotary actuator[59], e) McKibben artificial muscle [60], f) Pantograph actuator [61], g) Artificial muscle using electro-conjugate fluid [62], and h) Pleated pneumatic artificial muscle [63].

atures (*i.e.* shape memory alloys and thermal actuators) that cannot be used close to biological tissue in orthotic applications.

The first soft elastomeric inflatable actuator (EIA) can e traced back to a pneumatic jack patent submitted by L. A. Fleury [51] in 1919. The characterization of EIAs [52] are based on their motion path, as contracting, extending, bending, and twisting actuators [53]. The attention in this review is focused on contracting and extending actuators suited for lower limb assist applications.

Gorisson *et al.* [52] state that, it is the anisotropy (having properties that differ when measured in different directions) programmed in the flexible structure that determines the motion path [54, 55]. Expanding and contracting actuators typically have structurally symmetric cross sections in contrast to the asymmetry in bending actuators. The pressure expansion drives an extending actuator, while strain limiting components (*i.e.* inextensible fibers in a braid) convert an expansion into longitudinal contraction in contracting actuators. Fig. 2.1 present several examples of expanding and contracting EIAs.

2.2 Pneumatic artificial muscles

Pneumatic artificial muscles (PAM) are an SFA type that has attracted recent interest among soft robotic researchers [16, 64–66]. The very first PAM is attributed to Dimitri Sensaud de Lavaud (1929) and Garasiev (1930), with some argument among contemporary researchers [64, 67]. The next PAM is attributed to Morin (1947), which Morin and Woods later patented in 1953. The most noted PAM in literature is the fluidic actuator developed by McKibben in 1957, which coined the term "artificial muscle" [68].

PAMs have been defined as *"contractile and linear motion engines operated by gas pressure"* [64]. They tend to expand or contract upon pressurization or depressurization, applying pushing or pulling force on the load. The axial motion is linear and unidirectional. Most of the work on PAMs has focused on overpressure (above atm.), while there also are a few under-pressure (vacuum) devices [15, 69, 69–75], as well. Overpressure PAMs have several distinct rules [64]:

- A PAM shortens by increasing its enclosed volume.
- A PAM will contract against a constant load if the internal pressure is increased.
- A PAM will shorten at a constant pressure if its load is decreased.
- A PAM's contraction has a ceiling at which no force is developed, and the volume becomes maximum.
- Each pair of internal pressure and load has an equilibrium muscle length. (This contrasts with a pneumatic cylinder where cylinder force depends on pressure and piston surface area, force is constant regardless of displacement.)

Based on the construction of the PAM, it can be a contractor or an extensor muscle. The literature lacks muscles capable of both. Most research has been carried out on contractor muscles compared to extensor muscles. PAMs consist of soft material capable of elastic deformation to provide much safer interaction with their biological counterparts compared to conventional rigid actuators [76]. Table 2.1 shows the similarities between biological muscles and PAMs as derived from Tsagarakis [77] and Caldwell [78].

The key advantages and disadvantages observed regarding PAMs are as follows. The key advantages of PAMs are their ability to deliver a high energy density to a local application area, no reflected inertia, low added inertia, and, critically, inherent compliance. Their performance is similar to that of organic muscles. Their primary disadvantages include the inability to provide structural support due to the lack of stiff structures, the inability to provide accurate and precise motion, and the lack of compact feedback mechanisms for force and displacement that conforms to biological motions [79]. The available rigid methods negatively affect the advantages mentioned above. Soft actuators are typically under-actuated; hence they feature DoF that cannot be controlled [80]. Hence, to develop soft actuators with improved controlled accuracy, the focus has fallen on reducing the DoF to obtain uniaxial actuation.

TABLE 2.1: Comparison of biological muscles and PAMs

Parameter	**Organic muscle**	**PAM**
Displacement	35%	30–68%
Force/cm2	20–40 N	100–500 N
Power/weight	40–250 W/kg	500–2000 W/kg
Efficiency	45–70 %	32–50 %
Rate of contraction	25-2000%/s	35-700 %/s
Control	Good	Fair-Good
Operation in water	Yes	Yes
Temperature range	0 - 40° C	-30 - 80° C
Robustness	Excellent	Fair-Good
Self-repair/regeneration	Yes	Material dependent
Antagonistic operation	Yes	Yes
Energy source	Chemical	Pneumatic
Environment safe	Produces CO_2	Yes
Scalable from	µm-m	cm-m
Linear operation	Yes	Yes

2.3 Vacuum-driven soft actuators

Vacuum-driven actuation is gaining popularity in a variety of soft robotics applications, including the development of flexible arm robots [75, 81], crawling robots [81, 82], modular robots [83, 84], soft clutches [85], soft trusses [86], and wearable assistive devices [15]. Most of the literature's vacuum PAM (VPAM) aims to generate contraction motion. Additionally, others have utilized positive pressure in combination with vacuum to produce extension, bending [86], and rotational [81] motion.

If a positive pressure device ruptures or delaminates, it poses an explosive danger. Such explosions will injure the operator of a wearable gadget that employs positive pressure devices. When using higher pressures, the user's possibility for damage increases. Positive pressure devices are also more prone to performance degradation due to skin damage or seal failures [87].

In most general applications, the highest allowable differential pressure applicable in negative pressure devices is a single atmosphere or 100 kPa. In most practical applications, generating vacuum sources with pressures less than 10 kPa (abs.) may be costly and challenging, and most low-cost vacuum pumps can only provide a vacuum pressure of 30 kPa (abs.). As a result, the highest differential pressure may be in the 70–90 kPa range. As a result, the highest pressure differential represents a physical barrier that can only be surpassed under hyperbaric circumstances. Unlike positive pressure devices, vacuum-driven soft actuators are less prone to leakage or membrane failure. If a sufficient vacuum source capable of actuating the device is present, a vacuum-driven actuator will continue to work with the same or slightly reduced capacity with such damage. Most positive pressure devices are incapable of exhibiting such damage-resilient behavior.

Vacuum actuators have several drawbacks and restrictions as well. Unless hyper-

baric conditions are created, the maximum applicable pressure differential is limited to one atmosphere. This maximum pressure differential limits the maximum blocked forces that can be generated. Another limitation is that the breakdown of a vacuum-driven actuator's membrane or seal would result in the suction of the surrounding environment into the actuator sub-system. However, this will be advantageous for actuators that may need to evacuate fluids/particles from the environment in which they are functioning.

2.4 Vacuum-driven contractile actuators

Vacuum-driven actuators create force and motion by controlling the collapse of an air chamber. The negative pressure produced within a cavity in the actuator forces the ambient environment to compress the structure isotropically. As a vacuum source sucks out the fluid in the chamber and the pressure falls, contraction occurs as the chamber implodes due to atmospheric pressure. This implosion prevents radial expansion while increasing the contraction ratio, making it ideal for space-constrained applications.

Recent research describes a few different techniques for doing this, including inextensible film pouch collapse guided by a skeleton [72, 73, 75, 86], elastomeric volume collapse [83], beam buckling citeYang2016,Yang2017,Miller2018, and elastomer covered foam chamber collapse [71]. The functioning of these devices, including the origami-based vacuum PAMs, is detailed in [72, 88]. Fig. 2.2 describes some examples of these influential contemporary contractile vacuum actuators.

Some instances in the literature propose using both positive pressure and a vacuum source. Usevitch *et al.* [86] propose a two-chamber antagonistic PAM (APAM) capable of contraction, extension, and bending (Fig. 2.2 c)). To regulate the vacuum collapse, they propose using an inextensible thin-film bag with reinforcing ring supports. The two-chamber architecture needs both positive and negative pressure sources for actuation. Because there is no skeletal structure, the actuator requires positive pressure to remain in its unactuated condition. Yu *et al.* [82] propose a crawling robot based on an origami skeleton and a vacuum-driven foldable PAM (FPAM) (Fig. 2.2 i)). The suggested FPAM uses a paper skeleton enclosed in silicone skin. This design gets compressed in a vacuum and expands under positive pressure.

Another interesting vacuum actuation method described in the literature is beam buckling. Yang *et al.*'s [89] vacuum-actuated muscle-inspired pneumatic structures (VAMPs) create linear contraction and torsional motion by buckling beams in response to applied vacuum pressure (Fig. 2.2 h)). These actuators are composed of soft silicone and have a cellular structure comprising beams and columns. They accomplish a controlled collapse along a single axis by combining thinner beams with thick columns. The contraction reduces, and the force rises with the modulus of the material in the VAMP concept.

Recently, there has been an increase in interest in origami-inspired vacuum PAMs [72, 73]. These soft actuators contain foldable skeletons inspired by origami, encapsulated within a volume produced by a pouch composed of thin-walled, minimally extensible material, such as air-tight textiles and polyethylene (see Fig. 2.3). When the air inside the air pouch is evacuated (via a vacuum pressure), the actuator will experi-

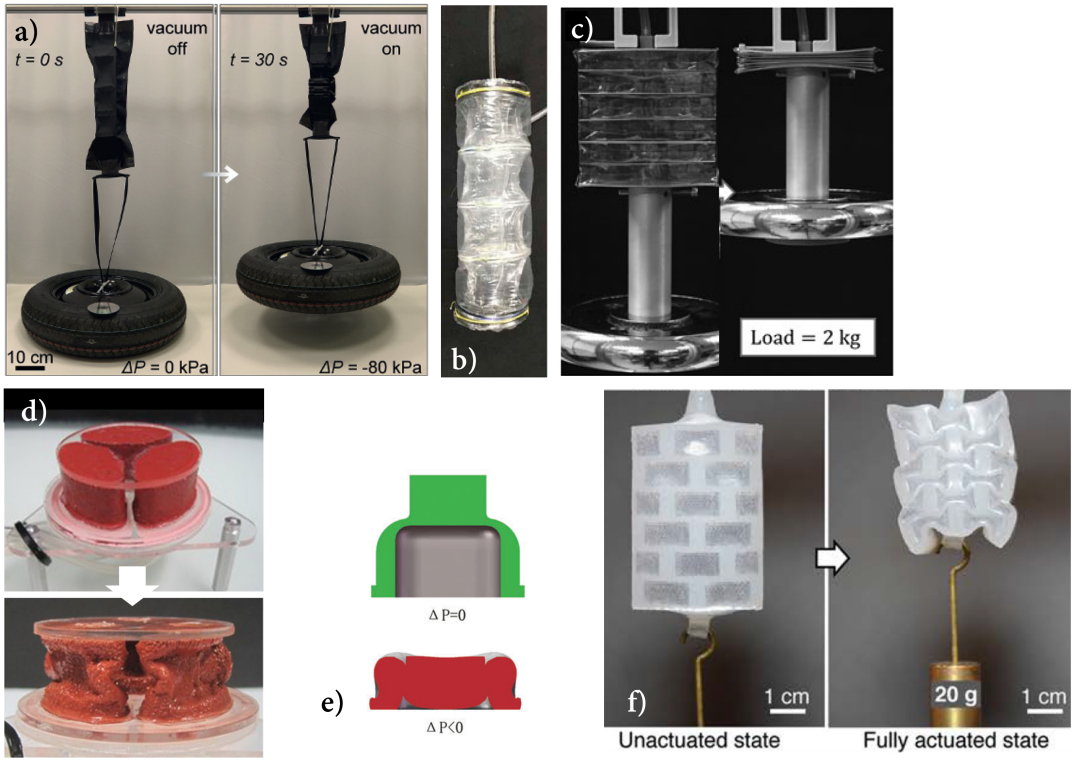

Fig. 2.2: Some examples of contemporary vacuum-driven contractile actuators. a) FOAM (Nylon skeleton with TPU skin) [72], b) APAM [86], c) OV-PAM [73], d) V-SPA [71, 84], e) a soft actuator utilizing elastomeric chamber collapse [83], f) VAMP design utilizing buckling of beams [69].

ence a controlled collapse in a direction controlled by the skeletal structure. Skeletal support is provided by small, rigid components that enable collapse only along the actuator's longitudinal axis when the volume inside the film pouch is evacuated. This design approach enables the easy and fast manufacture of lightweight, soft actuators with high force-to-weight ratios. These devices can produce large contraction ratios and linear forces with the applied vacuum pressure. Another distinguishing feature is that these actuators need less force to deform, allowing them to lift lighter weights at lower vacuum pressures than other PAMs that require more force to distort thicker structures [72]. One major drawback is that it becomes impossible to forecast the contraction without considering the connected load; hence, open-loop control for unknown loads will be difficult.

Li *et al.* [72] propose an origami-inspired artificial muscle that is fluid-driven (FOAM) (Fig. 2.2 b)). In this circumstance, they used zigzag-shaped skeletons enclosed in thick, thermally sealed film pouches. Their findings suggest that thicker film materials and a greater zigzag skeleton angle may be employed to improve a FOAM's maximum force. Thinner zigzag skeletons can attain higher contraction ratios. They utilized 0.34 mm and 0.48 mm thick nylon fabric pouches weighing 43 g and 56 g, respectively, to achieve maximum blocked forces of 201 N and 428 N. The contraction ratios of the identical actuators were 50% and 31%, respectively. Another lightweight

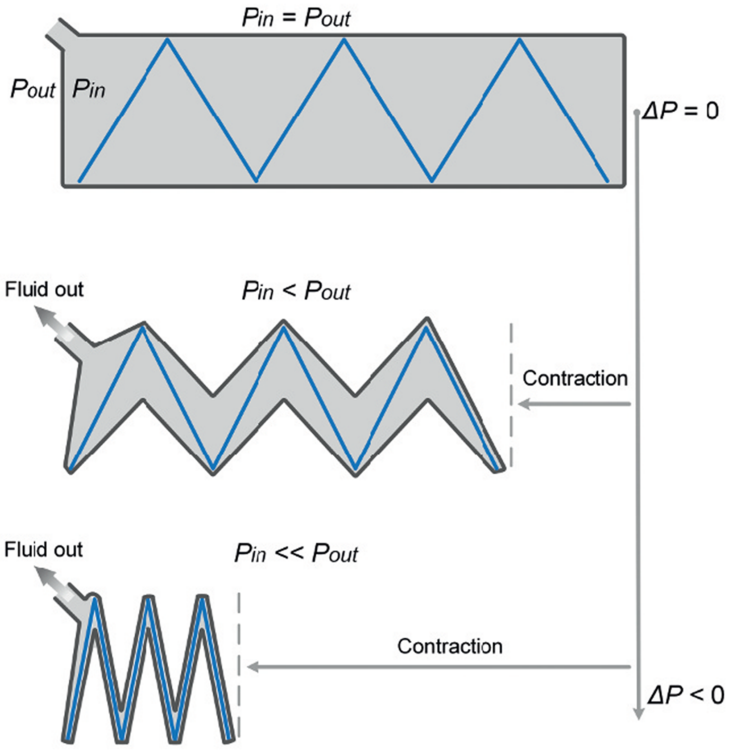

Fig. 2.3: The principal of operation of origami-inspired vacuum actuators [72].

FOAM (2.6 g) constructed of thin polyester material (film thickness: 0.038 mm and skeleton thickness: 0.254 mm) lifts a 3 kg (29.4 N) load at 20 kPa (abs.).

Lee *et al.* [73] present an origami-based vacuum PAM (OVPAM) with 400 N forces and a 90% contraction ratio (Fig. 2.2 d)). The OVPAM design uses polygonal cross-section supports to prevent longitudinal collapse during vacuum actuation. This design uses broad cross-sections to generate more force at lower vacuum pressures at the expense of larger actuators. The transverse supports are independent of one another, as opposed to [72]. Equilateral triangular cross-sections were combined with a pre-folded pouch to reduce the collapsed/contracted length of the actuator. An OVPAM with a length of 90 mm, a triangular side length of 90 mm (equivalent circular diameter of 104 mm), made of 0.07 mm PVC pouch and 3D-printed PLA top and bottom plates, weighing 53 g, has demonstrated 120 N (force-to-weight ratio: 230), with a 90% contraction ratio for loads 200 times its weight. Another OVPAM, composed of thicker 0.1 mm PVC film, with doubled top and bottom plates and 150 mm side length (equivalent circular diameter of 173 mm) weighing 160 g, was proven to lift a 40 kg load with 87% contraction (force-to-weight ratio: 250). They recommended utilizing flexible top and bottom plates to achieve a 100% contraction ratio.

2.5 Sensing in soft actuators

Though PAMs offer great potential in the development of soft robotic applications, the lack of integrated force and displacement feedback systems is one factor that is currently impeding their progress. PAMs could accomplish effective closed-loop control with the availability force and displacement feedback systems. For displacement feedback, several PAMs have attempted incorporating encoders [34], potentiometers [90], flexible force-sensing resistors [91], and hall effect sensors [78]. Force feedback has been obtained via strain [92] and gauge pressure [93] sensing.

However, because these approaches involve rigid and semi-rigid mechanisms, they add weight, change the requisite motion of the actuator, and negate the benefits of the actuator being soft. Conductive liquid metal sensors are also proposed as a softer feedback sensing method. Ga-In alloy-filled channels (see Fig. 2.4) have been utilized to provide displacement feedback on actuator deformation [94, 95]. These channels can alter the actuator's desired deformation. Furthermore, any damage to the channel will result in the leakage of the liquid metal, limiting the sensor's functionality and causing harm to the wearer.

Inductive sensing has recently become of interest among soft robotics researchers due to their response varying only upon the geometry in most general environments (see Fig. 2.4). Electrically conductive insulated wires made into a flexible yet inextensible braid have been utilized in the contraction sensing of McKibben-type soft actuators [88, 96, 97]. They have shown low measurement error (0.83 mm) with high sensitivity ($681\,nH/mm$) [96]. Inductive sensor-based feedback control has also yielded significantly good results that positively endorse their use in soft robotics actuator position control [97].

2.6 Assessment of PAM performance

As the main objective in the artificial muscle model of a PAM is to relate to biological muscle behavior, their assessment should also be done similarly to biological muscles [68]. Fig. 2.5 describes the three performance evaluations needed for a PAM.

- *Isotonic*: constant muscle tension
- *Isometric*: increasing muscle tension at constant muscle length

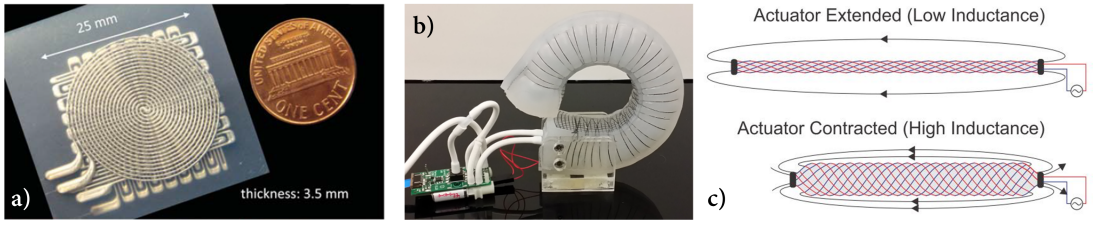

Fig. 2.4: Examples of soft sensors used in PAMs. a) and b) Eutectic Gallium-Indium (EGaIn) as a strain sensor [95], b) [94], c) Smart braid inductance sensor [96].

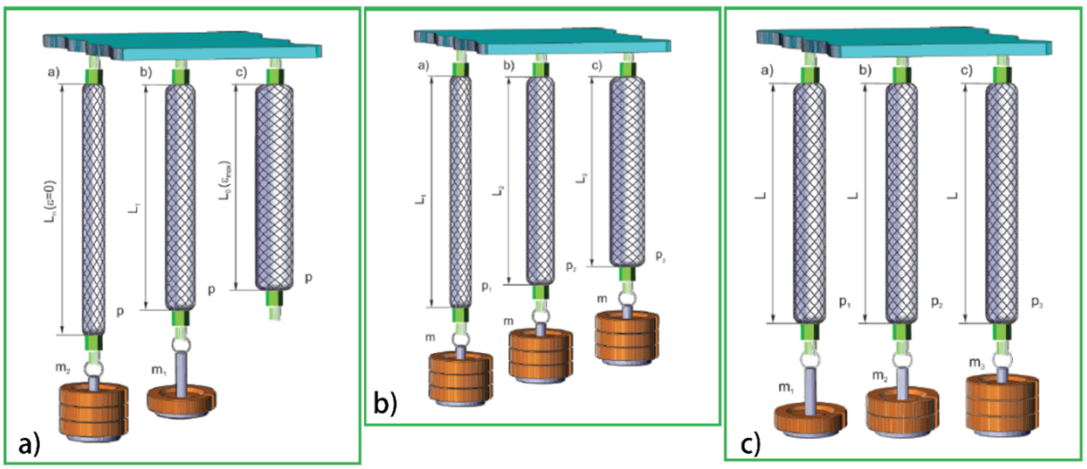

Fig. 2.5: Static characterization of PAMs [68]. a) determining isobaric characteristics, b) isotonic characteristics, c) isometric characteristics.

- *Auxotonic*: tension rises and then remains the same as the muscle contracts without changing its length

Isotonic properties are assessed by measuring muscle length at a constant load and changing applied pressure. Isometric properties are assessed by controlling the applied pressure to maintain constant muscle length as the load changes. The isobaric characteristics of an auxotonic contraction are measured by keeping the pressure constant and measuring the muscle length as the load varies [68].

2.7 Soft exosuits

Many recent reviewers of lower limb exoskeleton, assistive and rehabilitative devices identify the future of the technology lies with the development of wearable assistive devices based on softer materials that contain none, or minimal rigid components that can be easily worn underneath a conventional dress [98–100]. An exosuit, or specifically the 'soft exosuit', is the soft variant of the traditional rigid exoskeleton that can provide the above features.

A soft exosuit is a collection of principally soft, non-restrictive wearable components that can deliver augmentative/assistive/rehabilitative forces to a user. It should be able to augment select muscles/muscle groups and "utilize the wearer's skeletal structure to generate any compressive, bending and shear forces as required by the system" [13].

Soft exosuits differ from passive orthoses in the power delivery method to the user. A passive orthosis (a brace) will act as the rigid shell that will guide the force to the user's body. In contrast, a soft exosuit will apply circumferential forces to the user using connection cuffs [101] or tension forces to generate moments about biological joints [13, 102].

The most commonly referred lower limb exosuits found in the literature are Wehner *et al.* [13] from 2013 and Asbeck *et al.* [102] from 2015. Both publications are

from the Wyss Institute for Biologically Inspired Engineering at Harvard University, Boston, USA. These two centerpieces are part of a larger assortment of exosuit-related experimental publications [103–111], based mainly on the prototype shown by Asbeck *et al.* and J. Bae *et al.* [105].

One of the literature's most influential soft exosuit designs is the Wehner design [13]. Wehner *et al.* presents an ultra-lightweight exosuit utilizing soft actuators to augment the normal muscle function of healthy individuals (Fig. 2.6). This suit features custom-built McKibben-type actuators to assist hip, knee, and ankle joint motions by applying assistive torques in the sagittal plane. It provides motions of hip flexion and extension, knee flexion, and ankle dorsiflexion and plantarflexion (See Appendix 02 for the notations used for body planes and limb motions.).

In the human joint motion, specific paths on the skin surface undergo significant changes in length relative to one another, compared to others who undergo insignificant relative motion. Such *low-strain paths* have been defined as lines of non-extension [112]. This concept of lines of non-extension was first presented in the context of designing a wearable bio-suit for planetary exploration. Wehner *et al.* exploit this concept to configure a matrix of connectors to maintain stability during a normal range of motion, redirecting forces, and terminating at a key anchor point (see Fig. 2.6 c)). The distal end virtual anchors fix at the ankles, and the proximal end virtual anchors fix to the hips and shoulders, thus maintaining the forces normal to the skin and distributing the applied forces.

The second type of soft exosuits found in the literature is the Bowden cable-driven

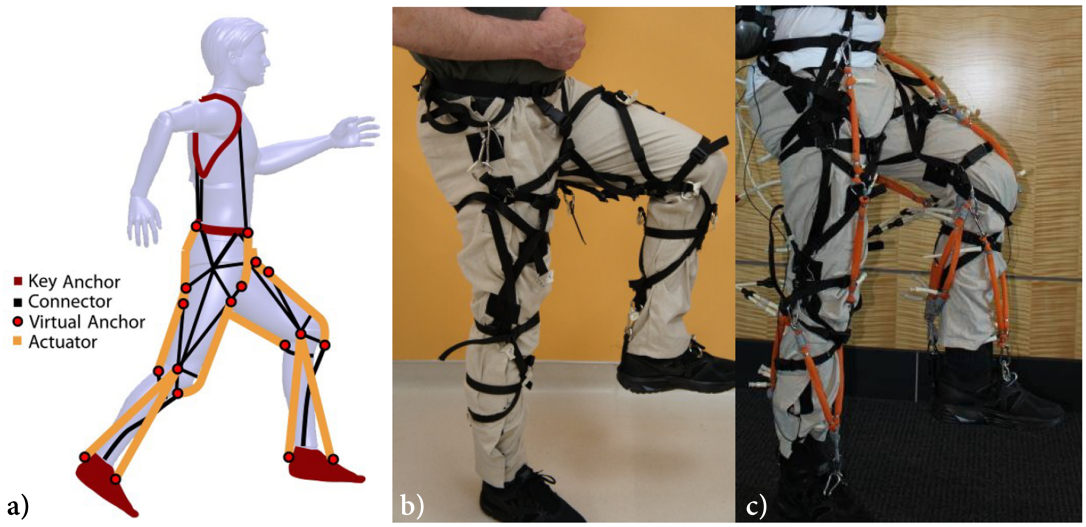

Fig. 2.6: The Wehner soft exosuit design [13]. a) The virtual anchor concept: black connector lines are along the lines-of-non-extension. b) soft exosuit with connector matrix webbing for virtual anchors. c) McKibben type soft actuators attached to virtual anchor points.

method presented by Asbeck *et al.* (portable) [102] and J.Bae *et al.* (tethered) [111]. Based on the virtual anchor concept, a series of webbing straps are used to secure the suit to the wearer, and a Bowden cable or two runs along the lower limb to a point/s on a foot attachment. The Bowden cable is attached to a DC motor-pulley configuration and is housed in a sheath on the webbing, routed along the lower limb. The Asbeck suit carries a single Bowden cable, driven by a hip-mounted body-worn actuator, running behind the lower leg and attaches to a heel anchor, behind the ankle, on the user's shoe. Alternatively, the J.Bae suit, which is extended later by Louis Awad [108, 109], carries two Bowden cables, which are initially driven by off-board motors using a trailing tether [105] and later by a body-worn actuator [108], attaches to the heel and the dorsal surface of the foot using anchor points on the webbing worn on the shoe. The Bowden cable-driven prototypes are illustrated in Fig. 2.7 [102, 108, 109].

Other notable lower limb exosuits in the literature come from researchers in Switzerland and Japan. A string-driven, wearable, upper body-powered dorsiflexion assist exosuit to improve minimum foot clearance is presented by Ohashi *et al.*i in [113]. Sasaki *et al.* presents a trouser embedded with two rubber balloon actuators above and below the knee posteriorly and one on top of the knee anteriorly [114]. Jin *et al.* [115, 116] proposes a winding belt-driven exosuit mounted on the trunk of a user for hip flexion assistance. Inspired by the Wyss Institute's research, Bartenbach *et al.* presented an alternative concept involving two anchors at the hip and one on the shank (the part of the leg between the knee and the ankle) and a knee module to increase the lever arm and protect the knee patella [7]. The Bartenbach suit is actuated by a motor-driven cable pulling on webbing segments above the knee instead of a foot attachment. Exosuits focusing on assisting upper limb motions are presented by Lessard *et al.* in the CRUX exosuit [117]. Fig. 2.8 presents these exosuits.

Based on the concepts proposed by contemporary researchers [13, 28, 76], a soft exosuit can be defined as follows:

"Soft exosuits are wearable devices designed to assist with walking or other activities, capable of exerting assistive forces through reversible shape and elastic rigidity changes. They should be lightweight to minimize inertia and not disrupt joint movement. They should not constrain the natural movement of the joints when passive. Additionally, they should be safe for direct contact with humans, fit a person without extensive adjustment and calibration, and be comfortable for the wearer."

2.7.1 Advantages and disadvantages over rigid exoskeletons

2.7.1.1 Advantages over rigid exoskeletons

1. Rigid exoskeletons are usually coupled to the wearer by pads, straps, or similar interface strategies. As the biological joints are flexed/extended, the rigid links add considerable inertia to the movement that needs to be overcome by the user/exoskeleton. Though all current rigid exoskeletons seek to minimize these effects, there is a considerable hindrance to natural gait kinematics and dynamics. Converting the components to soft, lightweight materials can remove this effect in assistive devices [13].

2. It is challenging to remove misalignments between the biological and exoskele-

ton joints. The presence of static misalignments can lead to dynamic misalignments up to 10 cm during typical motions [118]. Current rigid exoskeletons have attempted to overcome this by including redundant, passive degrees of freedom, increasing the system weight, resulting in more inertial impedance [11].

3. Rigid exoskeleton systems are used with software, electrical and mechanical limits to safeguard users and those around them. However, there is an undeniable risk factor associated with these rigid, heavy and primarily metallic systems. Even a fall while wearing a rigid exoskeleton can physically harm the wearer and bystanders. The inherent material compliance and safety provided by soft exosuits dramatically reduce this risk and provide cushioning capabilities to absorb some impact forces that might otherwise harm the wearer and bystanders.

4. The mounting and the removal of rigid exoskeletons systems is a complicated process that typically requires additional assistance [116].

2.7.1.2 Drawbacks of exosuits

Soft exosuits suffer several drawbacks compared to rigid lower limb exoskeletons [119].

1. An exosuit alone cannot fully transfer a load from any part of a user's body to the ground. Hence, there will be a need for a skeletal structure for load bearing.

2. The torque and force generated by an exosuit are forced onto the user's skin, resulting in skin irritations and even skin damage.

3. Exosuits have poor torque efficiency compared to rigid exoskeletons.

2.7.2 Knee rehabilitation assist devices

With the increasing numbers of elderly and patients requiring knee rehabilitation globally, the availability of assistive rehabilitation devices that would allow physiotherapists to cater to multiple patients at a given time reduce their workload. Contemporary literature presents only a few such devices; hence, this area needs attention. Rigid exoskeleton systems have been used for knee rehabilitation assistance. Weinberg *et al.* [120], present an active knee rehabilitation orthotic device (AKROD) that uses an electro-rheological fluid (ERF) driven resistive variable damper to support knee flexion and provide resistance to prevent knee buckling (Fig. 2.9 a)). This rigid system weighs 3.8 kg. They have only provided kinematic analysis without any evaluations of the assistance provided. Sridar *et al.* [121] presents a soft actuator driven, knee extension assist exosuit (Fig. 2.9 b)), that provides 20% partial assistance (4.4 Nm). They have used thermoplastic polyurethane for (of thickness: 0.15 and 0.038 mm) the fabrication of the soft inflatable actuator. Their suit shows a muscle activity reduction of 7% during level walking in the rectus femoris muscle group. Finally, Park *et al.* [28] presents a soft wearable robotic device for knee flexion and extension (Fig. 2.9 c)). They utilize a lightweight (8.4 g) soft actuator designed to be flat in the unactuated

state via zero-volume chambers. During actuation, the chamber inflates, losing its low-profile nature. The device can exert only 2.5 N and 7 N, during flexion and extension of a model of an infant's leg (lower leg weight of about 220 g). Hence, the produced motion assist is inadequate for practical use in rehabilitation assistance.

2.7.3 Sit-to-stand-transition assist exosuits

With the world's aging population, sit-to-stand transition (StSt) assist exosuits have gained attention in the recent literature [7, 14]. StSt is a muscular action that begins in a sitting position and finishes with the individual standing upright. As a result, during the first portion of STSt, the wearable assist system must allow for comfortable sitting. As a result, the StSt assist exosuit's actuators and the exosuit itself should be soft and flexible. Actuators with wide cross-sections will restrict comfortability while seated. Therefore they should be low-profile to optimize user comfort. The use of heavy actuators capable of delivering larger forces imposes an unwanted inertial penalty on the user; hence, a more efficient method is to utilize soft, low-profile actuators with a high force-to-weight ratio.

Contemporary STSt assist exosuits in the literature have relied on motor-driven cables as the actuating mechanism. Employing inextensible webbing straps as fixturing, anchoring, and force-directing channels have been a popular design technique for the exosuit. Webbing straps are a typical exosuit design technique that takes advantage of the non-extension lines mentioned in [13]. The Bartenbach exosuit employs a hip-mounted motor system with a Bowden cable to provide assistive forces [7] (Fig. 2.10 a) and b)). The webbing straps are attached to the pelvis and the ankle. The Bartenbach design, as a passive exosuit prototype, outlines the proposed usage of an exosuit in anti-gravity STSt assistance. The Schmidt exosuit reported in [14] expands the concept mentioned above to an experimental prototype that shows for the first time a decrease in the knee and hip extensor muscle activation during STSt (Fig. 2.10 c) and d)).

2.8 Summary

This chapter summarized recent literature on soft robotics, soft fluidic actuators, pneumatic muscle actuators, vacuum-driven contractile actuators, sensing methods used in soft actuators, soft actuator performance assessment methods, and soft exosuit applications in lower limb motion assist. The development of soft robots and exosuits has gained attention due to their potential to operate safely in real-world environments, mimic natural compliance, and embed control and intelligence into structures. Soft fluidic actuators (SFAs) have become popular for soft robotics due to their ease of fabrication, safety, power-to-weight ratio, and lower cost. Pneumatic artificial muscles (PAMs) are one type of SFA that can provide high energy density, compliance, and safe interaction with biological counterparts. Vacuum-driven soft actuators are one type of SFA that can provide advantages such as; lower risk of rupture, explosion, and subsequent damage, ideal for contractile motion, can efficiently utilize collapsible structures for actuation, resilient to actuator damage, and the ability for simple control. Developing integrated force and displacement feedback systems for soft actuators is an im-

portant area in soft actuator development, and inductive sensing is a promising option. Soft exosuits, such as the Wehner design and the Bowden cable-driven methods can deliver augmentative, assistive, and rehabilitative forces through soft, non-restrictive materials and have the potential to be worn easily underneath regular clothing. The future of soft exosuit technology lies in developing devices based on soft actuators that are low-profile or compliant to match body contours and have high force-to-weight ratios.

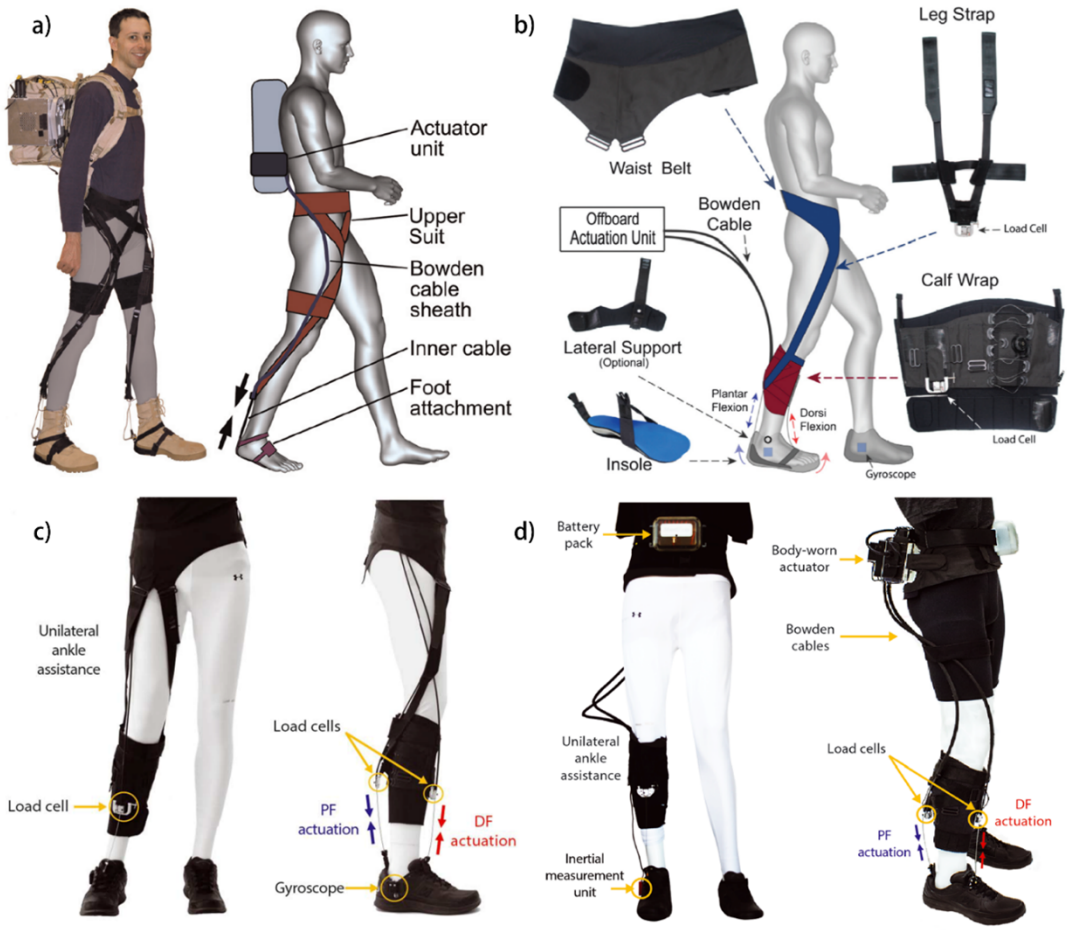

Fig. 2.7: Bowden cable driven exosuits: Asbeck, Bae, and Awad [102, 105, 109] a) Asbeck exosuit [102] (left) with components labeled (right), b) Bae exosuit [105] with offboard actuated antagonistic assistance for ankle motion assist. Functional textile anchors (waist belt, leg strap, calf wrap, and an optional lateral support module) interact with an in-shoe insole to generate assistive ankle plantarflexion and dorsiflexion forces when the contractile elements of the exosuit (Bowden cables located adjacent to the ankle) are retracted by an offboard actuation unit. c) Bae exosuit developed further by Awad [109], depicting Bowden cable actuation worn on the lower limb. d) Awad exosuit [109] incorporating trunk-mounted battery-pack and body-worn actuator.

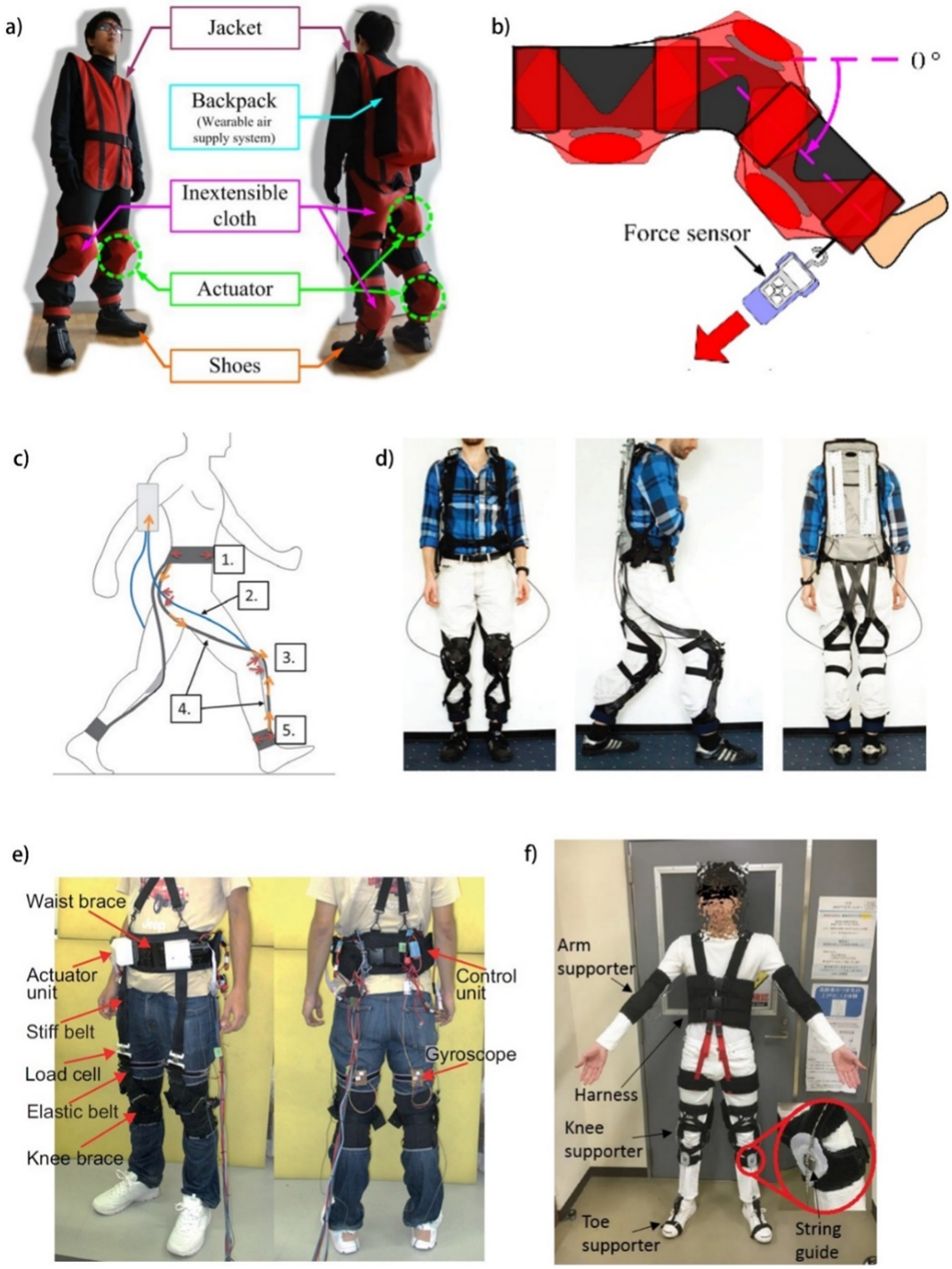

Fig. 2.8: Other contemporary exosuits. a) Sasaki [114] exosuit comprising trousers integrated with a soft balloon actuator and a backpack containing the air supply system. b) how the balloon actuators are embedded in the trouser. c) concept model of the Bartenbach exosuit [7], (1) and (5) are anchor points at the hip and above the ankle, respectively, (2) Bowden cable for actuation, (3) knee guard to increase lever arm and patella safety, (4) webbing elements. d) Bartenbach exosuit prototype. e) Structure of the Jin exosuit [115], f) Structure of the Ohashi exosuit [113].

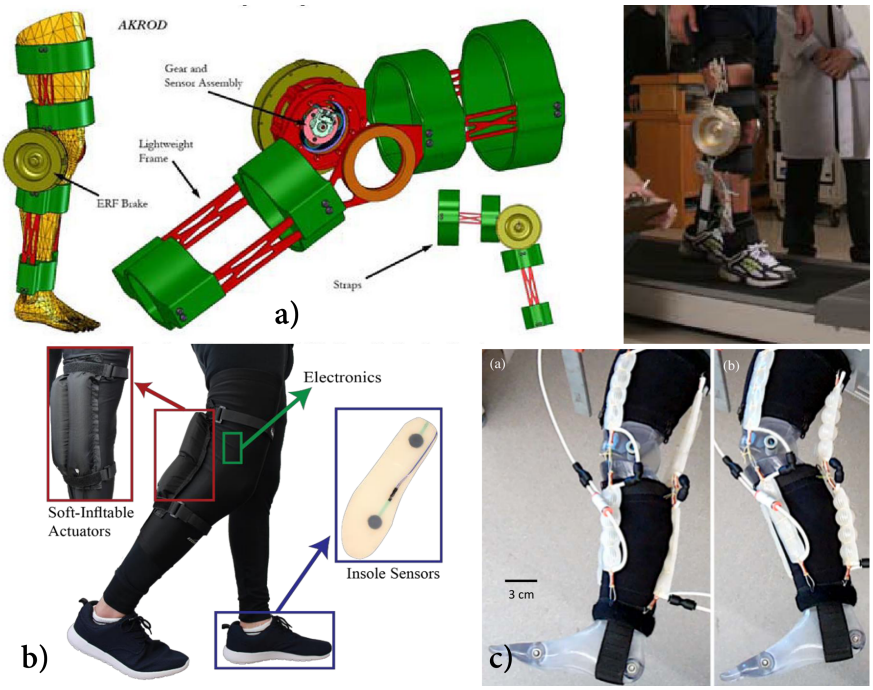

Fig. 2.9: Knee rehabilitation assist devices found in literature. a) rigid Active Knee Rehabilitation Orthotic Device (AKROD) [120], b) soft inflatable knee exosuit [121], and c) Soft wearable knee motion assist device [28].

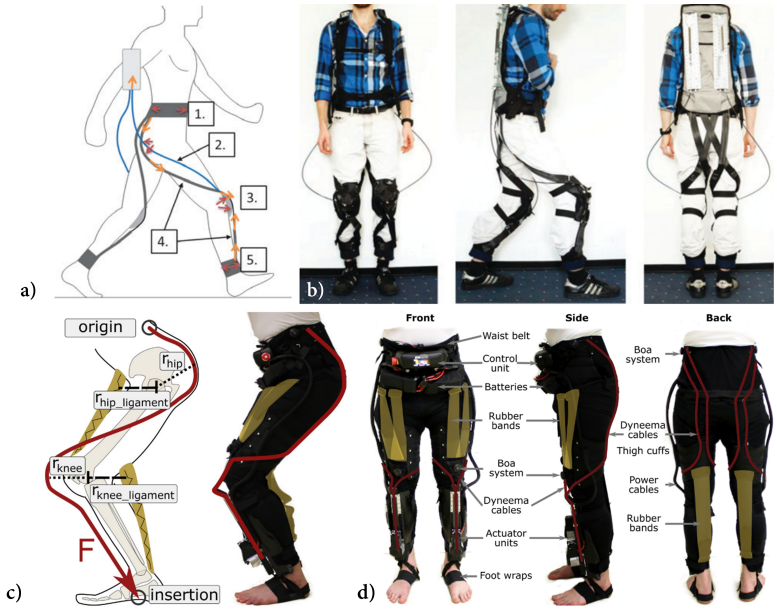

Fig. 2.10: Sit-to-Stand-transition assist exosuits. a) Conceptual design of the Bartenbach suit [7], b) Initial prototype of the Bartenbach suit [7], c) Concept and the force transfer path of the Schmidt suit [14], and d) major componenets and views of the Schmidt suit [14].

CHAPTER 3

DEVELOPMENT OF SOFT LINEAR ACTUATORS

3.1 Introduction

The concept of origami-inspired vacuum actuators is used to develop the novel soft linear actuators presented in this thesis. Hence, a collapsible structural skeleton is incorporated within another easily collapsible air-tight enclosure to create the actuator. Thin, flexible, but inextensible film materials are used to create this air-tight volume. The air within this enclosed space can be evacuated by connecting this volume to a vacuum source. The structure will collapse when this fluid within the volume is evacuated. Without any internal structure, the actuator's longitudinally opposite walls will collapse with minimal contraction. Hence, the collapsible skeletal structure controls this collapse and directs it in a single direction to obtain an effective contraction. If the skeleton structure has spring properties, this skeleton structure will further assist in returning the structure once the actuating vacuum signal is removed and the cavity is connected to the ambient atmosphere.

Soft contractile actuators developed for wearable soft assistive exosuits have several primary requirements. They should be;

- longitudinally flexible,
- lightweight,
- having a high force-to-weight ratio that can assist limb motion reducing inertial penalties,
- unobtrusive,
- having no/minimal wearer discomfort, and
- transparent to the user as well as any observers.

This thesis presents two origami-inspired, vacuum-driven actuators that aspire to provide the above requirements and describe their concept, design, and fabrication. The proposed designs are two high-ranking designs selected from developed conceptual solutions. First, a thin monofilament vacuum-driven soft contractile actuator with a small diameter cross-section is developed, and it is then combined to develop multifilament structures for force scaling. Then, a vacuum-driven soft low-profile contractile actuator is developed, and its low-profile shape is modified for force scaling.

3.2 Conceptual Design

A potential contractile soft actuator must be primarily longitudinally flexible, compliant, and non-intrusive to fit the identified design requirements for exosuit integration. Existing literature points to two potential solution paths. The design can be thin and flexible, where the cross-sectional diameter is significantly larger than the actuator

length, or have a low-profile cross-section, where the cross-sectional height is smaller than the cross-sectional width. Fig. 3.1 presents these two primary concepts. The collapsible skeleton structure also needs to be longitudinally flexible to meet the requirement for longitudinal flexibility while maintaining the controlled collapse. The thin and flexible concept developed the Thin Vaccum Actuator (ThinVAc) presented in section 3.3. The Low-profile Vaccum Actuator (LPVAc) described in section 3.4 results from the low-profile cross-section design.

This work proposes the use of a desktop vacuum system. A vacuum pump connected to a vacuum chamber of a significantly larger volume than the volume of the proposed actuator will create the vacuum source for actuation. Chapter 4 describes the specific arrangement of the vacuum system used in this work.

3.3 Thin Vacuum Actuator (ThinVAc)

This section presents the concept, design, and fabrication of a thin, vacuum-driven contractile actuator (ThinVAc). To obtain the desired characteristics for soft contractile actuators suited for wearable soft assistive exosuits, the proposed actuator is designed to be highly flexible and have a small diameter cross-section. The design concept applied here is a thin wire stainless steel (SS) helical spring of a circular footing enclosed in a collapsible thin-walled pouch(See Fig. 3.2. This thin-walled pouch functions as the closed air volume that may be evacuated via a vacuum source. The thin wire stainless steel spring is a skeleton framework that keeps the ThinVAc's cross-section intact during the collapse. The ThinVAc may longitudinally contract without collapsing into itself by keeping the cross-sectional area constant throughout the evacuation of the internal air volume. The SS spring permits only a longitudinal structure collapse, allowing the ThinVAc to function as a contractile actuator.

The requirement for the thin-walled skin is to provide a volume that is airtight and easily collapsible. Among the suitable materials, 1) low-density polyethylene (LDPE) and 2) thermoplastic polyurethane (TPU) is selected considering their collapsibility, previously observed success [72, 75], off-the-shelf availability, and ease of fabrication of enclosed volumes using simple thermal sealing methods [47, 75].

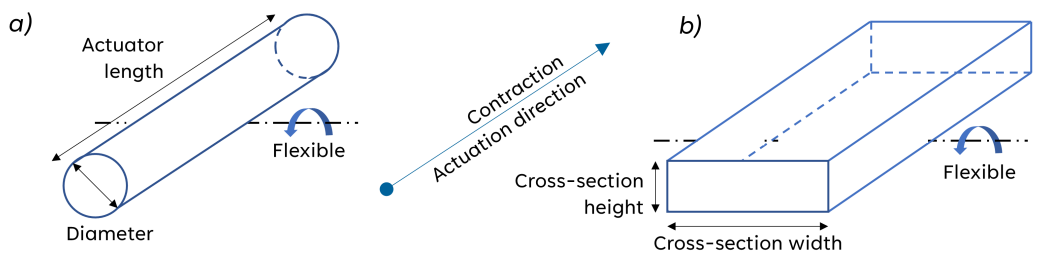

Fig. 3.1: The potential design paths for a contractile soft actuator for use in soft exosuits; a) the thin and flexible design, b) the low-profile design.

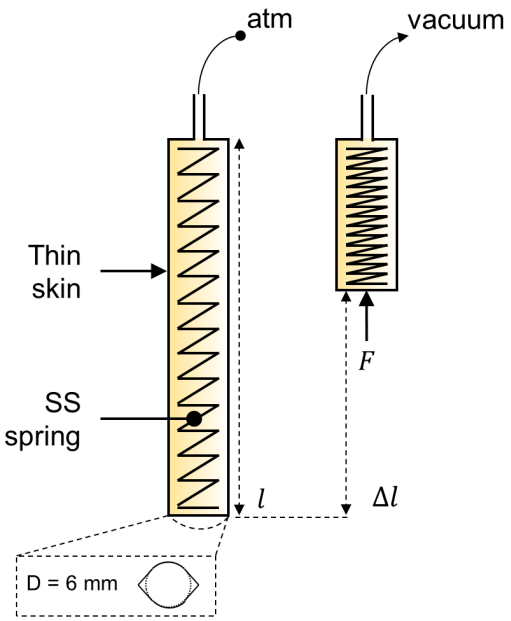

Fig. 3.2: Concept of the proposed thin vacuum actuator (ThinVAc).

A 6 mm diameter helical spring composed of 0.3 mm SS wire was chosen to develop the prototypes for testing and characterization. Stainless steel springs of three lengths were made on a lathe machine using the hot drawing process. The number of turns per length, wire diameter, and outer spring diameter was kept constant. The main characteristics of the spring used in the proposed ThinVAcs are shown in Table 3.1.

3.3.1 LDPE-ThinVAc

To produce the LDPE-based ThinVAc, an LDPE film with a thickness of 0.0125 mm was used to produce the thin-walled tube. The LDPE film was initially cut to 10 mm x L mm, including seal margins on all sides. The length L included the spring's length, two seal margins, and the positioning of a crimped insert for load attachment. Two 2 mm wide thermal seals were created by joining two LDPE film layers to form a tube, and the SS spring was then inserted. A polyurethane (PU) tube piece (5 mm in length) was connected to one side of the spring to serve as a solid connection, to which a

TABLE 3.1: Characteristics of the SS spring used in the ThinVAc

	Small	**Medium**	**Large**
Outer diameter [mm]		6 mm	
Wire diameter [mm]		0.3 mm	
Turns per 25 mm length		8 turns / 25 mm	
Spring Length [mm]	50	100	200
Spring constant [N/m]	60 N/m ± 1.4 N/m	34 N/m ± 2.1 N/m	16 N/m ± 2.9 N/m

flexible tubing serving as the vacuum line was attached. This end was bonded using cyanoacrylate adhesive to keep the LDPE film and flexible tubing in place. The tube was then sealed using thermal seals at the opposite end of the spring. During testing, a grommet was utilized to provide a stable mounting point for load attachment. The fabricated LDPE-ThinVAc is shown in Fig. 3.3. The fabricated 50, 100, and 200 mm ThinVAc weighed 0.75 g, 0.92 g, and 1.24 g, respectively.

3.3.2 LDPE-ThinVAc Multi-filament actuators

The proposed LDPE-ThinVAc monofilaments were coupled to enhance the parallel force for a given length, similar to biological muscle actuators of numerous muscle fibers. Several 50-, 100-, and 200-mm monofilament actuators were joined to build multifilament structures. As illustrated in Fig. 3.4, multifilament structures of 5, 10, and 15 monofilaments were constructed. To link the vacuum line to the individual monofilament actuators, a manifold constructed of acrylic sheets laser-cut into shape, as illustrated in Fig. 3.4 a), is used. A grommet is used at the distal end of the actuator, similar to monofilament actuators, to allow anchoring for testing and actuation.

A polyurethane (PU) tube of 8 mm OD was chosen to enable faster evacuation of the multi-filament structure (see Fig. 3.4). The PU tube was attached and sealed to an acrylic sheet manifold. Fig. 3.4 a) shows how the acrylic sheets were laser-cut and assembled. The manifold comprises an acrylic plate that connects the PU tubing and another that connects to ThinVAc's latex tubing. A hollow portion was sandwiched between the two to improve the evacuation of the combined multi-filament actuator. Fig. 3.4 b) and c) show the completed multi-filament actuator combinations. Fig. 3.4 b) depicts 15 filament actuators with 50, 100, and 200 mm lengths. Multi-filament combinations of 5, 10, and 15 ThinVAc monofilaments of 200 mm length are shown in

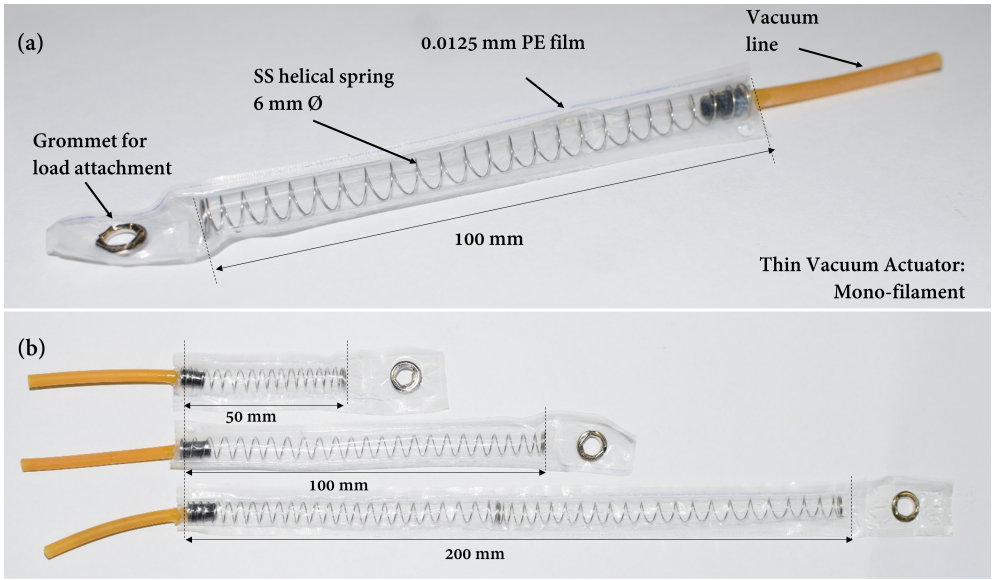

Fig. 3.3: The proposed thin vacuum actuator (ThinVAc). a) the main components of a 100 mm long ThinVAc. b) ThinVAcs of 50 mm, 100 mm, and 200 mm lengths.

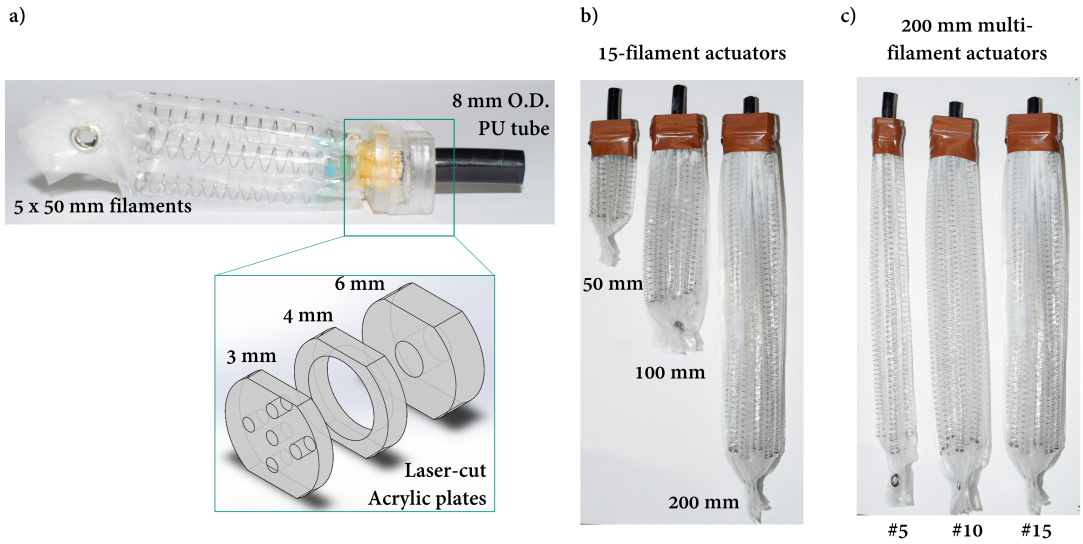

Fig. 3.4: The proposed multi-filament actuator design and fabricated actuators. a) 5 nos. of 50 mm monofilaments combined; insert shows the design of the acrylic connection plates. b) 15 filament actuators, c) 200 mm monofilaments combined in 5, 10, and 15 nos.

TABLE 3.2: Weight of each Multifilament actuator combination

	#5	**#10**	**#15**
50 mm	7 g	10 g	16 g
100 mm	9 g	12 g	19 g
200 mm	10 g	18 g	25 g

Fig. 3.4 c). Table 3.2 shows the weight of each multi-filament actuator combination.

3.3.3 TPU-ThinVAc

To produce the TPU fabric-based ThinVAc, a 0.2 mm thick nylon fabric coated on one side with TPU was used to create the thin-walled tube. The skeletal structure was provided by a 200 mm length helical SS spring (identical to the one used in the LDPE-ThinVAc). The SS spring was placed inside the TPU fabric pouch, which was then made into an enclosed pouch using thermal sealing. The fabrication process is described below. The main components and the fabricated TPU-ThinVAc are shown in Fig. 3.5.

The TPU-ThinVAc fabrication steps:

1. Cut two TPU fabric strips (L mm x 10 mm). *Note: Length L includes spring length + allowances for the thermal seals and grommets.*
2. Stack the two fabric pieces together with the TPU layer inside.
3. Create one thermal seal longitudinally along one edge of the stacked strips.
4. Create two transverse seals at the top and bottom, keeping a pouch length of 200 mm. *Note: leave a gap in the top seal for later insertion of the vacuum tube.*
5. Insert the vacuum tube via the gap in the top seal and complete the seal using cyanoacrylate glue.
6. Punch two holes at the top and bottom outside, transverse the thermal seals, and integrate grommets for fixing.

3.3.4 TPU-ThinVAc multi-filament actuator

The proposed TPU-ThinVAc monofilaments were coupled to enhance the parallel force for a given length, similar to biological muscle actuators of numerous muscle fibers. As the TPU-ThinVAc was more flexible than the LDPE-ThinVAc, an alternative design was used to create the multi-filament structures. Considering the TPU fabric's inherent ability to be layered, the multi-filament structure was made in a layered arrangement, as shown in Fig. 3.6. The TPU-ThinVAc was combined to create 3 and 5-multiple actuator configurations similar to the multi-filament LDPE-ThinVAc.

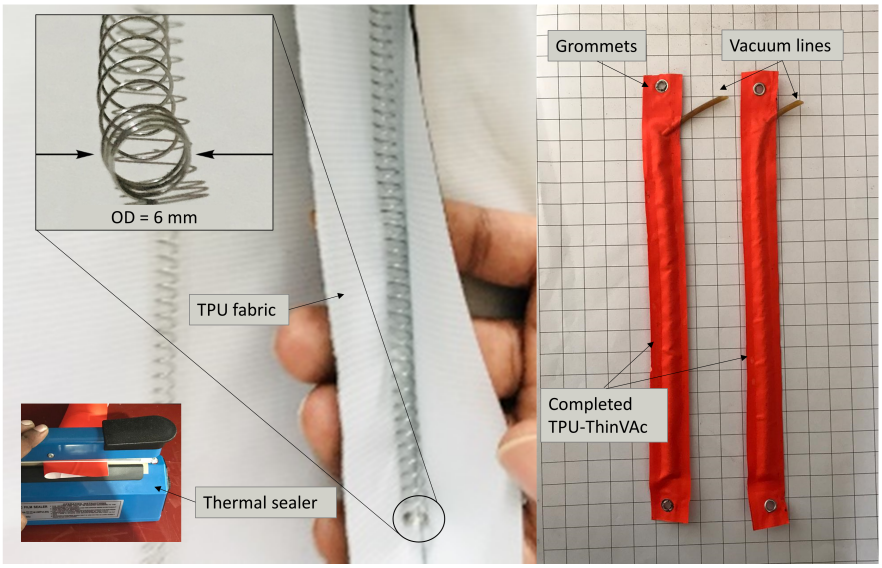

Fig. 3.5: The main components used to fabricate the TPU-ThinVAc, and the final fabricated TPU-ThinVAc.

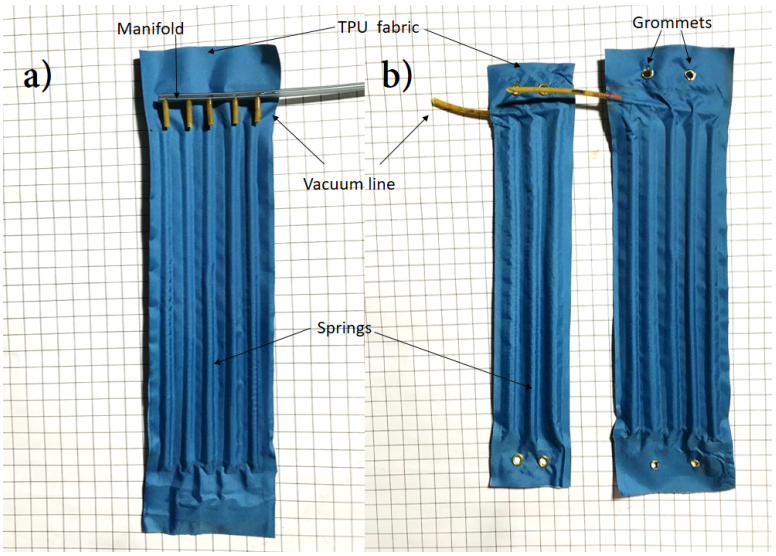

Fig. 3.6: Multi-filament TPU-ThinVAcs: 3-filament and 5-filament. (a) The vacuum manifold used for the multi-filament TPU-ThinVAc. (b) The fabricated 3-filament and 5-filament TPU-ThinVAc

Similarly to the fabrication of TPU-ThinVAc, rectangle strips of TPU fabric were cut based on the required number of actuators n ($12\,x\,n$ mm x L mm). L includes the spring length (200 mm) and allowances for seals and attachments. Two methods were used for creating the seals for the mono- and multi-filament TPU-ThinVAcs. In the LDPE-ThinVAc, the thermal seams were made using a desktop thermal sealer in the monofilament TPU-ThinVAc. The desktop thermal sealer could not be used in the multi-filament design due to space limitations between the filaments. As a solution, the multi-filament seals were made using an electric iron [47]. The tip of the electric iron was used to trace the thermal seals along the TPU fabric strips. A Polytetrafluoroethylene (PTFE) strip was placed between the iron tip and the TPU strips to prevent it from burning up during the sealing process.

It was observed in initial testing that the vacuum channel collapsed during actuation, negatively affecting the contraction and the force. Therefore, a manifold design was used to connect to the vacuum source. Two vacuum manifolds were designed with three- and five-channels. PU and flexible latex tubes were used to create the manifolds (see Fig. 3.6 a)). Thermal sealing integrated the vacuum line manifold and springs into the multi-filament structure. Like the monofilament design, cyanoacrylate glue was used to seal the vacuum connections, and grommets provided attachment points at the top and bottom. Fig. 3.6 b) depicts the completed 3- and 5-multiple filament actuators.

3.4 Low-profile Vacuum Actuator (LPVAc)

This section presents the concept, design details, and fabrication process of a novel low-profile vacuum actuator (LPVAc). The proposed actuator is designed to be low-

profile to obtain the desired characteristics for soft contractile actuators suited for wearable soft assistive exosuits. This design contrasts with the ThinVAc design by replacing the springs with a circular footing, with an obround-shaped helical spring to minimize the height of the actuator and achieve a low-profile actuator while retaining the flexibility and the origami-inspired vacuum-driven contractile actuator properties (see Fig. 3.7). Similar to the standard helical spring used in the ThinVAc, the obround-shaped spring acts as a skeleton framework that keeps the ThinVAc's cross-section intact during the collapse. The LPVAc may longitudinally contract without collapsing into itself by keeping the cross-sectional area constant throughout the evacuation of the internal air volume. The obround-shaped spring permits only a longitudinal structure collapse, allowing the ThinVAc to function as a contractile actuator. This collapse would allow the LPVAc to be better integrated into wearable exosuit designs with minimum interference and discomfort.

The two major components of the LPVAc are the low-profile spring that serves as the skeleton framework and the thin film pouch. An obround-shaped low-profile spring is selected, where the width is significantly larger than the height. This spring is modeled after a common loading spring found on a rifle magazine. This low-profile spring may be made using standard methods, such as winding around a rectangular block and heat treatment to program in the desired form. Due to their simplicity of fabrication, galvanized iron (GI) and mild steel (MS) were chosen for the prototype spring manufacturing. Fig. 3.8 depicts the dimensions of the manufactured low-profile spring and the fabricated actuator.

The low-profile nature of the proposed actuator will be based on the width and the height of the obround spring. Hence, this property can be considered $Low - Profileness = Width/Height$. Three variants of the proposed obround-shaped spring were fabricated. Table 3.3 summarizes their details.

Low-density polyethylene (LDPE) film was chosen to produce the inextensible, thin-walled pouch based on prior success [72, 75], widespread off-the-shelf availabil-

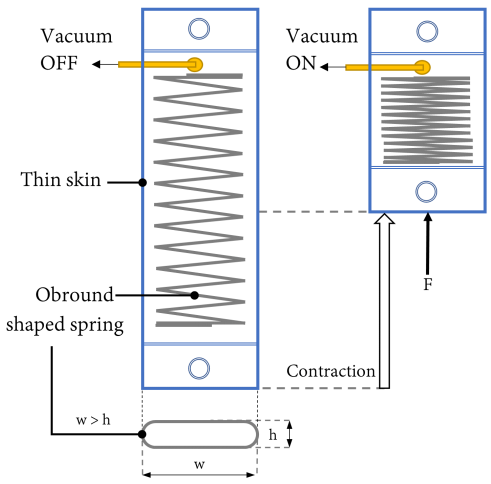

Fig. 3.7: Concept of the proposed low-profile vacuum actuator (LPVAc).

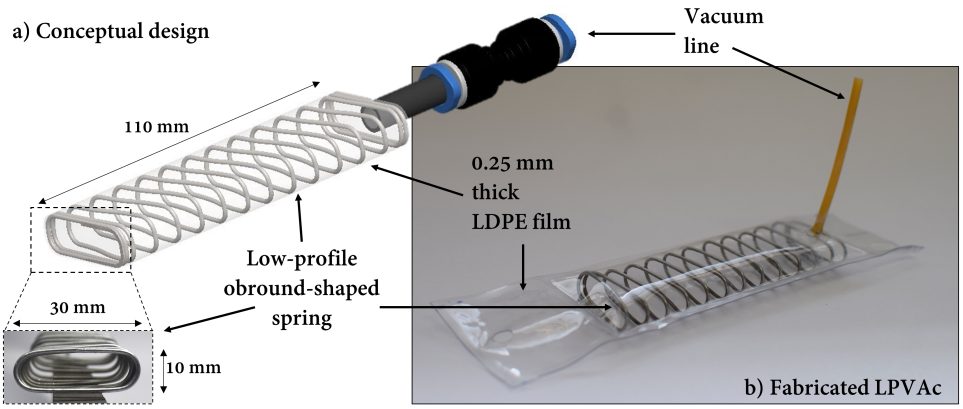

Fig. 3.8: Conceptual design of the LPVAc and the fabricated actuator.

ity, and ease of fabrication via thermal sealing. Rectangular film strips were cut to make the bag. The strip length was estimated to account for the spring length of 110 mm, the actuator height of 10 mm, warping when producing the thermal seals, and the additional adjustable length for attachments (minimum total length: 110 mm). Preliminary tests were conducted on various film thicknesses to determine which was best suited. Low-thickness film trials revealed issues with thermal seal maintenance, leakage owing to imperfections/damages on the film surface, damage from contact with the spring, and trouble connecting tubing to the actuator. As a result, a 0.25 mm thick LDPE film was chosen for actuator testing. The main steps of fabricating the proposed LPVAc are described in Fig. 3.9. The fabricated LPVAc weighed 14 g.

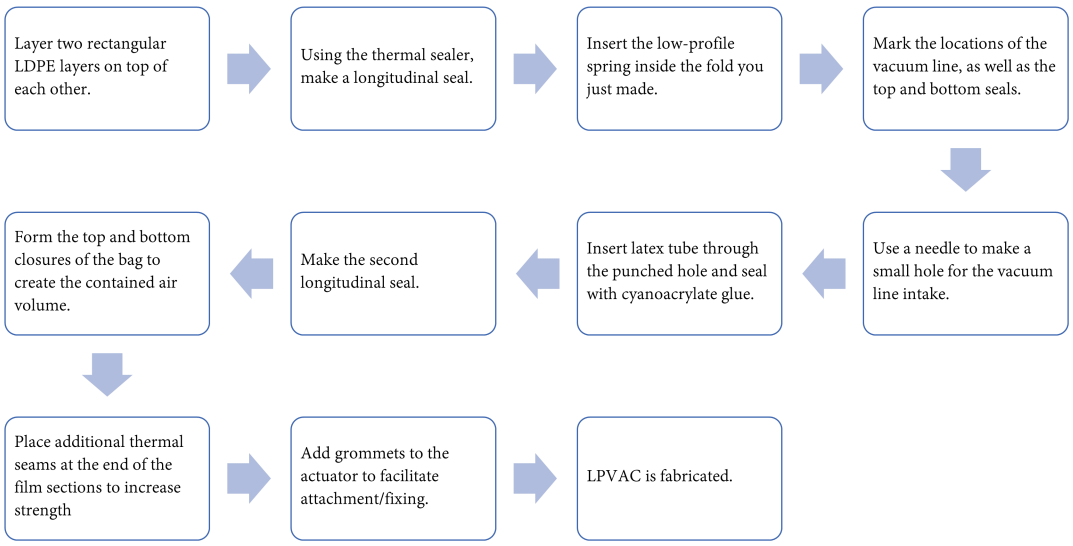

Fig. 3.9: The main steps of fabricating the proposed LPVAc.

TABLE 3.3: The main parameters of the fabricated LPVAcs

Spring footing shape	Obround		
Wire materials	Galvanized iron (GI) & Mild steel (MS)		
Wire diameter (mm)	1.2 mm		
Spring length (mm)	110		
Turns/length	11 turns/100 mm		
LDPE film thickness	0.25 mm		
Finished actuator weight	14 g		
	Spring A	Spring B	Spring C
W x H (mm)	30 x 15	30 x 10	40 x 10
Cross-section area (mm^2)	402	279	379
W/H ratio	2	3	4

3.4.1 Integrated sensing for the LPVAc

A limitation in most modern soft robotic actuators is the absence of proprioceptive sensing. In contrast to rigid actuation options that readily come with integrated position feedback solutions, soft robotic systems lag in integrated sensing solutions. One reason for this limitation is that incorporating sensing mechanisms into the actuator tends to negatively affect the desired motion/force of the soft actuator. Hence, for better-integrated sensing with minimal effect on the actuator, there is a need to utilize the change in properties inherent to the soft actuator for obtaining sensory feedback.

The proposed LPVAc utilizes a metallic spring, which undergoes longitudinal compression during actuation. The inductance measured across the top and bottom of a metallic spring is dependent on its length [88]. Hence, the (compressed) length of the LPVAc during actuation can be estimated by measuring this inductance. This phenomenon is employed to develop an integrated displacement sensing solution for the LPVAc.

When a capacitor and an inductor are connected in parallel, they create a parallel LC circuit, as shown in Fig. 3.10. Such a circuit is called an oscillatory or LC tank circuit. The values of L and C will determine the oscillation frequency. Here, the inductive reactance increases, and the capacitive reactance decreases, with increasing frequency [122].

The frequency at which both the inductive and capacitive reactances are equal is the resonant frequency (f_{Res}) [122]. The resonant frequency f_{res} is given by;

$$f_{res} = \frac{1}{2\pi\sqrt{LC}} \tag{3.1}$$

Here, the inductance L is in Henrys [H], the capacitance C is in Farads [F], and the resonance frequency f_{Res} is in Hertz [Hz].

A commercially available inductance-to-digital-converter module (LDC 1614, Texas Instruments, USA) measured the spring inductance. The LDC1614 schematic and its module are shown in Fig. 3.11. Table 3.4 describes the features of the LDC1614 module.

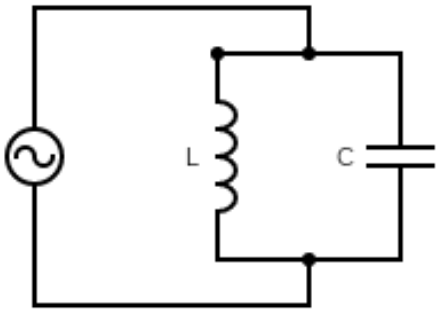

Fig. 3.10: A parallel LC tank circuit.

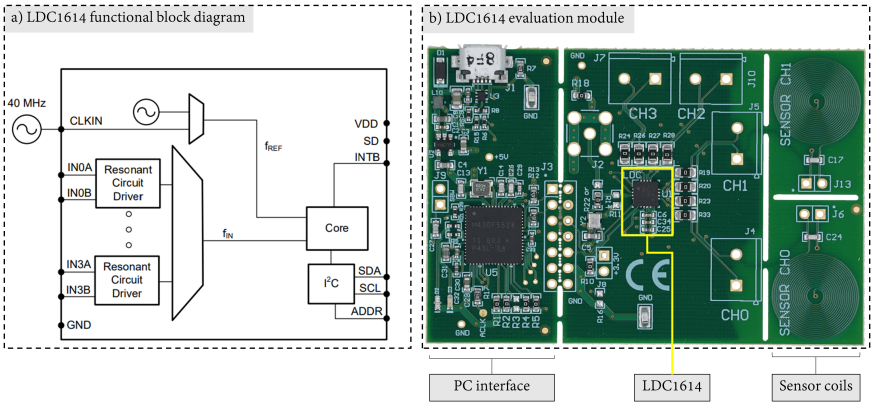

Fig. 3.11: LDC1614 functional block diagram and module [123].

A capacitor was connected across the top and bottom of the spring to create a parallel LC tank to measure the spring inductance using the LDC1614 module. The LDC1614 module measures the LC tank's resonant frequency (f_{res}). The output from the LDC module is given as [123];

$$\frac{DATA}{2^{28}} = \frac{f_{res}}{f_{ref}} \tag{3.2}$$

Here, $DATA$ is the raw output from the LDC module given as the ratio of the circuit resonant frequency f_{res} to the reference frequency f_{Res}.

The capacitor C was selected as 1 nF, and the reference frequency f_{ref} was 43 MHz. Hence, by the combination of eq. 3.1 and eq. 3.2, measured inductance L (in μH)can be simplified as:

$$L\,[\mu H] = \frac{9.69}{DATA^2}\,10^6 \tag{3.3}$$

A thin, flexible conductive thread was soldered to the top and the bottom ends of the Obround-shaped spring. Then this thin wire was drawn through the seam of the actuator, and the capacitor was connected at the top of the LPVAc as shown in Fig. 3.12. Then this parallel LC tank was connected to channel 1 of the LDC module.

TABLE 3.4: The main features available on the LDC1614 module [123].

Parameter	Value/Type
No. of channels	4
Resolution	28 bit
Communication	I2C/USB

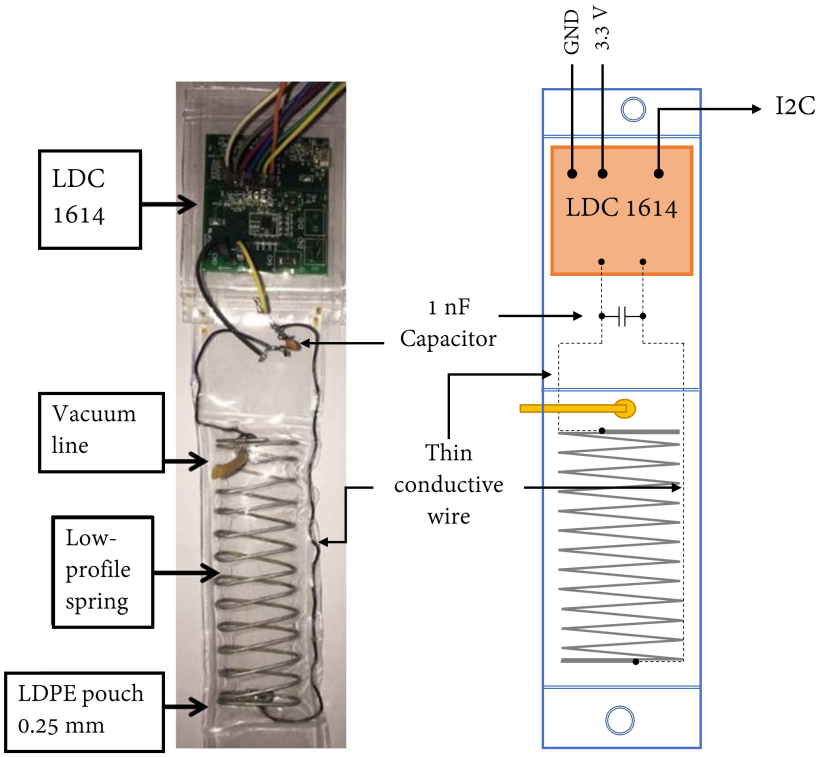

Fig. 3.12: LPVAc with the integrated inductive displacement sensing module.

Further to the fabrication process described earlier, an extra pouch was created on the top of the LPVAc to house the LDC module (see Fig. 3.12)

3.5 Summary

Two main categories of novel, vacuum-driven, soft contractile linear actuators are proposed. The primary novelty lies in developing thin, vacuum-driven low-profile actuators for soft robotic applications. The proposed actuators use inextensible yet flexible, thin-film materials to create enclosed volumes. The cross-sectional shape is maintained throughout the actuation using springs that act like collapsible skeletal structures. Upon evacuation of the enclosed air volume, the actuator collapses guided along the spring. The presence of the spring limits the collapse of the structure to the longitudinal axis.

This section presented two soft actuator designs with thin and low-profile cross-

sections: ThinVAc and LPVAc. The ThinVAc uses a thin-film skin (LDPE or TPU) enclosing a small diameter (6 mm OD) stainless steel spring. The LPVAc uses an LDPE skin enclosing a specially designed, obround-shaped low-profile ($30\,mm \times 10\,mm$) spring (made from GI and MS). The ThinVAc monofilament was combined to create multifilament actuators to scale the force. The use of differently proportioned low-profile springs allowed force scaling of the LPVAc. Table 3.5 compares the developed mono-and multifilament actuators. An integrated sensing solution for the LPVAc was developed based on inductive sensing.

TABLE 3.5: A comparison of the developed actuators.

Actuator	Weight $[g]$	X-section area $[mm^2]$	length $[mm]$	Volume $[ml]$
LDPEThinVAc 50mm	0.75	28.3	50	1.4
LDPEThinVAc 100mm	0.92	28.3	100	2.8
LDPEThinVAc 200mm	1.24	28.3	200	5.7
TPU-ThinVAc 200mm	1.99	28.3	200	5.7
LPVAc-A	14	402	110	44.2
LPVAc-B	14	278	110	30.6
LPVAc-C	14	378	110	41.6
LDPEThinVAc 5x100mm	9	225	100	14.2
LDPEThinVAc 15x100mm	19	875	100	42.5
LDPEThinVAc 5x200mm	10	225	200	28.3
LDPEThinVAc 10x200mm	18	600	200	56.6
TPUThinVAc 3x200mm	4.94	86	200	17
TPUThinVAc 5x200mm	7.93	145	200	28.3

CHAPTER 4

ACTUATOR PERFORMANCE EVALUATION

This chapter presents the experimental characterizations conducted to establish the performance of the proposed soft linear contractile actuators. Isobaric, isotonic, and isometric performance characterization of the ThinVAc and the LPVAc were conducted. Further, the inductive sensor integrated into the LPVAc was calibrated, and its performance characteristics were identified. Later, these actuators were used in exosuit applications, and those experiments and their analysis are presented in chapter 6.

For the following experiments, a 21-liter vacuum chamber evacuated by a single-stage vacuum pump (FY-1C-N, Value Vacuum Technology) was used as the vacuum source. The general layout of the experimental setup is shown in Fig. 4.1. The vacuum pressures mentioned in the following experiments and analysis are given as either absolute pressure values [x kPa (abs.); where 0 kPa indicates perfect vacuum] or differential pressure to the atmospheric pressure.

4.1 Performance evaluation of the ThinVAc

Isometric, isotonic/isobaric performance analysis was conducted for both types of ThinVAc. The following section describes this experimental evaluation process and

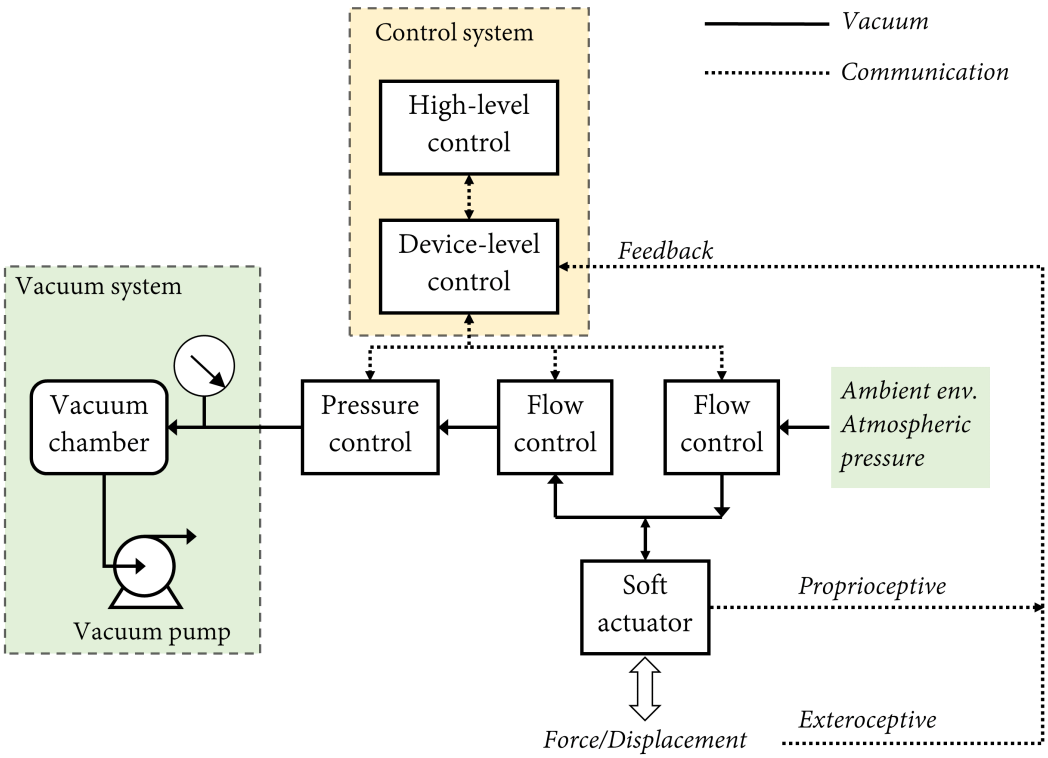

Fig. 4.1: The general layout of the experimental setup used in the experimental analysis.

its results. The experiments were conducted for both the LDPE- and TPU-based ThinVAcs. 50, 100, 200 mm length LDPE-ThinVAcs, and 200 mm TPU-ThinVAc monofilaments, and the 100 mm x 5, 100 mm x 15, 200 mm x 5, and 200 mm x 10 LDPE-ThinVAc, and 200 mm x 3, and 200 mm x 5 TPU-ThinVAc multi-filament structures were experimentally evaluated.

The experimental setup depicted in Fig. 4.2 a) was employed to evaluate the produced blocked force based on the vacuum pressure applied. A ThinVAc with a constant length was installed on a universal testing machine (M350- 10AT, Testometric), and the isometric force was measured using a load cell. The isotonic and isobaric contraction of the ThinVAc was assessed using the setup in Fig. 4.2 b). The contraction was captured through a digital camera and estimated offline using ImageJ software.

4.1.1 Contraction performance of the ThinVAc

The no-load contraction of the ThinVAcs are presented in this section. The contraction of the ThinVAcs' are shown in Fig. 4.3. Fig. 4.3 a) shows that LDPE-ThinVAcs have good scalability with varied actuator length. The TPU-ThinVAc shows higher range of contraction compared to the LDPE-ThinVAcs. Fig. 4.3 b) shows that the LDPE-ThinVAc's contraction as a ratio of length is similar, and higher compared to that of the TPU-ThinVAc. A summary of the ThinVAc maximum contraction performance at 20 kPa (abs.) is given in Table 4.1.

4.1.2 Force-displacement characteristics of the ThinVAc

The force-displacement performance of the developed ThinVAcs is presented in this section. Varying loads were attached to the experimental setup shown in Fig. 4.2 b). Fig. 4.4 presents the force-displacement characteristics of the LDPE-ThinVAcs and the TPU-ThinVAc. The force-displacement performance is linear in the 0 - 2 N range for both types ThinVAc.

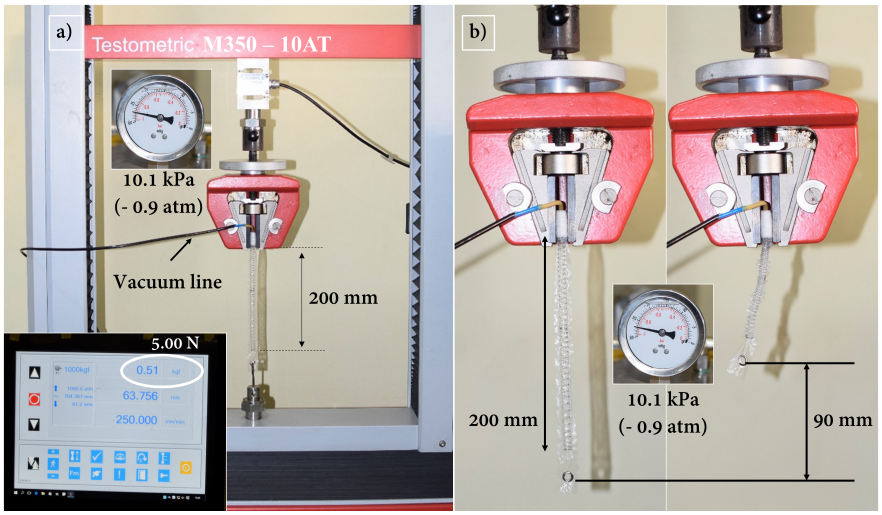

Fig. 4.2: The experimental test setups used to characterize the ThinVAc. a) Maximum force evaluation and b) displacement evaluation.

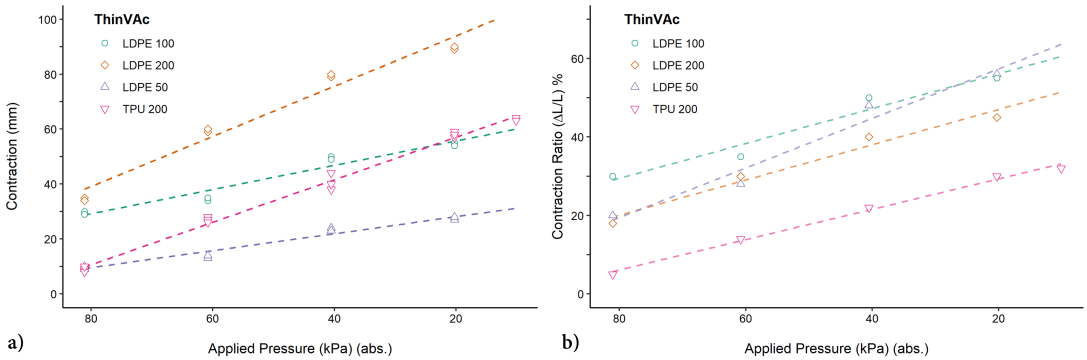

Fig. 4.3: No-load contraction of the ThinVAcs. a) Contraction in length [mm], b) Contraction as a ratio $[\Delta L/L]$.

TABLE 4.1: ThinVAc no-load contraction performance at 20 kPA (abs.)

ThinVAc		Max. Contraction	
Type	Length	[mm]	[%]
LDPE	50	30	60
LDPE	100	55	55
LDPE	200	90	45
TPU	200	60	30

It can be observed that the best method to analyze the ThinVAc contraction performance is by comparing the contraction ratio (CR) $[\Delta L/L]$. The CR of the LDPE-ThinVAc with varying load is shown in Fig. 4.5. Fig. 4.5 indicates that the CR of the LDPE-ThinVAc is similar over the different lengths, and hence, it can be used as a length-independent measure of its performance.

Hence, the CR is used as a measure to compare the contraction performance of LDPE and TPU-ThinVAc. This comparison is shown in Fig. 4.6. LDPE-ThinVAc presents higher contraction performance than the TPU-ThinVAc. This difference in contraction performance can be attributed to the higher thickness and stiffness of the TPU fabric compared to the LDPE film.

4.1.3 Blocked force performance of the ThinVAc

The maximum blocked force characteristics of the ThinVAcs are shown in Fig. 4.7. This isometric characterization was conducted using the experimental setup described in Fig. 4.2 a). Fig. 4.7 presents the regression fit functions produced using the least-squares technique for each monofilament actuator's maximum blocked force performance. In this equation, x is the applied differential pressure in kPa, and y denotes the estimated blocked force in N. ThinVAc maximum blocked force shows a linear increase with an applied pressure differential. The TPU-ThinVAc shows lower blocked force compared to LDPE-ThinVAc of the same length. Table 4.2 summarizes the performance characteristics of the monofilament ThinVAc.

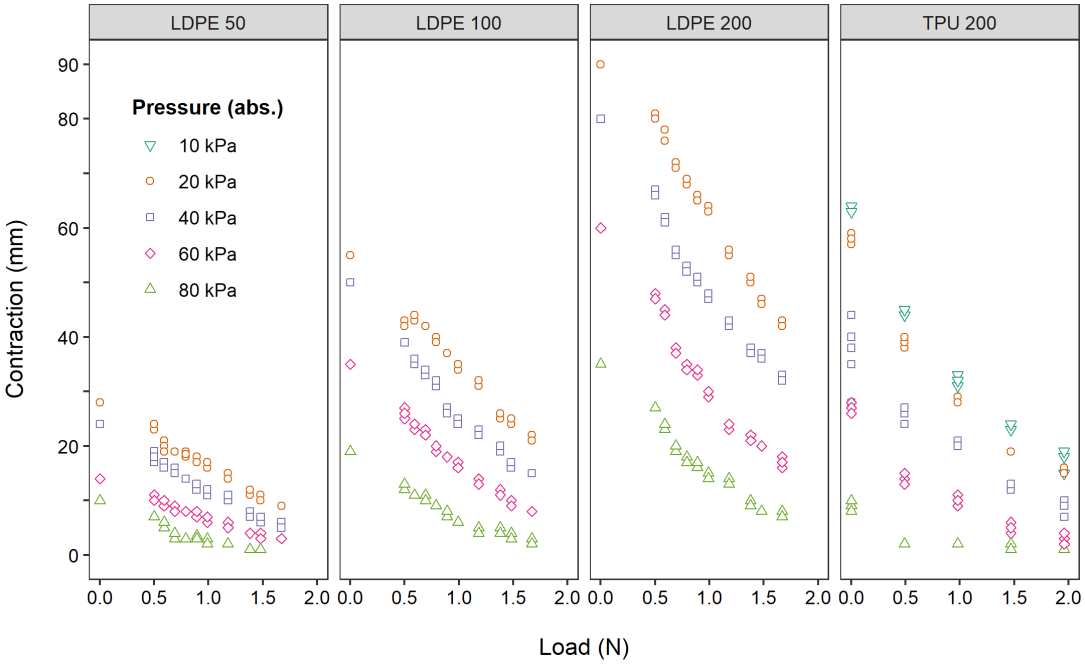

Fig. 4.4: ThinVAc force-displacement characteristics.

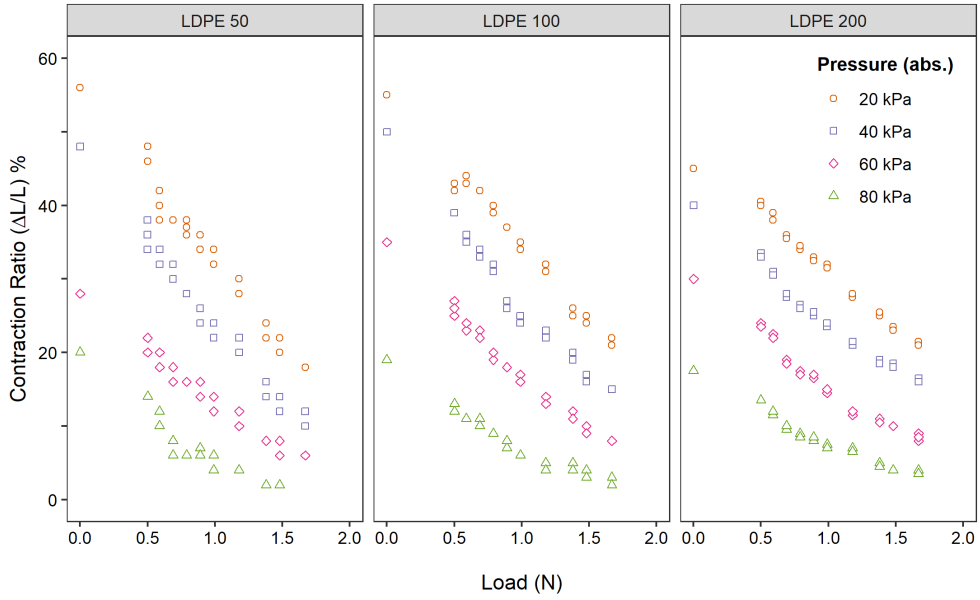

Fig. 4.5: LDPE-ThinVAc force-displacement characteristics (CR).

4.1.4 Applications of the proposed ThinVAc

This section describes experimental studies carried out to establish the applicability of the proposed ThinVAc in soft robotic applications. To conveniently attach the ThinVAc to the test structures, a 3D-printed attachment was adopted. Rubber bands/zip ties secured the LDPE tube to the spring's top and bottom attachment.

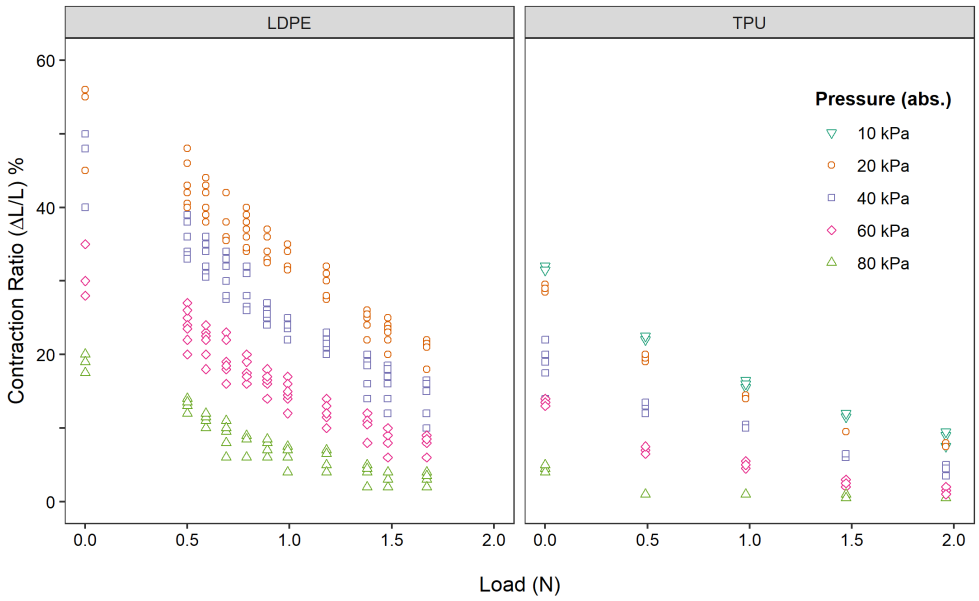

Fig. 4.6: ThinVAc force-displacement characteristics (CR).

TABLE 4.2: A summary of characteristics of the monofilament ThinVAcs.

Actuator type	LDPE		TPU	
Spring length [mm]	50	100	200	200
Actuator weight [g]	0.75	0.92	1.24	2
Max. contraction [mm]	30	55	90	60
Max. contraction ratio [%]	60	55	45	30
Max. force [N] at 10 kPa (abs.)	3.1	4.3	5.2	4.5
Max. stress [kPa] at 10 kPa (abs.)	87.2	120.9	146.2	126.8
Max. force-to-weight ratio	421.8	476.9	427.9	229.6

4.1.4.1 Actuation of soft structures

The ThinVAc's intrinsic flexibility enables for simple attachment around complex-shaped structures. An LDPE-ThinVAc is used to actuate a soft toy to illustrate this capability. As shown in Fig. 4.8, a 100 mm LDPE-ThinVAc monofilament actuator is connected to each arm of a soft toy. Within 0.24 s of activation, the ThinVAc lifts the soft toy's arm. The ThinVAc monofilament readily adapts to the contour of the soft toy's arm, as seen in Fig. 4.8. The monofilament can also be incorporated inside for discrete actuation without reducing the toy's softness.

4.1.4.2 Actuation of a compliant gripper

A compliant gripper enables precise gripping of relatively small items while also providing the benefits of inherent compliance. Including a soft actuator can increase the gripper's compliance and safety even further. As illustrated in Fig. 4.9, a 50 mm ThinVAc is incorporated as the actuator in a compliant gripper 3D-printed from PLA.

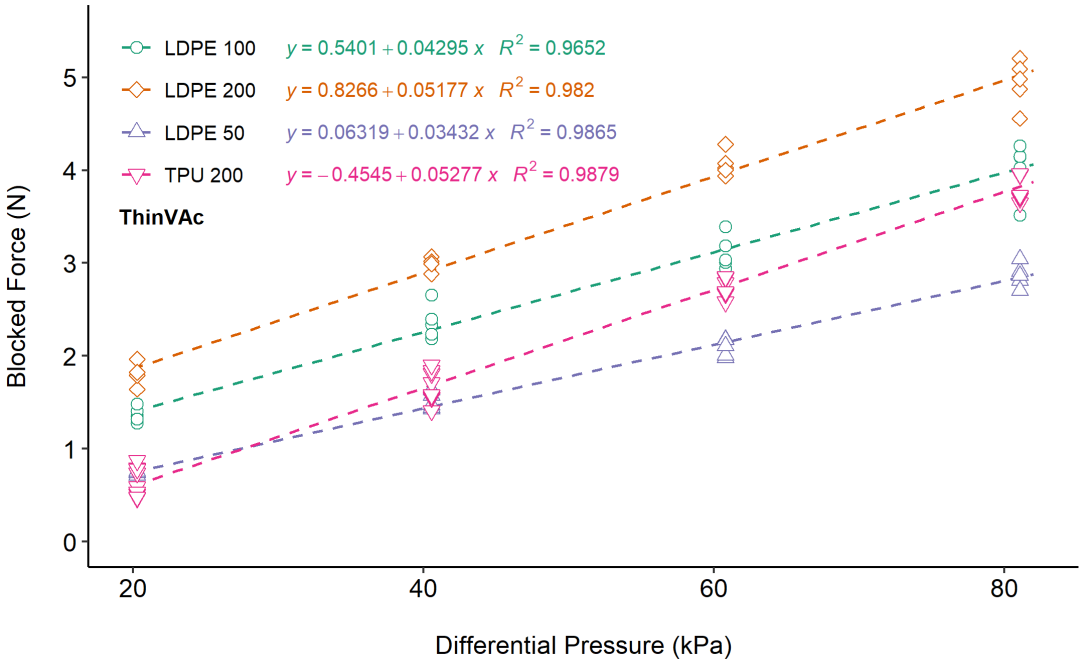

Fig. 4.7: The maximum blocked force performance of the ThinVAc.

The gripper's unactuated finger opening is 40 mm. The actuation signal is a vacuum pressure step input of 20 kPa (abs.). A tripod-mounted digital camera captures the tip movement at 30 frames per second. The movement of the tip is post-analyzed using motion analysis software to get the tip trajectory (Kinovea, ver. 0.8.15). As depicted in Fig. 4.10, the tip of the top finger moves downward 17 mm in 0.33 s, exhibiting an over-damped time response.

4.1.5 Blocked force performance of multi-filament ThinVAc

The experimental evaluation of the blocked force characteristics of the multi-filament actuators is presented in this section. The multiple combinations of the ThinVAcs described in sections 3.3.2 and 3.3.4 are used for the experimental evaluation here.

4.1.5.1 Blocked force performance: LDPE-ThinVAc multi-filament actuators

The blocked force performance of the LDPE-ThinVAc multi-filaments was experimentally evaluated using an isometric test setup (see Fig. 4.2 a)). Fig. 4.11 illustrates the observed blocked force performance of the multi-filament actuators. The graph depicts the regression fit functions produced using the least-squares technique for each multi-filament actuator's maximum blocked force performance. In this equation, x is the applied differential pressure in kPa, and y denotes the estimated blocked force in N. When the number of ThinVAc in the 100 mm multi-filament actuator is tripled from 5 to 15, the blocked force increases by a factor of 2.77. Similarly, increasing the number of ThinVAc in the 200 mm multi-filament actuator from 5 to 10 increases the blocked force by a ratio of 1.87. The behavior seen in Fig. 4.11 demonstrates strong linear-

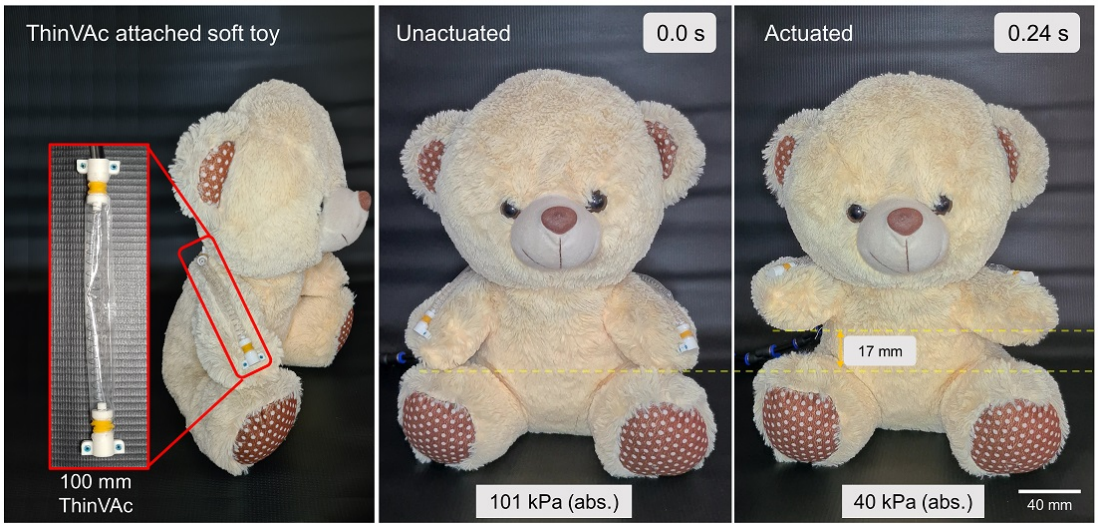

Fig. 4.8: Actuation of a soft toy using a 100 mm LDPE-ThinVAc.

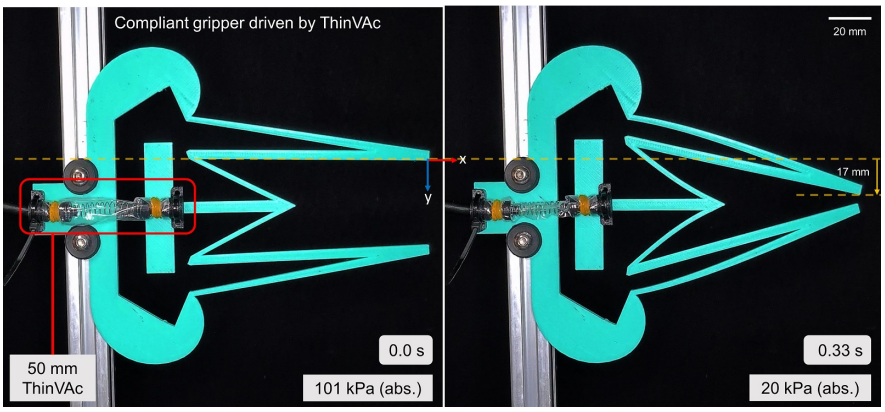

Fig. 4.9: Actuation of a compliant gripper by the ThinVAc.

ity and scalability between actuator combinations. This scalability will become useful in the design of multi-filament actuators for soft robotic applications. The computed force-to-weight ratios for the multi-filament actuator designs (see Table 4.3) indicate promising results for successful implementation in soft robotic applications requiring low-weight, high-force, yet low-profile actuators. It demonstrates that multi-filament combinations with more filaments have higher force-to-weight ratios.

Conventional pneumatic artificial muscles of identical sizes have difficulty operating unless employed in a linear configuration. The ThinVAc monofilaments are inherently highly flexible. This property allows the ThinVAc multi-filament structures to be actuated even when bent or in deformed orientations (See Fig. 4.12). This flexibility in operation will be an advantage when integrating with space-limited wearable systems that follow body contours. As shown in Fig. 4.13, the LDPE-ThinVAc multi-filament actuators provide good contraction performance comparable to the monofilaments.

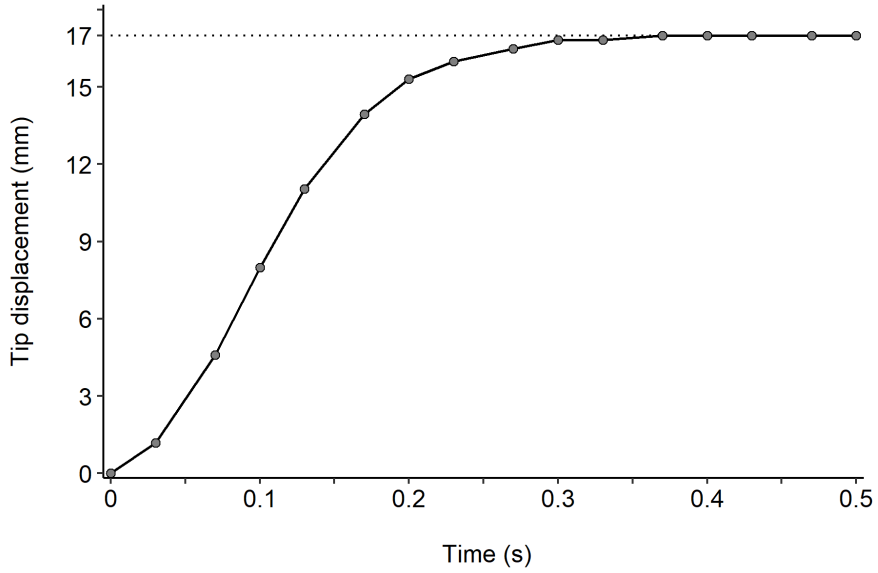

Fig. 4.10: Time domain response of the compliant gripper tip motion.

TABLE 4.3: A summary of LDPE-ThinVAc multi-filament actuator performance

	Max. blocked Force (N)	Weight (g)	Force-to-Weight ratio	Crosssection area (mm^2)	Max. Stress (kPa)
100 mm x 5	19.13	9	217	225	85.02
100 mm x 15	54.04	19	291	875	61.76
200 mm x 5	25.11	10	257	225	111.6
200 mm x 10	48.06	18	273	600	80.1

4.1.5.2 Blocked force performance: TPU-ThinVAc multi-filament actuators

This section presents the isometric or blocked force performance of the TPU-ThinVAc multi-filament actuators. The same experimental setup used to evaluate the LDPE-ThinVAc was employed here. The maximum blocked forces delivered by the 3- and 5-filament TPU-ThinVAcs were 8 and 14 N, respectively. This force is equivalent to lifting 156 times or 180 times their self-weight. The experimental results indicate a linear relationship between differential pressure and the blocked force, similar to the TPU-ThinVAc monofilaments. Like the TPU-ThinVAc monofilament, the maximum blocked forces vary linearly with the applied vacuum pressure differential (see Fig. 4.14).

4.2 Performance evaluation of the LPVAc

4.2.1 Spring properties

The skeletal structure of the LPVAc comprises a helical shape of a novel footing. Initially, it was needed to evaluate whether the behavior of this obround-shaped spring was similar to that of conventional springs. Contemporary literature has mentioned

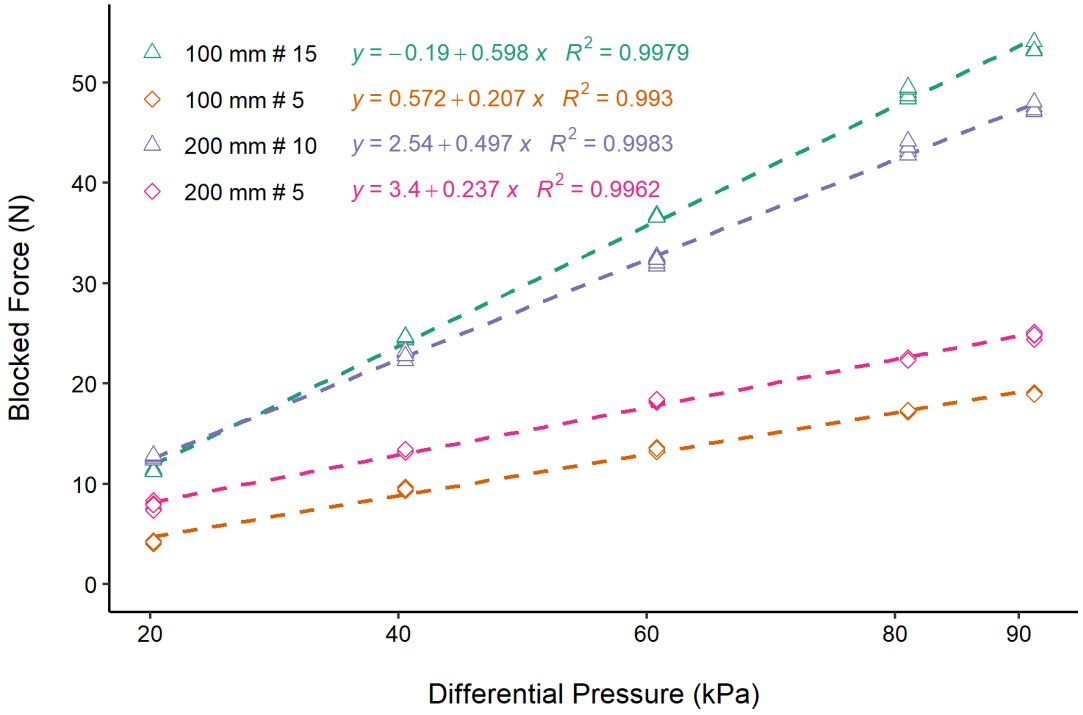

Fig. 4.11: The blocked force characteristics of the LDPE-ThinVAc multi-filament actuators.

that the deflection of the spring under axial load and the stresses developed within might be affected by the obround shape [124]. Hence, the force-displacement characteristics of the obround-shaped spring were experimentally evaluated. Fig. 4.15 presents the experimental results. The relationship between force and displacement was observed to be linear. Hence, it was acceptable to assume that the obround-shaped spring behaves under Hooke's law, $F_{spring} = -kx$, where x is the spring displacement. The spring coefficients of the obround-shaped springs were estimated from the experimental results as mild steel spring: 127 N/m and galvanized iron spring: 136 N/m.

4.2.2 Contraction performance of the LPVAc

The experimental test setup illustrated in Fig. 4.16 was used to determine the isometric, isotonic, and isobaric properties of the LPVAc.The isobaric (no-load) and isotonic contraction performance characterization was conducted using the test setup in Fig. 4.16 b).

The proposed LPVAc's contraction performance was characterized using the experimental setup illustrated in Fig. 4.16 b). The isotonic contraction performance was evaluated with a fixed connected load and varying vacuum pressure for GI and MS spring-based LPVAcs. Fig. 4.17 a) shows the contraction of the LPVAc under an attached load of 200 g at 20 kPa (abs.). The contraction performance of the LPVAc at the same load is shown in 4.17 b). The experimental results demonstrate a linear relationship between displacement and applied vacuum pressure. Compared to the

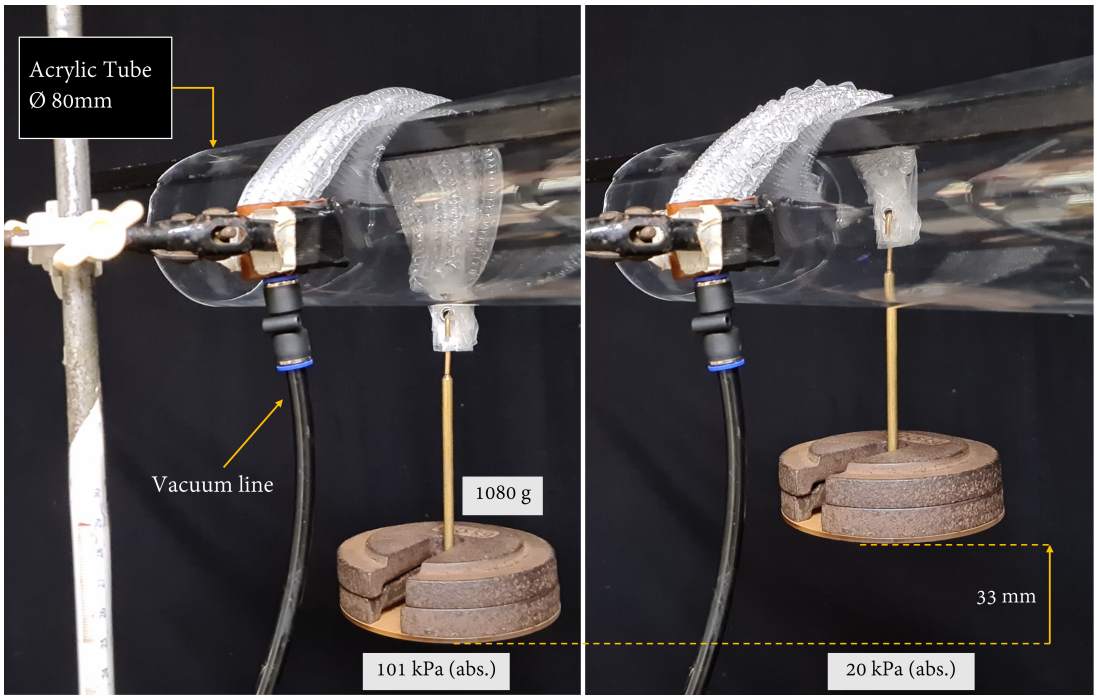

Fig. 4.12: The LDPE-ThinVAc multi-filament muscle actuator can be actuated while deformed. An LDPE-ThinVAc multi-filament actuator made up of ten 200 mm monofilament actuators raise a weight of 10.6 N (1080 g) at 20 kPA (abs.) while being bent.

GI spring-based LPVAc, the MS spring-based actuators demonstrated slightly higher displacement at higher vacuum pressures.

A maximum strain of 65 percent (contraction ratio: 182 percent) was observed at no-load and 20 kPa (abs.) vacuum pressure (see Fig. 4.18).

4.2.3 Force-displacement characteristics of the LPVAc

The proposed LPVAc's force-displacement characteristics were assessed using the experimental setup illustrated in Fig. 4.16 b). MS spring-based LPVAcs were chosen for this experiment due to their higher displacement performance, as illustrated in Fig. 4.17 b). The connected load was adjusted to 20 N, with vacuum pressure ranging from 60 kPa (abs.) to 10 kPa (abs.). Fig. 4.19 demonstrates that the force-displacement characteristics are linear and scalable with increasing load and vacuum pressure, respectively.

4.2.4 Blocked force performance of the LPVAc

The proposed LPVAc's isometric or the maximum blocked force performance was assessed using the experimental setup depicted in Fig. 4.16 a). The LPVAcs were attached to a test load placed on a digital scale and fastened to the test frame. When the LPVAc is activated, this test load is an immovable structure preventing contraction. After the test loads were put on the scale, the digital scale reading was set to zero. Then

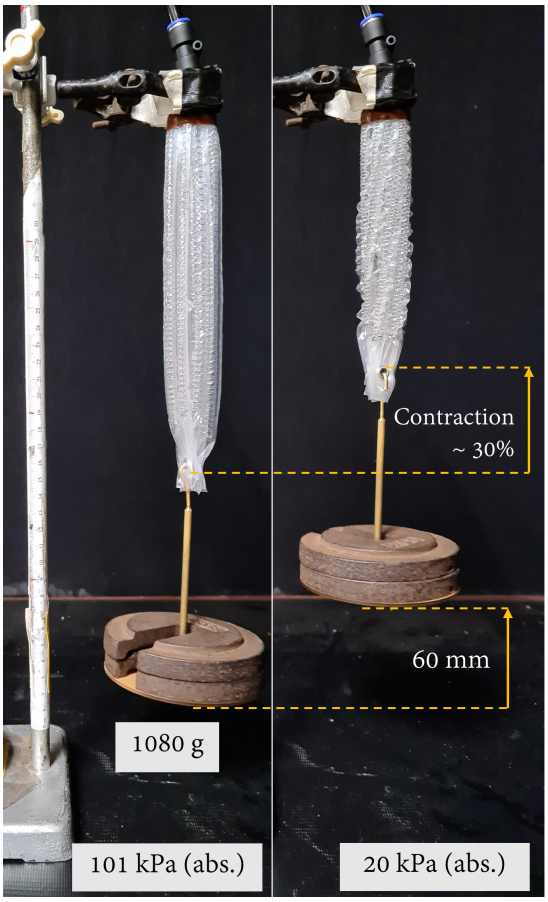

Fig. 4.13: A 200 mm x 10 LDPE-ThinVAc multi-filament actuator lifting a 10.6 N load at 20 kPa (abs.).

the digital scale records the applied blocked force as a negative value once the LPVAc is activated. The maximum value shown here was recorded as the actuator's maximum blocked force. The experimental blocked force data (Fig. 4.20) indicate a linear relationship between blocked force and applied vacuum pressure. The experimental data are shown in Fig. 4.20 corresponds to spring B (see Table 3.3). LPVAc, comprising spring B, produces a maximum blocked force of 32.5 N at 10 kPa (abs.).

4.2.5 Blocked force performance with varying width-to-height ratio

Two more low-profile springs with varied width and height combinations were fabricated to investigate the influence of low-profileness on the blocked force performance of the LPVAc (see Table 3.3). As the W/H ratio increases, the curved surface area of the LPVAc decreases while the flat rectangular area increases. As previously described, the blocked force performance of different spring combinations was evaluated. Table 4.4 shows the blocked force performance of each LPVAc as the W/H ratio is varied.

Fig. 4.21 shows that the LPVAc blocked force is scalable with varying W/H ratios. The blocked force increases with increasing differential pressure as the W/H ratio increases. The increase in the W/H ratio may be considered the cause for the higher blocked force performance. Spring C, which has the most significant W/H ratio

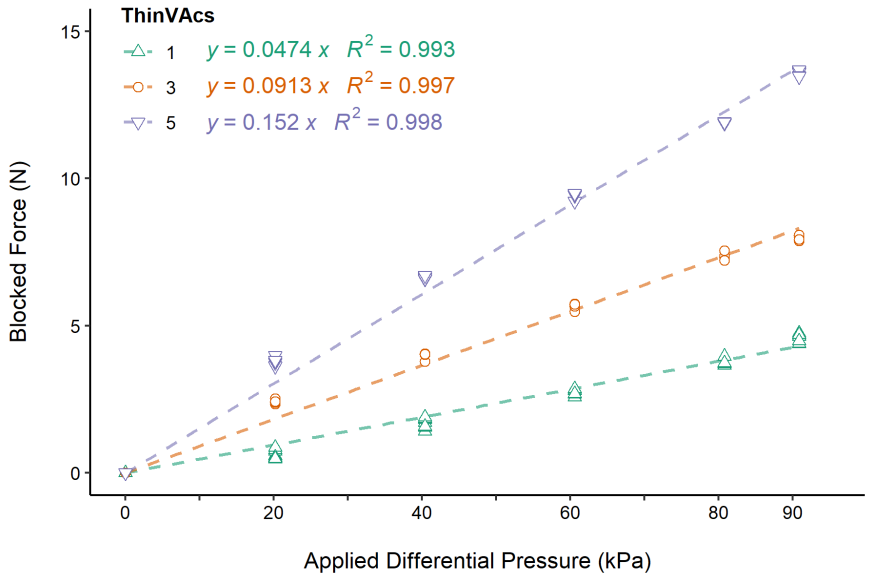

Fig. 4.14: The maximum blocked force performance of the TPU-ThinVAc multi-filament configurations. Monofilament results are given as reference.

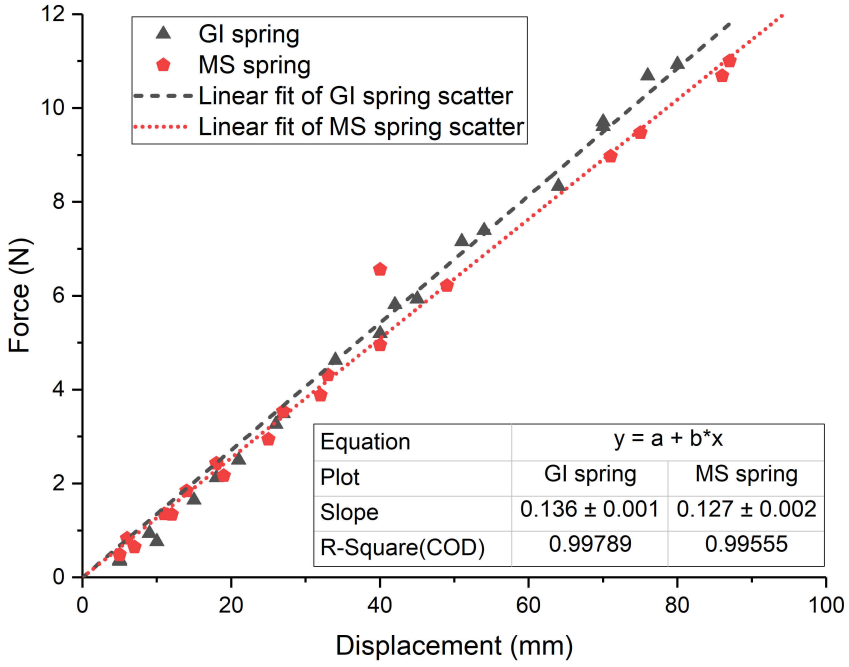

Fig. 4.15: The experimental force-displacement properties of round-shaped low-profile springs made of galvanized iron (GI) and mild steel (MS). The results demonstrate that using a standard helical spring model to describe the behavior of a obround-shaped helical spring is valid.

($W/H = 4$), produces the highest blocked force of 39.05 N at 10 kPa (abs.).

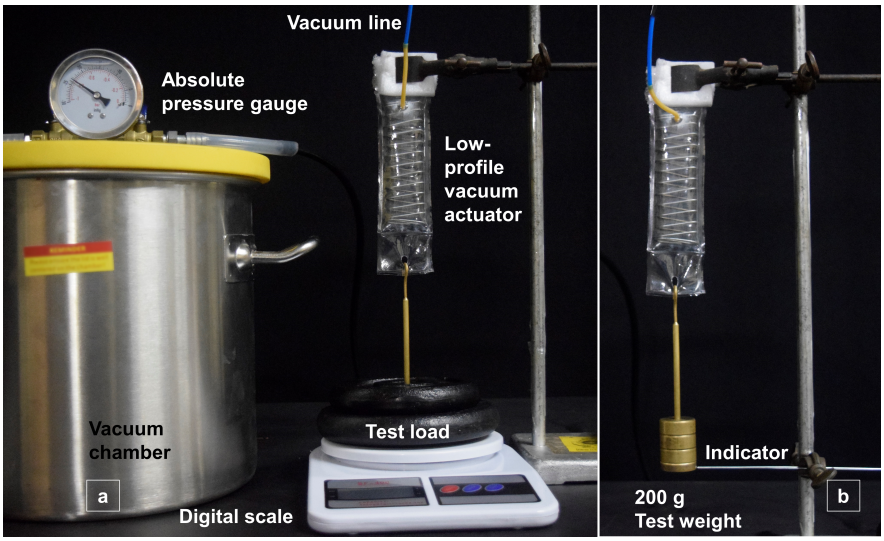

Fig. 4.16: The experimental test setups used to characterize the LPVAc: Maximum force evaluation (a) and displacement evaluation (b).

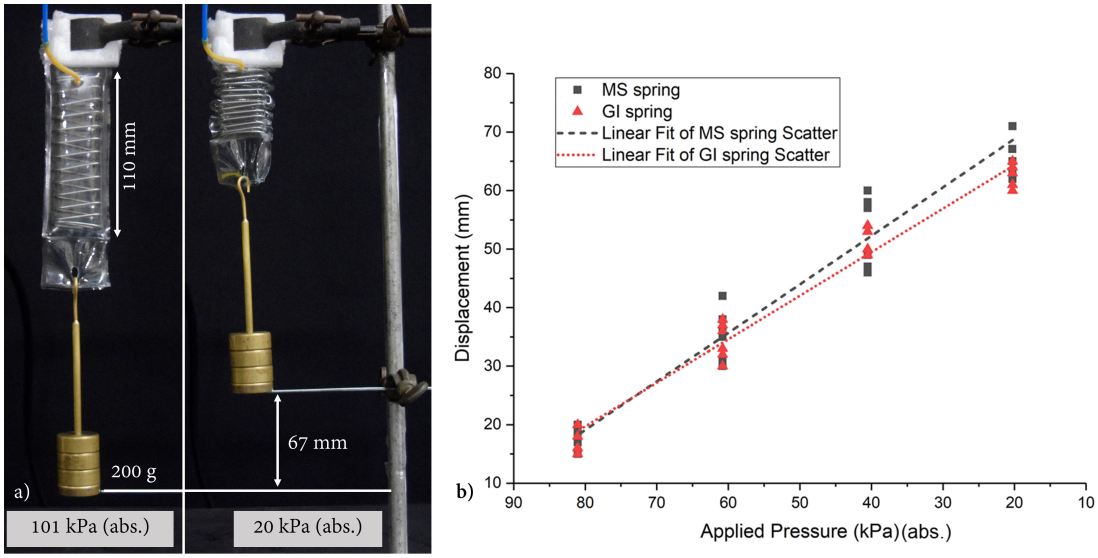

Fig. 4.17: LPVAc contraction performance at 20 KPa. a) The LPVAc lifts a 200 g load by 67 mm (strain 61%) at 20 kPa (abs.). b) The isotonic contraction performance (load: 200g) of the LPVAc (both GI and MS) is linear.

TABLE 4.4: LPVAc blocked force performance with varying W/H ratio

Spring	W/H	Maximum Output Force (N)	Maximum Output Stress (kPa)	Force-to-weight ratio
A	3	32.5	116.68	237
B	2	29.35	73.06	212
C	4	39.05	103.16	285

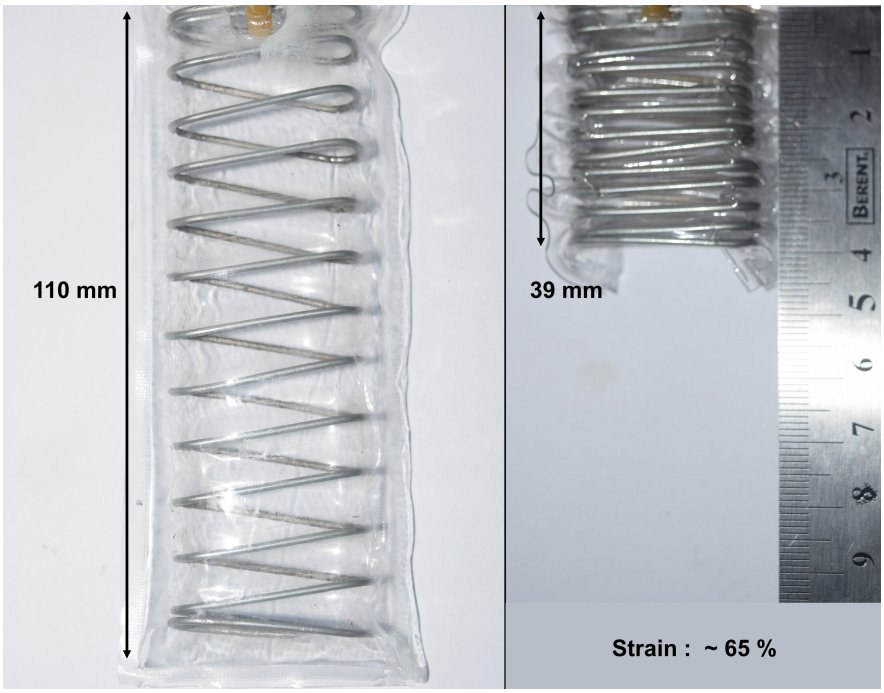

Fig. 4.18: Maximum strain observed: 65% at 20 kPa (abs.).

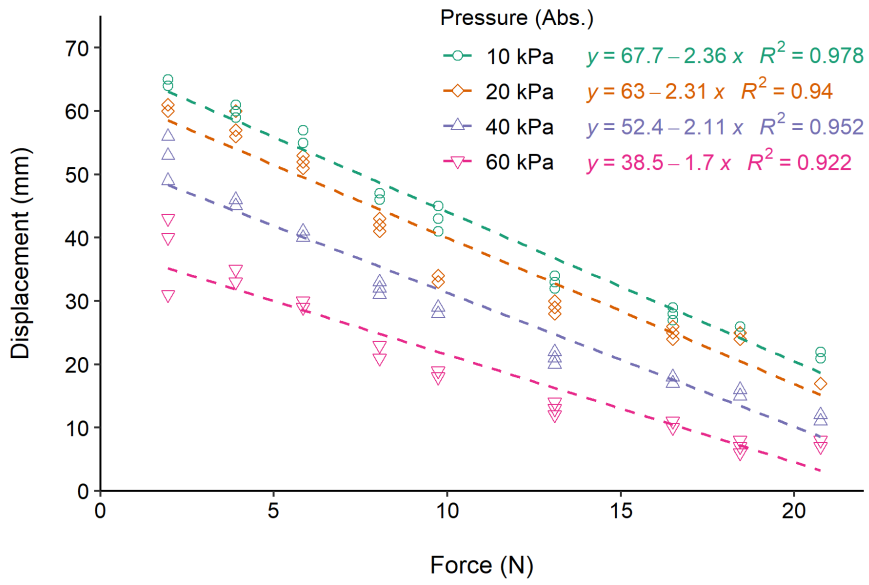

Fig. 4.19: The displacement of the LPVAc with applied load for four vacuum levels is shown. The dashed lines are the linear regression fits produced using the least-squares approach for the experimental values.

4.2.6 Integrated displacement sensor calibration

This section describes the experimental assessment used to derive the sensor equation and its performance characteristics. The test setup described earlier in Fig. 4.16 b) was used for this evaluation, with a test load of 200 g. As the LPVAc was actuated, the spring inductance was measured using the LDC1614 module. No difference in

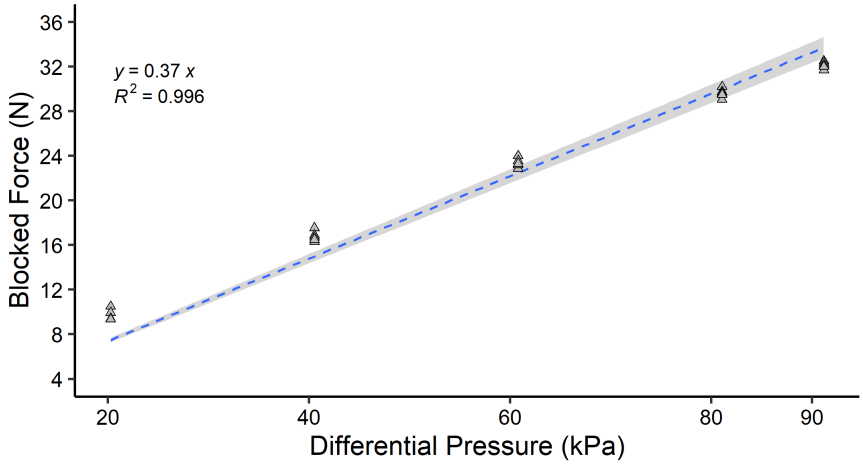

Fig. 4.20: The LPVAc's blocked force performance (using spring B) as the applied differential pressure varies is shown. The colored region represents the 95% confidence interval for the least-squares fit.

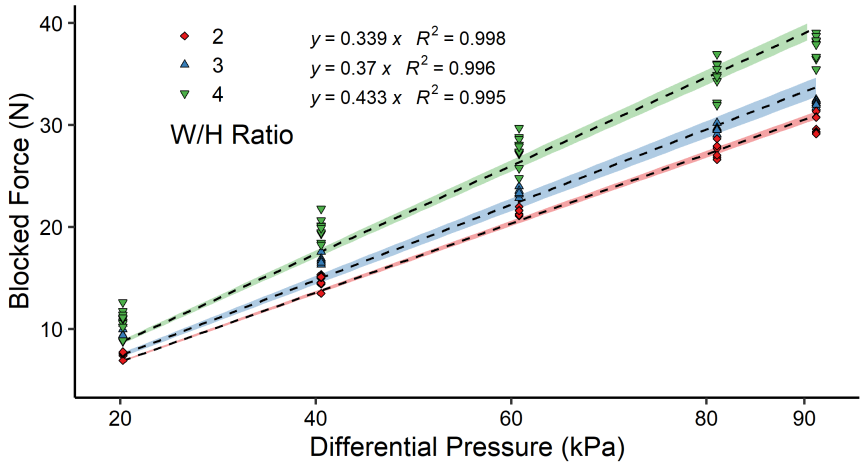

Fig. 4.21: The LPVAc's blocked force performance as the W/H ratio varies. The colored region represents the 95% confidence interval for the least-squares fit.

force or displacement was observed between the LPVAc with the thin wire integrated to enable inductive displacement sensing. Fig. 4.22 depicts the sensor performance. The least-squares approach was used to calculate the relationship between measured spring inductance (L) and actuator displacement (D). As seen in Fig. 4.22, there is a linear relationship between the displacement and the measured inductance, with an R^2 of 0.97.

The computed sensor equation is presented in eq. 4.1, where D is in mm and L is in μH.

$$L = 0.0022\,D\ +\ 0.75 \tag{4.1}$$

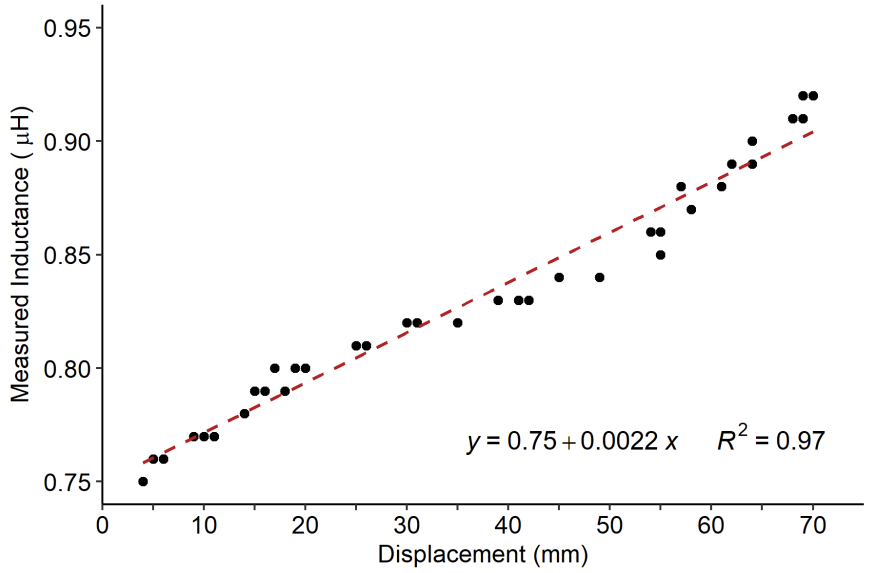

Fig. 4.22: The obtained least-squares fit for the observed inductance vs. actuator displacement.

4.2.7 Characterization of the integrated sensor

4.2.7.1 Hysteresis and repeatability

The LPVAc was activated and released by raising and lowering the vacuum pressure to study the performance of the hysteresis. The same test setup used for the sensor calibration was used here. Fig. 4.23 depicts the sensor's hysteresis performance. The hysteresis seen was calculated to be 1.49 percent.

Repeated measurements at predetermined places were taken to evaluate the sensor's repeatability. The LPVAc was contracted to three preset locations [48 mm, 60 mm, and 72 mm], and readings were collected for 20 iterations at each preset contraction. Fig. 4.24 depicts the fluctuation of sensor output with repeated measurements.

Table 4.5 contains a statistical analysis of these measurements. The sensor exhibits high repeatability, with standard deviations of 2.35 mm, 2.3 mm, and 1.65 mm for each preset position.

TABLE 4.5: Performance measures for repeatability of the integrated sensor

No. of Iterations	Test 1	Test 2	Test 3
	20 *iterations*		
Preset contraction [mm]	72	60	48
Mean sensor reading [mm]	71.9	59.17	46.47
Std. deviation [±mm]	1.65	2.3	2.35
Mean error [mm]	1.9	-0.84	-1.54
Measurements $\leq$ 5 % error [%]	80	75	65
Measurements $\leq$ 10 % error [%]	100	95	95

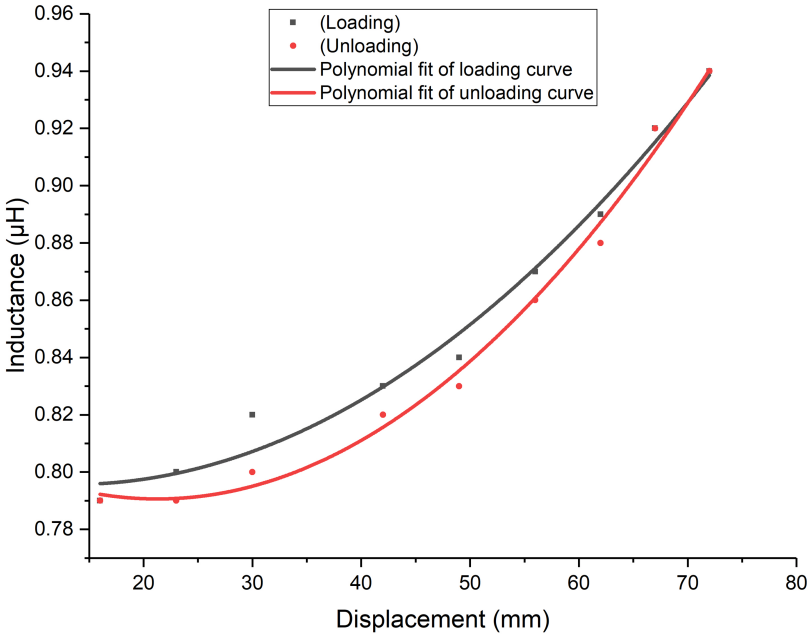

Fig. 4.23: Hysteresis performance of the integrated sensor.

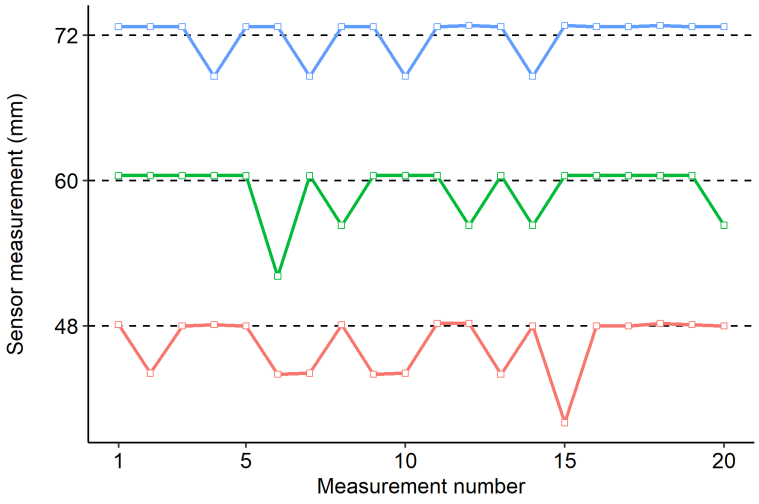

Fig. 4.24: The repeatability performance of the inductive displacement sensor for three preset displacement positions [48, 60, and 72 mm] (n=20).

4.2.7.2 Sensitivity and measurement error

The sensor transfer function describes its sensitivity. The sensor transfer function was obtained earlier in the calibration step (eq. 3.3).Hence, the sensor sensitivity is 0.0022 H/mm (See Fig. 10). Fig. 4.25 depicts the absolute error percentage recorded in sensor feedback. The mean error percentage is 5.24 $\pm$ 2.66 percent. The experimental evaluation found no sensible sensor measurement fluctuations with either temperature or applied vacuum pressure.

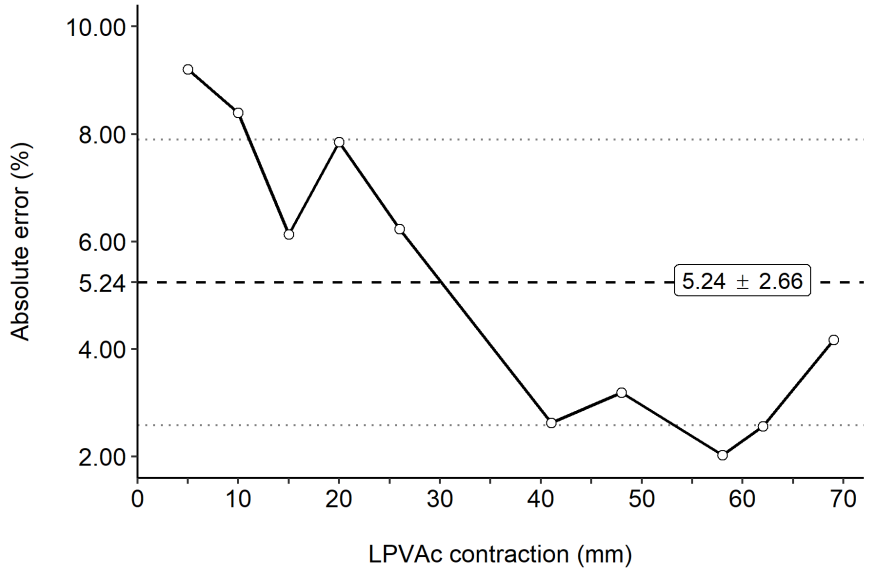

Fig. 4.25: The measurement error observed over the LPVAc's actuation range is shown. 5.24 ± 2.66 percent was determined as the mean absolute error percentage.

4.2.8 Using the integrated sensor for feedback control of the LPVAc

Fig. 4.26 depicts the test setup used for the performance assessment of the proposed integrated sensor in actuator displacement control. A microcontroller development board (mega2560, Arduino) was used as the central controller. Two relay-driven solenoid-actuated open/close flow control valves (FCVs) (911-707, Dorman) were utilized to link the actuator to the vacuum source for actuation and the atmosphere for release. The position data from the integrated sensor (LDC1614, Texas Instruments) was used to actuate the LPVAc. The sensor input was used by an on-off controller run on the microcontroller development board with lower and upper thresholds (vacuum and atmosphere). The sensor feedback data from the sensing module was serially transmitted to and saved on the PC using I2C. Fig. 4.27 presents the block diagram of the feedback control system.

In this experiment, a square wave displacement reference signal was employed. The square wave had a 20 mm amplitude and a frequency of 0.25 Hz. The LPVAc was activated within the measured range of 5 to 25 mm. The sensor's LPVAc displacement value was computed using the characteristic equation established previously in eq.3.3. Using a digital camera and a marker on the LPVAc, the actual LPVAc displacement was measured. This visual input was post-processed on a PC with digital video analysis software (Kinovea, ver. 0.8.15). A third-order Savitzky–Golay filter with a filter length of 21 was used to smooth the gathered data [125].

The results of the feedback control experiment are given in Fig. 4.28. The input signal is shown in blue, the sensor feedback signal is shown in red, and the actual location of the LPVAc is shown in black. The findings demonstrate that the proposed sensor may be employed for effective feedback control of the LPVAc. The sensor accurately measures the real location of the LPVAc, allowing the controller to move the LPVAc in the correct square wave motion.

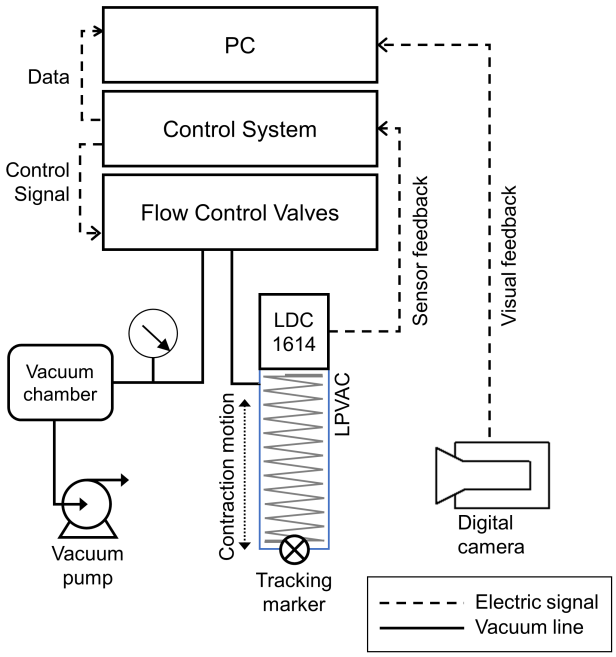

Fig. 4.26: The experimental setup for evaluating feedback control performance.

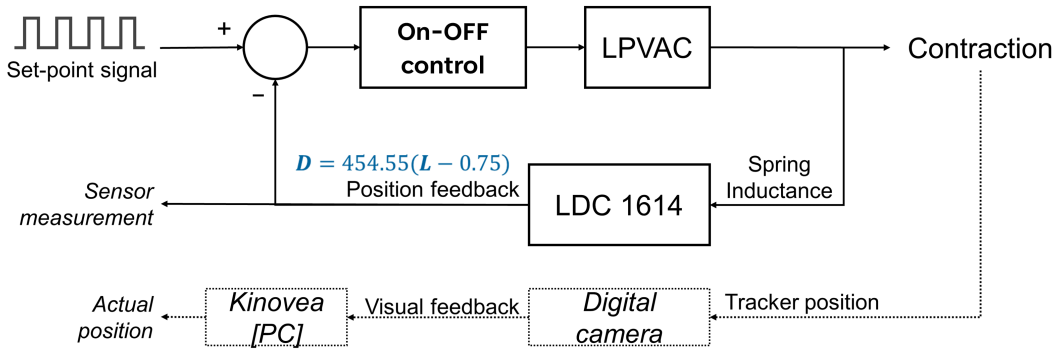

Fig. 4.27: The block diagram of the control system used for the feedback control performance evaluation test.

4.3 Summary

This chapter presented the experimental evaluation of the contraction and blocked force performance characteristics of ThinVAc and LPVAc. The ThinVAc and the LPVAc show good contraction and blocked-force properties suitable for assistive soft exosuit applications. The performance of the inductive sensor developed for the LPVAc was also experimentally characterized. This sensor is used in conjunction with a bang-bang type controller to evaluate the closed-loop controllability of the actuator. The LPVAc is controlled in a closed loop to assess the ability of the actuator to follow a given square wave signal. The LPVAc can successfully follow a square wave signal with minimal error at 0.25 Hz. Table 4.6 compares the developed actuators with

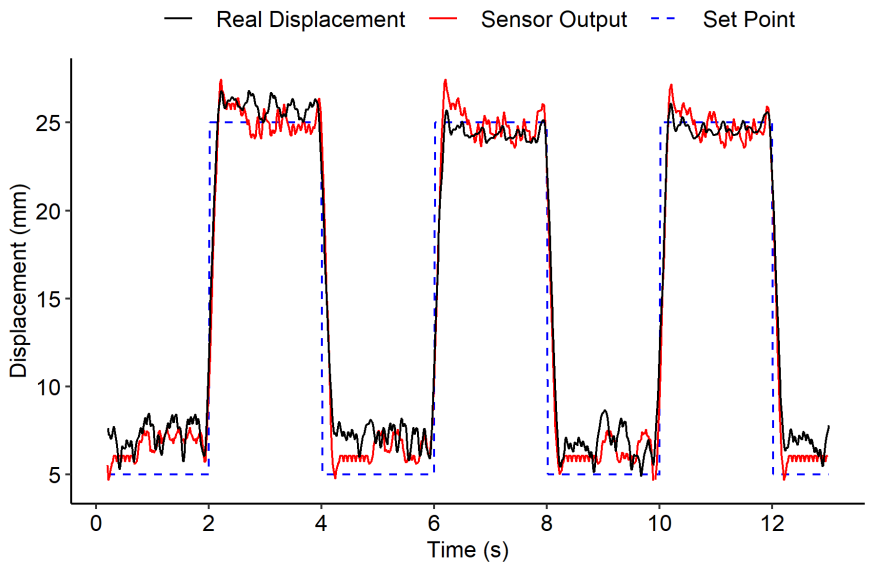

Fig. 4.28: The sensor response and actual displacement seen during the actuator's feedback control test.

those in the literature. The LPVAc, ThinVAc, and multi-filament designs show smaller cross-sectional areas, lower weight, higher maximum blocked forces, and maximum delivered stress compared to contemporary vacuum-driven contractile actuators (see Fig. 4.29).

TABLE 4.6: ThinVAc force performance in comparison to literature.

Actuator	Weight (g)	Area (mm^2)	Max. Force (N)	Max. Stress (kPa)	Force-to-weight ratio
FOAM-1 [72]	43	705	201	285	477
FOAM-2 [72]	56	736	428	582	779
OV-PAM-1 [73]	53	3507	120	34	231
OV-PAM-2 [73]	160	9743	392	40	250
APAM [86]	-	81	70	863	-
FPAM [82]	2.52	100	0.098	1	4
VAMP-1 [69]	-	952	61.88	65	-
VAMP-2 [69]	-	952	0.93	1	-
VAMP-3 [69]	-	952	9.32	10	-
LP-VPAM [126]	-	380	26.4	69	-
LDPE-ThinVAc: mono					
50 mm	0.75	28.3	3.1	110	421
100 mm	0.92	28.3	4.3	152	477
200 mm	1.24	28.3	5.2	184	428
TPU-ThinVAc: mono					
200 mm	1.99	28.3	4.5	159	231
LPVAc: Mono					
Spring A (30 x 15)	14	402	29.35	73	214
Spring B (30 x 10)	14	278	32.5	117	237
Spring C (40 x 10)	14	378	39.05	103	285
LDPE-ThinVAc: multi					
5 x 100 mm	9	225	19.13	85	217
15 x 100 mm	19	875	54.04	62	290
5 x 200 mm	10	225	25.11	112	256
10 x 200 mm	18	600	48.06	80	272
TPU-ThinVAc: multi					
3 x 200 mm	4.94	86	8	93	165
5 x 200 mm	7.93	145	14	97	180

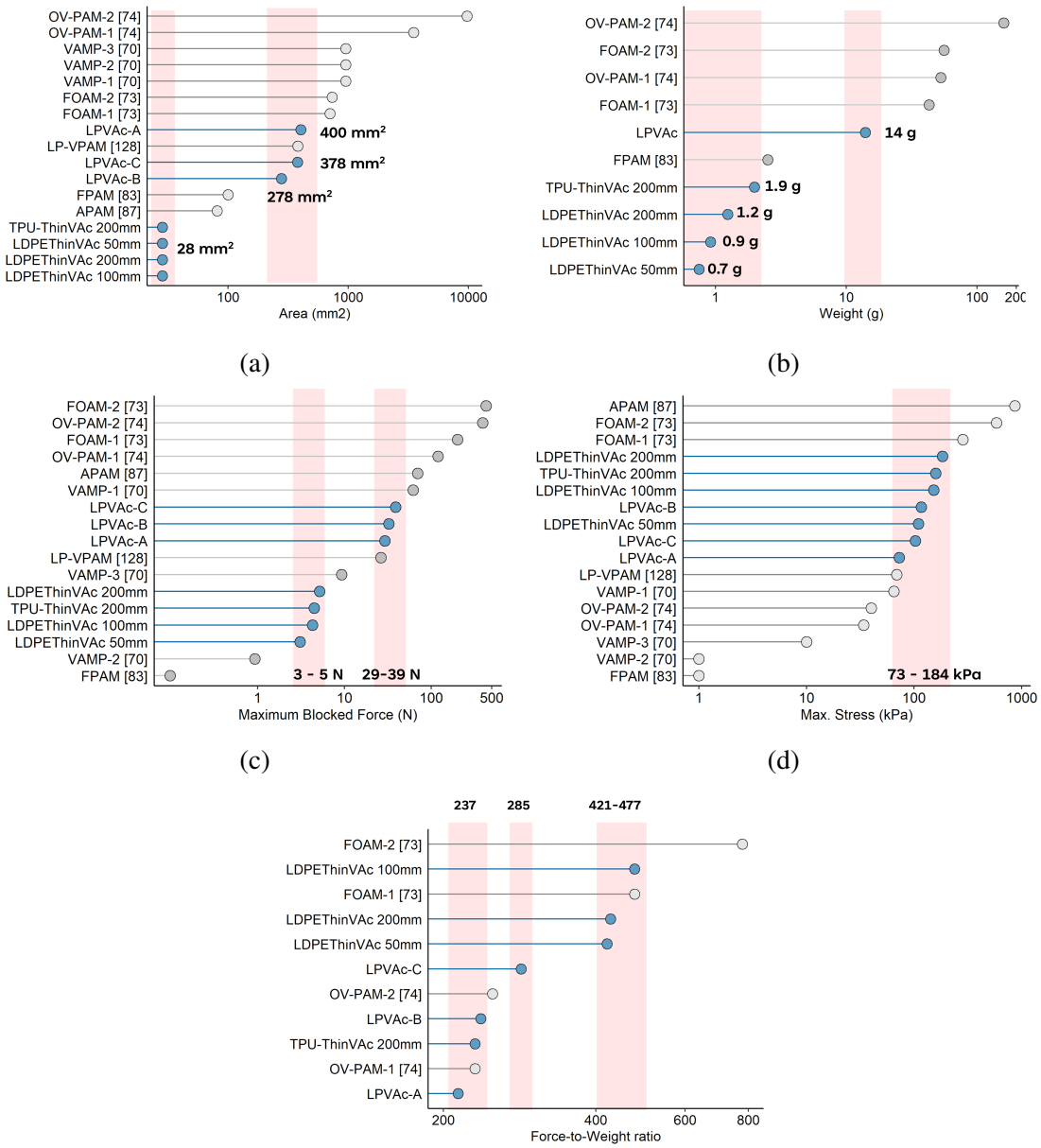

Fig. 4.29: Comparison of the developed soft actuators in comparison with related vacuum actuators in literature; a) cross-sectional area, b) self-weight, c) maximum blocked force, d) maximum stress, and e) force-to-weight ratio.

CHAPTER 5

NUMERICAL MODELS FOR CONTRACTION AND FORCE

The recent models presented for contraction and force estimation of skeleton-based contractile vacuum actuators rely on measuring the skin curvature between the skeletons during collapse [72, 73]. These researchers used proprioceptive sensors fixed externally to conduct these measurements. The use of such sensors is impractical in real-world wearable applications. As a result, models that do not rely on such real-time data and can forecast performance based on actuator shape and applied differential pressure are required. As a result, this thesis suggests using a numerical modeling technique to create models that anticipate ThinVAc contraction and blocked force performance. First, a numerical model of the ThinVAc contraction is presented. Second, a model is provided to explain the ThinVAc blocked force performance, which is then extended to forecast the blocked force of the multi-filament actuator.

5.1 LDPE-ThinVAc contraction model

A regression model was developed to describe the LDPE-ThinVAc contraction performance using numerical analysis of the experimental data. The contraction of the LDPE-ThinVAc was experimentally evaluated under isotonic conditions. The experiments were carried out using three actuator lengths (50 mm, 100 mm, and 200 mm) and four pressure levels (20, 40, 60, and 80 kPa(abs.)). Regression fitting was performed using the least-squares approach to identify and model the displacement characteristic of the LDPE-ThinVAc. Several regression models were initially considered, such as single-parameter and multi-parameter regression.

A single-parameter regression model for contraction vs. load requires 12 equations to explain all possible configurations (three LDPE-ThinVAc lengths and four applied vacuum levels). Therefore, a multiple-parameter regression model is selected to describe the LDPE-ThinVAc monofilament contraction. The unitless contraction ratio (see eq. 5.1) is used as the performance metric to evaluate contraction performance independent of actuator length. The single and multi-parameter regression models are compared in Appendix 05. The multi-parameter model considered for the contraction of the LDPE-ThinVAc is shown in eq. 5.2.

$$\text{Contraction ratio (CR) [no units]} = \frac{\text{strain}(\Delta L)}{\text{initial length}(L)} \tag{5.1}$$

$$\text{CR} = aP + bL + c \tag{5.2}$$

Here, P is the applied pressure in kPa (abs.), L is the driven load in N, and a, b, and c, are the regression coefficients. The least-squares method was used to estimate these three coefficients. The estimated coefficients and their goodness of fit are presented in Table 5.1. It can be seen from the goodness-of-fit results that the estimated multi-parameter model will closely follow the experimental values.

The performance of the eq. 5.2 in estimating the LDPE-contraction is shown in Fig.

TABLE 5.1: The goodness of fit parameters for the multi-parameter LDPE-ThinVAc monofilament contraction model.

Model	Contraction ratio ~ Pressure + load
R^2	0.95
Adj. R^2	0.95
RMSE $[\Delta L/L]$	0.026
RMSE $[\Delta L/L\,\%]$	2.6

Parameter	Coefficients	t Stat	P-value
a	-0.0043	-70.7535	5.6555×10^{-21}
b	-0.1537	-42.4613	4.5691×10^{-140}
c	0.05706	113.7994	7.2425×10^{-281}

5.1. The model closely follows the experimental data, and the RMSE for each pressure level and the full pressure range is shown in Table 5.2 for each actuator length. It can be seen that the model can describe the contraction performance with a maximum RMSE of 3.5%.

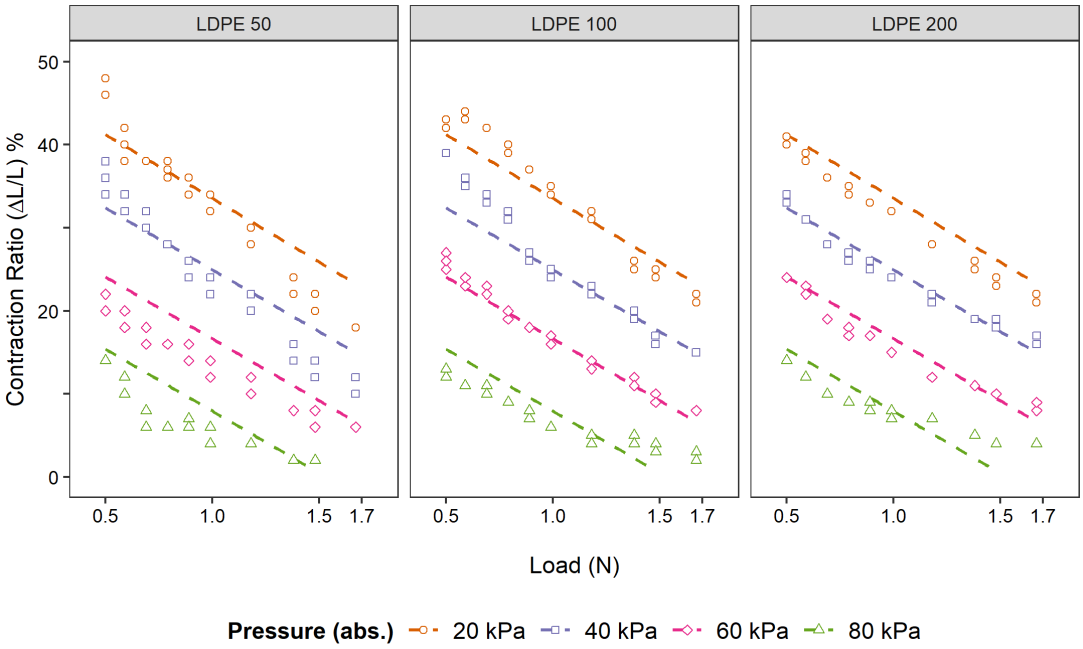

Fig. 5.1: Multi-parameter regression contraction model for the LDPE-ThinVAc describes the experimental data with minimum error.

TABLE 5.2: RMSE of contraction ratio (%) at each pressure level and the full range for the proposed multi-regression model for the LDPE-ThinVAc

LDPE ThinVAc	Pressure level 20 kPa	40 kPa	60 kPa	80 kPa	Over full range
50 mm	3.48	2.68	2.62	2.44	2.87
100 mm	2.60	3.38	1.74	2.77	2.69
200 mm	1.92	1.12	1.51	3.22	2.10

5.2 TPU-ThinVAc contraction model

A multi-parameter regression model similar to that of LDPE-ThinVAc was developed to describe the contraction performance of the TPU-ThinVAc. Just like in the case of the LDPE-model, the same parameters of absolute pressure (kPa) and driven load (N), as in eq. 5.2. The RMSE is calculated for each pressure level, and the full pressure range is shown in Table 5.3. The model can describe the contraction performance with an overall RMSE of 1.5%.

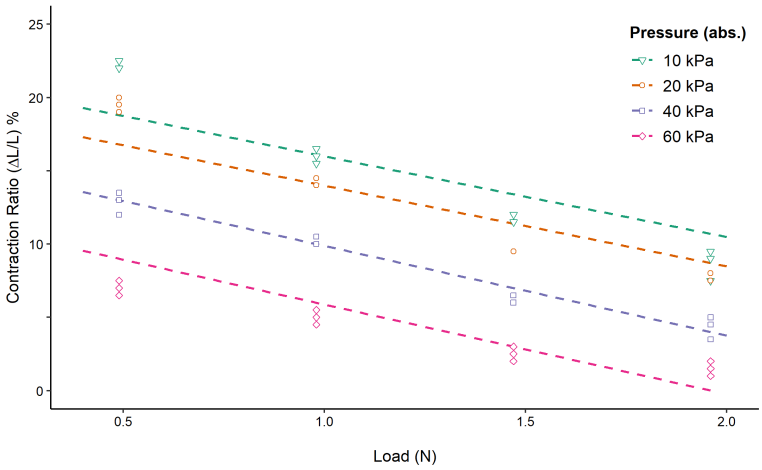

Fig. 5.2: Multi-parameter regression contraction model for the LDPE-ThinVAc describes the experimental data with minimum error.

TABLE 5.3: RMSE of contraction ratio (%) at each pressure level and the full range for the proposed multi-regression model for the LDPE-ThinVAc

ThinVAc type	Pressure level 10 kPa	20 kPa	40 kPa	60 kPa	Over full range
TPU 200	2	1.6	0.6	1.4	1.5

5.3 LDPE-ThinVAc blocked force model

The LDPE-ThinVAc monofilaments were bulked in combinations of 5, 10, and 15 to create multi-filament actuators. The LDPE-ThinVAc monofilaments, as well as multi-filament structures, both showed good blocked force scalability (see Fig. 4.7 and Fig. 4.11 respectively).

As described earlier in chapter 4, linear regression models were calculated to represent the blocked force behavior of the LDPE-ThinVAc monofilaments (See Table. 5.4). The blocked force characteristics of the multi-filament combinations shown in Fig. 4.11 suggest scalability to the number of LDPE-ThinVAc monofilaments. Hence, the feasibility of developing a multiplicative model for the multi-filament structures using the regression fit models for the monofilaments was considered.

TABLE 5.4: Regression fits for the LDPE-ThinVAc blocked force performance

	Regression model
50 mm	$F_{mono} = 0.03432\,dP + 0.0632$
100 mm	$F_{mono} = 0.04259\,dP + 0.5401$
200 mm	$F_{mono} = 0.05177\,dP + 0.8266$

F_{mono} is the blocked force in N.
dP is the applied differential pressure in kPa.

The ThinVAc monofilament blocked force model (shown in Fig. 4.7) was multiplied by the number of filaments in the multi-filament structure to obtain its blocked force, using eq. 5.3. Here, for a given length, $F_{blocked-multi}$ is the blocked force from the multi-filament structure, n is the number of integrated filaments, and $F_{blocked-mono}$ is the blocked force equation for the respective monofilament from Table 5.4.

$$F_{blocked-multi} = n \times F_{blocked-mono} \tag{5.3}$$

The prediction obtained from eq. 5.3 is plotted in Fig. 5.3. The dashed line indicates the experimental data. The initial fit depicted results from multiplying the monofilament model by the number of strands using 5.3. The estimate given by the multiplicative model is higher than the expected value.

The blocked force at atmospheric pressure (in the unactuated condition) should be zero. Hence, the y-intercept should be zero at the origin. Therefore, to account for this, the following linear correction term C_{dP} is appended to eq. 5.3. Here, n is the number of monofilaments, and C_{mono} is the constant value from the respective monofilament blocked force model (*i.e.* for 50 mm LDPE-ThinVAc, $C_{mono} = 0.0632$).

$$C_{dP} = n \times C_{mono} \tag{5.4}$$

The linear correction term C_{dP} is deducted from the initial model eq to get the corrected fit. 5.3. The revised model in Eq. (5) matches the experimental data better, as shown in the corrected fit in Fig. 5.3.

$$F_{blocked-multi} = (n \times F_{blocked-mono}) - C_{dP} \tag{5.5}$$

TABLE 5.5: RMSE values for the initial and correction fit for the multiplicative model for the LDPE-ThinVAc multi-filament actuators

Multi-Filament Combination	RMSE (N) Initial Fit	Corrected Fit	Reduction (%)
5 x 100 mm	2.64	0.5	81
15 x 100 mm	11.08	3.21	71
5 x 200 mm	2.1	0.97	54
10 x 200 mm	6.97	1.52	78
Average	6.76	1.86	73

Table 5.5 displays the RMSE values for the initial and corrected models. When the influence of the y-axis intercept is removed, the average error decreases by 73% when compared to the baseline model in eq. 5.3. Table 5.6 compares multi-filament actuator combinations' predicted and experimental maximum blocked force values. The maximum blocked force can be described with a maximum error of less than 9%, and the average error for each combination is 3.28 %.

5.4 TPU-ThinVAc blocked force model

A normalized model was used instead of the multiplicative model for the LDPE-ThinVAc to predict the blocked force of the TPU-ThinVAc multi-filament actuators. The experimental data shown in Fig. 4.14, the multi-filament actuators do not show direct scalability from the monofilament. In theory, a multi-actuator with n-filaments should be able to generate n-times the force of a monofilament actuator. Experimental

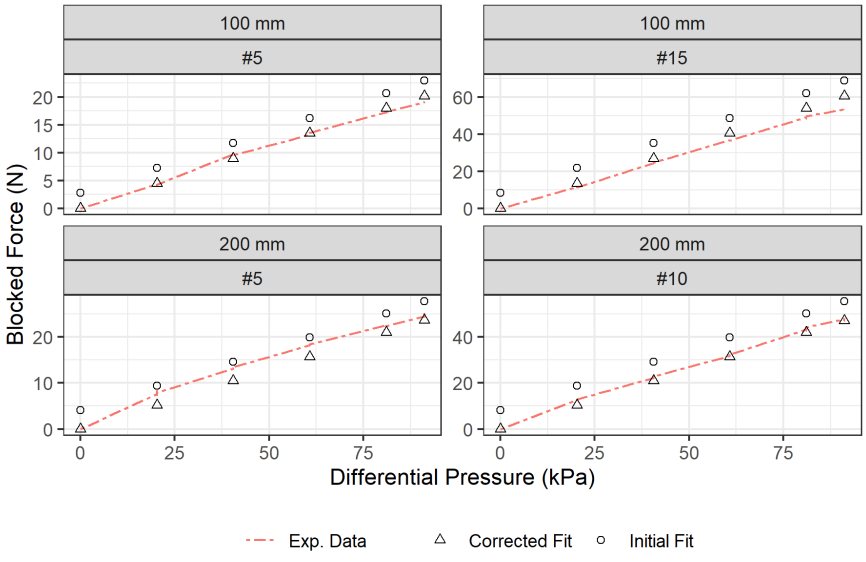

Fig. 5.3: The multiplicative blocked force model for the LDPE-ThinVAc multi-filamant actuators.

TABLE 5.6: Comparison of predicted and experimental values for blocked force for the LDPE-ThinVAc

	5 x 100 mm	15 x 100 mm	5 x 200 mm	10 x 200 mm
Experimental maximum blocked force (N)	19.13	54.04	25.11	48.06
Predicted maximum blocked force from the multiplicative model (N)	19.58	58.75	25.04	47.21
Absolute Error percentage (%)	2.37	8.71	0.28	1.76

results show blocked forces 1.9 times and 3.2 times larger than the monofilament actuator for 3- and 5-filament actuators, respectively. The presence of multiple consecutive thermal seals that cause an increase in the contraction resistance of the TPU-ThinVAc multi-filament actuators can be considered the reason for this reduction.

The TPU-ThinVAc multi-filament actuator does show good scalability between 3- and 5-TPU-ThinVAc combinations. Hence, the filament number normalized the blocked force generated from the multi-filament to obtain a unit blocked force. This unit-blocked force model was used to predict the blocked force for the multi-filament actuators. The prediction correlates well with the experimental results, as shown in Fig. 5.4.

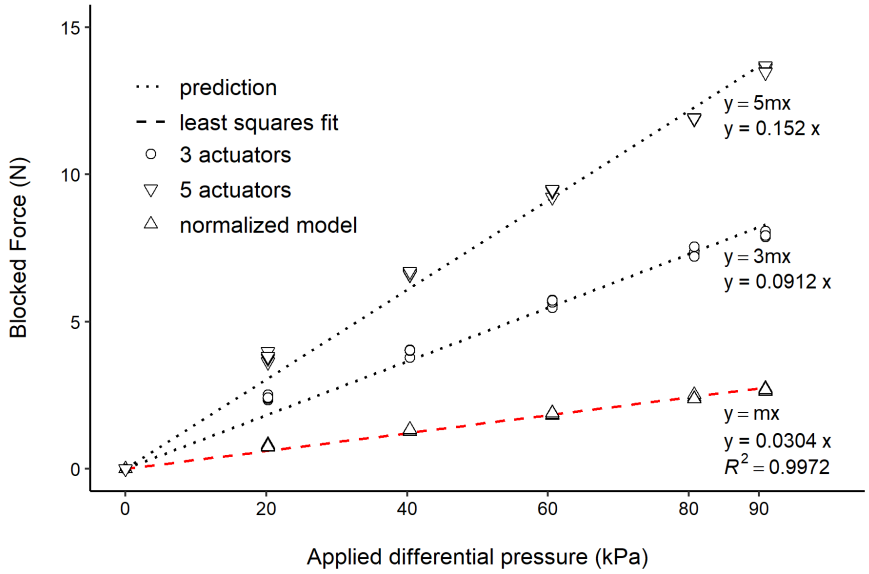

Fig. 5.4: The blocked force model for the TPU-ThinVAc multi-filamant actuators.

Table 5.7 displays the RMSE values and compares maximum experimental and predicted blocked force values. The overall RMSE for the model is 0.33 N and 0.44 N for the 3- and 5-actuator configurations. The full range RMSE is 4.1%, and 3.1%, respectively. The proposed model can describe the maximum blocked force with less than a maximum error of 2.6% and 1.43% for the 3- and 5-actuator configurations, respectively.

TABLE 5.7: TPU-ThinVAc multi-filament blocked force model evaluation

	3-Filament	5-filament
RMSE (N)	0.33	0.44
RMSE (% of full range)	4.1	3.1
Experimental Maximum blocked force (N)	8.08	14.02
Theoretical maximum blocked force from the multiplicative model (N)	8.29	13.82
Absolute Error percentage (%)	2.6	1.43

5.5 Summary

This chapter presented numerical models to describe the contraction and the blocked force performance of the developed ThinVAc. Existing models require external sensory feedback to describe the contractile and blocked force performance of vacuum-driven contractile soft actuators. Hence, the use of numerical models is proposed. Multi-parameter regression models were developed to describe the contraction performance of the LDPE and TPU ThinVAc, monofilaments. These models enable the designer to use applied absolute pressure and the load to determine the contraction ratio of the ThinVAc with minimal RMSE. Linear regression models were calculated to represent the blocked force behavior of the LDPE-ThinVAc monofilaments. The blocked-force characteristics of the multi-filament LDPE-ThinVAc were predicted using a multiplicative model using the observed scalability of monofilament results. Similarly, a normalized model was developed to predict the blocked-force performance of the TPU-ThinVAc multi-filaments. Both blocked force models for the multi-filament structures exhibit low RMSE.

CHAPTER 6

EXOSUIT DEVELOPMENT AND TESTING

This chapter presents the application of the developed soft linear actuators in wearable applications. The inherent safety, compliance, high force-to-weight ratios, and structural flexibility provided by soft robotics systems have recently gained the attention of researchers developing lower limb assistive solutions [14, 28, 111, 127]. To successfully apply soft actuators in wearable applications, they must provide adequate forces to move user limbs while being flexible enough to fit around body contours. First, the proposed ThinVAcs in a knee rehabilitation assist system is shown. Next, the LPVAc is used in a novel exosuit for sit-to-stand transition assistance.

6.1 Knee rehabilitation assist device

6.1.1 Introduction

Knee disorders are a prominent issue that affects human lower limb motion [128]. A leading management technique of knee disorders is physiotherapy-based knee rehabilitation [129]. Some primary causes necessitating knee rehabilitation are osteoarthritis, total knee replacement (TKR), and stroke [130]. Three main muscle groups targeted in knee rehabilitation therapies are the quadriceps-femoris muscles, the hamstrings, and the calves [131]. Leg flexion and extension exercises are essential for developing and healing these muscles. The lack of physiotherapists to meet the growing number of patients is a significant problem in knee rehabilitation. As a result, there is a need to create devices that would assist a physiotherapist in attending to multiple patients simultaneously. Few examples of rigid assistive devices for knee rehabilitation [120] and very few examples of soft devices [28] can be found in recent literature. One major limiting factor is the absence of flexible, lightweight actuators that can easily conform and contour along human limbs for integration with soft wearable (exosuit) support systems. The following section describes the proposed ThinVAc in a lower leg extension system for knee rehabilitation assistance.

6.1.2 Knee extension assist system

A model lower limb was used to test the viability of the proposed TPU-ThinVAc in motion assist during knee extension. A model comprising a thigh, a knee, a shank, and a foot was fabricated from acrylic sheets. The knee joint was designed to rotate in the sagittal plane. The TPU-ThinVAcs were anchored above and below the knee (thigh and shank), mimicking the muscle placement across the human knee.

The model lower limb was designed to represent the 95^{th} percentile male lower limb dimensions (shank length = 450 mm [132], foot length = 250 mm [133]). The model is fabricated from laser-cut acrylic sheets and the sheets are glued together using acrylic adhesives (see Fig 6.1). The shank weighs 850 g, and the foot 250 g. The leg model was rigidly attached to a fixed frame for experimentation.

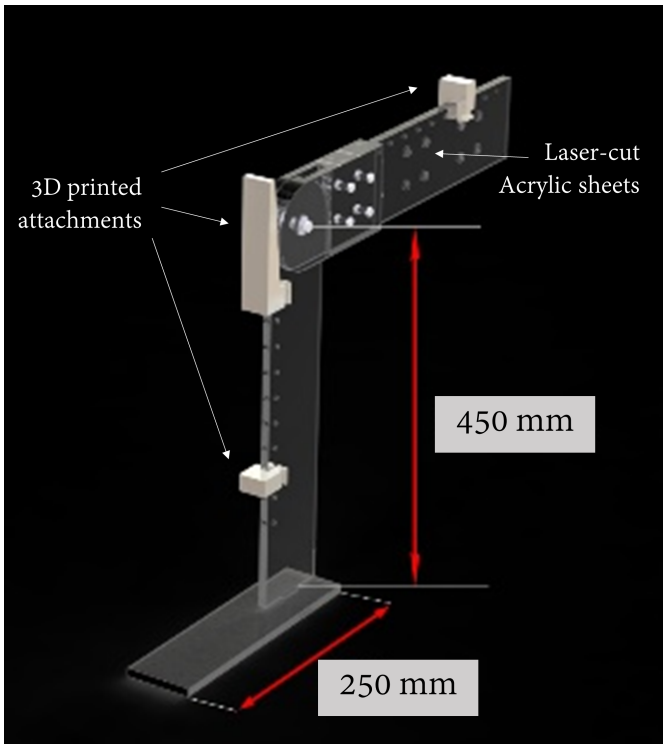

Fig. 6.1: CAD model of the lower limb model for knee extension assistance test.

The knee extension test used two LDPE-ThinVAc multi-filament actuators (10 x 200 mm and 15 x 100 mm). The multi-filament actuators were attached to the thigh plate above the knee with a fixture and a mounting bracket attached to the shank with inextensible wire (see Fig. 6.2 a) and 6.3 a)). The movement of the shank upon actuation is captured using a tripod-mounted digital camera at 30 frames per second. Motion analysis software (Kinovea, ver. 0.8.15) was used to analyze the trajectory of markers placed on the foot tip and ankle. The ankle marker's trajectory is utilized to calculate the knee extension angle. As the actuation signal, a vacuum pressure step input of 20 kPa (abs.) was given at 0 s. The shank response is underdamped, as seen in Figs. 6.5 and 6.5. Table 6.1 describes the shank response time-domain characteristics.

As shown in Fig. 6.3 a) inset, the ThinVAc multi-filament actuators can be compliant to irregular-shaped structures and stretched out to easily achieve a low profile.

TABLE 6.1: Shank response with ThinVAc actuation.

	15 x 100 mm	10 x 200 mm
90% rise time [s]	0.27	0.4
±5% settling time [s]	1	0.83
Overshoot [%]	162	119
Max. shank angle [°]	30	19

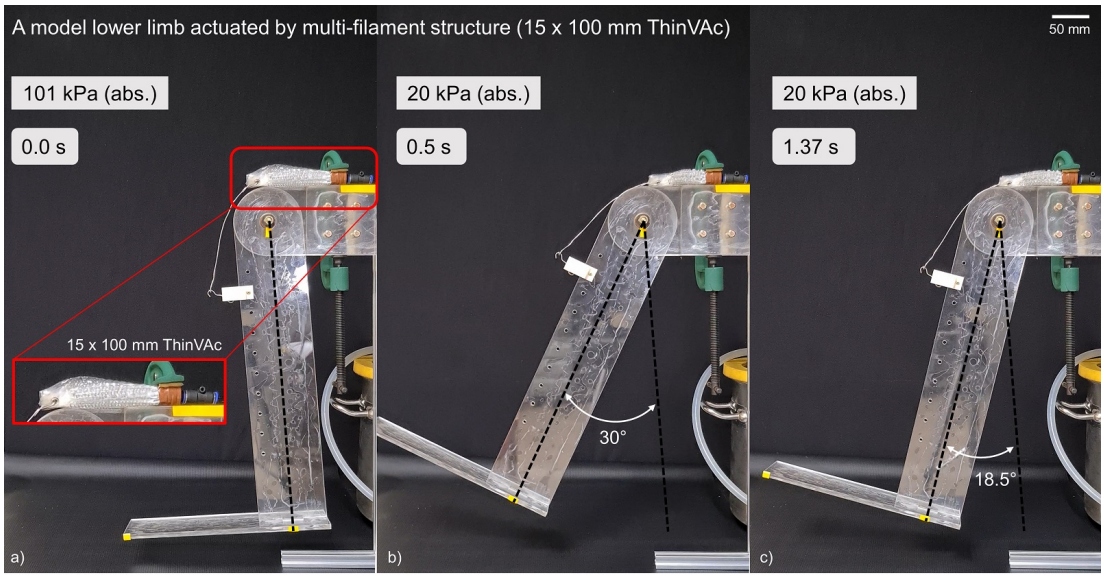

Fig. 6.2: A 15 x 100 mm multi-filament actuator used to actuate the model lower leg for knee extension.

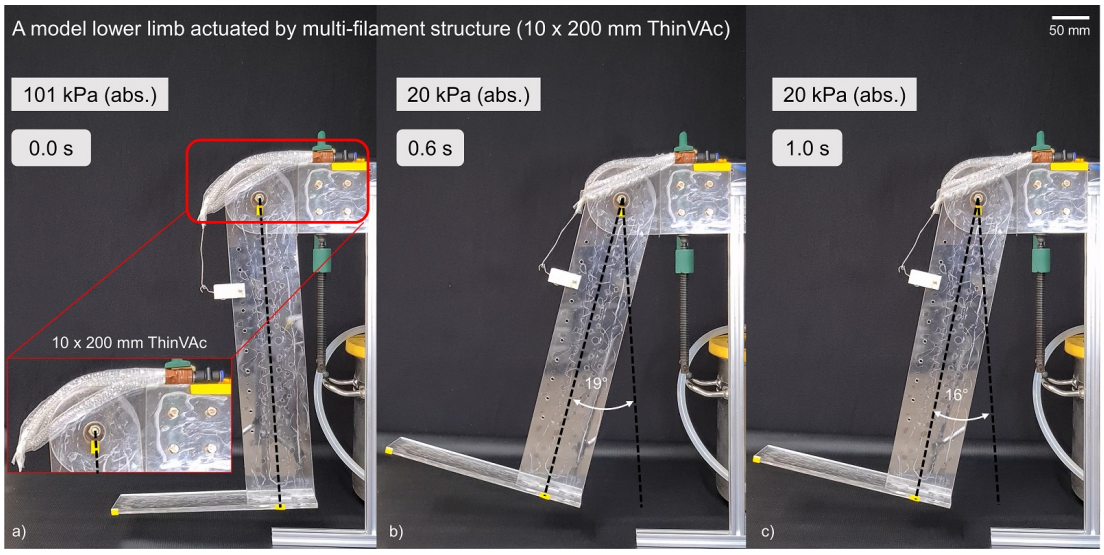

Fig. 6.3: A 10 x 200 mm multi-filament actuator used to actuate the model lower leg for knee extension.

6.2 Sit-to-stand-transition assist exosuit

6.2.1 Introduction

Walking is an activity of daily living that plays a significant role in a person's functional independence and quality of life [134]. Hence, lower-limb muscle weakness that limits mobility can negatively affect their health and livelihood, cause secondary medical disorders, and lead to physical and psychological dependency on caregivers [135]. Stroke, spinal cord injuries, other trauma, obesity, and age can lead to temporary and permanent mobility impairments and functional decline. In managing these situations

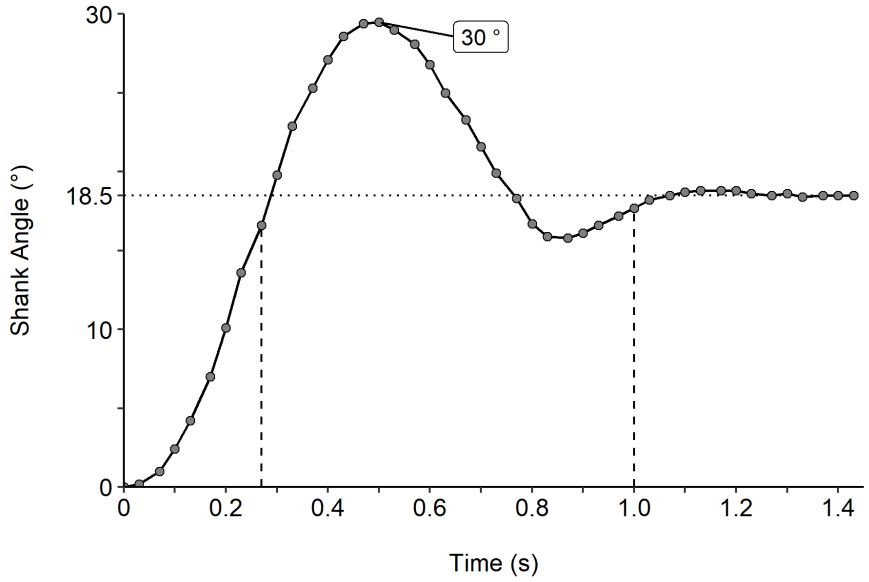

Fig. 6.4: Shank angle response as a function of time for actuation by a 15 x 100 mm multi-filament actuator.

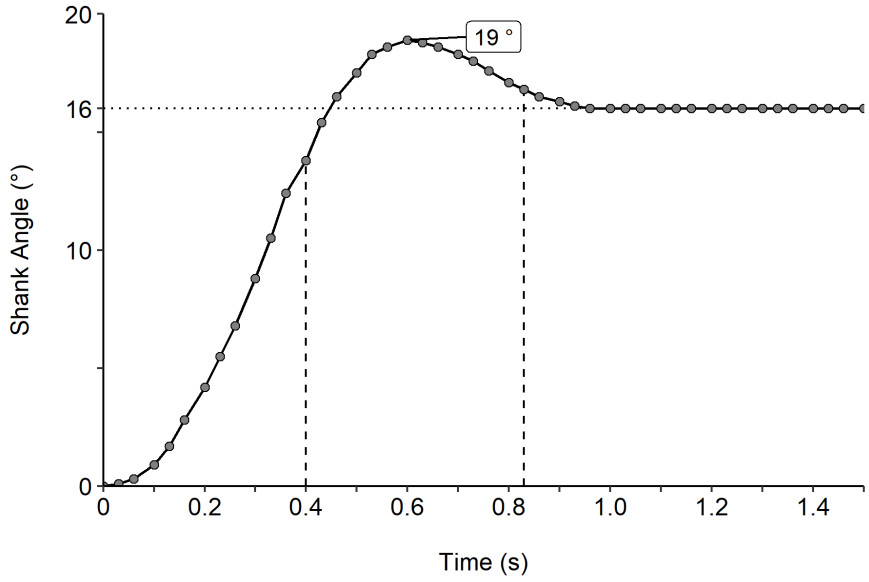

Fig. 6.5: Shank angle response as a function of time for actuation by a 10 x 200 mm multi-filament actuator.

to maintain/recover independent motion functionality, a key factor is the promotion of continuous attempts at mobility [7].

The difficulty in transitioning from seated to standing posture is one of the common obstacles faced by persons with impaired mobility and functional decline with age. We can support such persons during this sit-to-stand transition (StSt). Such support will encourage more frequent attempts at independent mobility and reduce secondary medical complications associated with a sedentary life [7]. Conventional assist solutions for StSt have included passive devices such as canes, walkers, and personal caregivers.

However, the associated social stigma of dependence on such external assistance negatively affects patients, promoting sedentary behavior.

Provision of an StSt assist solution that is easy to use in daily living, inconspicuous to an observer but provides adequate assistance to promote more frequent attempts at StSt, will lead to a less sedentary life and an improved quality of life. Soft exosuits have come up as an excellent solution for this. The following sections will describe the proposed LPVAc in developing and experimenting with an StSt-assist soft exosuit.

6.2.2 Exosuit design

Sit-to-stand transition is a motion that takes place against gravity and relies mainly on the strength of lower limb muscles. The primary body movements associated with StSt are hip and knee extension. During these extensions, the primary muscles recruited are the quadriceps femoris (QF) and gluteus maximus (GM). The GM muscles provide most of the anti-gravity lifting force compared to QF [136]. Therefore, an artificial muscle can be used with GM to assist StSt. This requirement necessitates that the assistive actuator (LPVAc in this scenario) be placed in a mono-articular arrangement with the wearer's GM muscle. A novel exosuit prototype was designed and fabricated to assess the LPVAc in StSt-assist. Fig. 6.6 presents this prototype soft exosuit and how it is worn while standing.

The Wehner design [13] inspired the proposed soft exosuit. Wehner presents using physical (key) and virtual anchor points to transfer forces across the lower limbs through non-extension lines. Based on this concept, the LPVAc is anchored parallel to the GM muscle on the posterior lower limb. One anchor point is a webbing strap wrapped around the hip, while the other is the thigh support. This application uses webbing straps (25 mm wide) as anchors and force guides. The LPVAc is proximally anchored to the hip belt using a box stitch and distally anchored to a soft thigh sup-

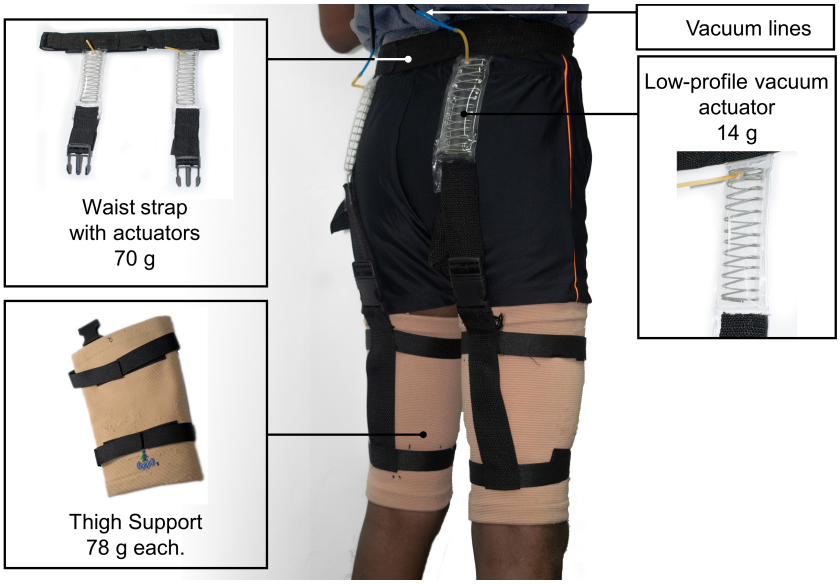

Fig. 6.6: The proposed novel mono-articular StSt-assist soft exosuit. The weight of each sub-component is given in the figure.

port sleeve (2040, OppoMedical, USA). Two Velcro straps were sewn onto the thigh support to tighten it in place after donning, while another webbing strap was sewn in parallel to the biceps femoris muscle connecting the tightening straps. These straps are used to direct the force applied by the LPVAc along the thigh support. Each leg had one LPVAc attached, using two LPVAcs per subject. Depending on the wearer's height, the distal connections have a quick-release clasp for simple donning, doffing, and adjustment.

The proposed exosuit weighs 324 g in total, excluding the weight of the vacuum pump, chamber, and valves. Most of the exosuit's weight is carried on the hips, close to the body's center of mass, reducing the metabolic penalty and biomechanical constraints to motion.

6.2.3 Performance evaluation of the exosuit

Three healthy participants were enlisted to evaluate the efficacy of the planned exosuit in STSt-assist (details in Table 6.2). The test protocol used for the StSt assist performance evaluation is described in Fig. 6.7. Before each experiment, every participant went through a guided trial run. All participants were then asked to conduct a Front plank with hip extension to measure their GM muscle's maximum voluntary contraction (MVC) EMG signal [137]. The maximum value of three trails was selected as their GM MVC for post-processing EMG normalization. Each test subject conducted 10 repetitions of StSt with and without the exosuit. All clothing was kept the same throughout the trials. The StSt was conducted on a 12-bpm metronome.

TABLE 6.2: Test subject details and observed sEMG signal reduction

Subject (m/f)	Age (Y)	Weight (kg)	Height (m)	BMI (kg/m^2)	Reduction (%)
1 (m)	26	45	1.65	16.5	66.93
2 (m)	27	64	1.65	23.5	42.28
3 (m)	27	65	1.60	25.4	26.72
				mean $\pm$ SD [%]	45.31 $\pm$ 20.28

6.2.4 EMG capture test setup

A Delsys Bagnoli-16 desktop EMG system was used for the EMG data capture (See Fig. 6.8). The Bagnoli system comprises a 16-channel amplifier, input modules, connection cables, and surface-mount wired EMG sensors. The output from the amplifier is uploaded to the Delsys EMGworks software running on a desktop PC in real time.

Fig. 6.9 b) shows the experimental test setup. A chair of 46 cm of popliteal height was selected to match DIN 18040-1 requirements (which define the design guidelines for public restrooms). As seen in Fig. 6.9 b) inset, the LPVAc does not interfere with

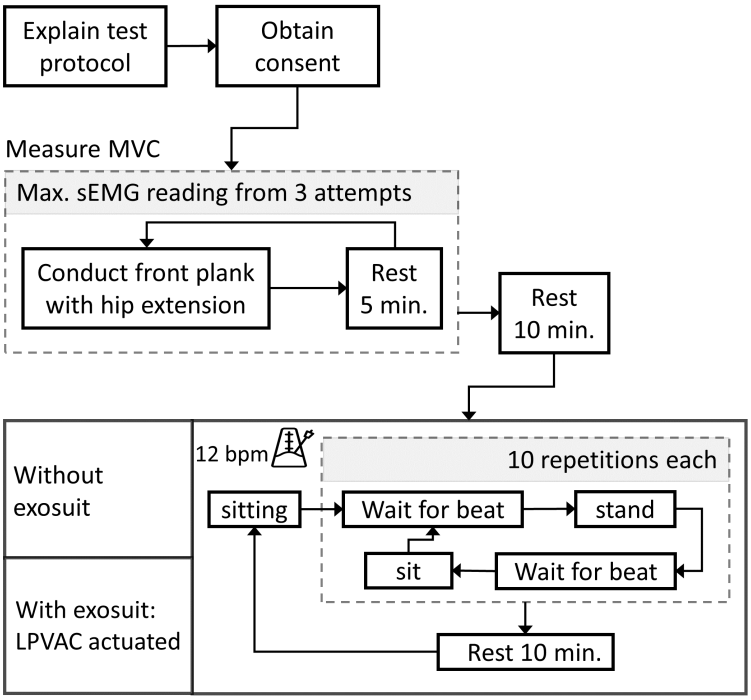

Fig. 6.7: The test protocol used for StSt assist performance evaluation.

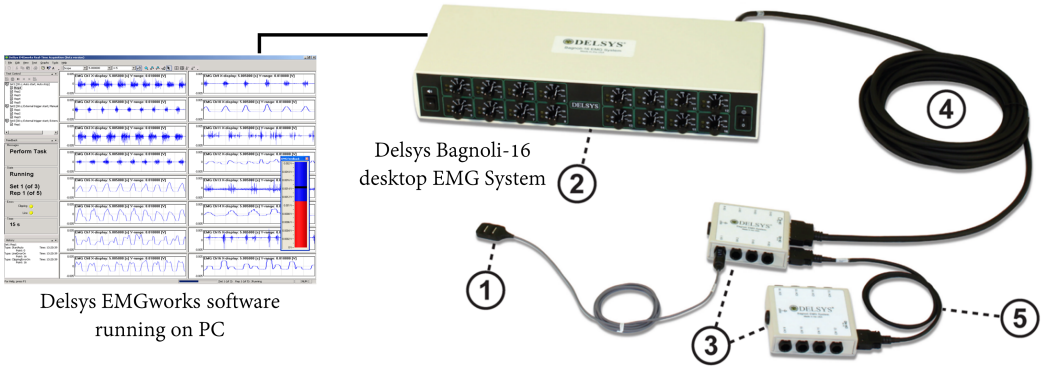

Fig. 6.8: The Delsys Bagnoli-16 desktop EMG system. 1) surface-mount wired EMG sensor, 2) 16-channel main amplifier, 3) input modules, 4) input module cabling, and 5) inter-module cabling.

normal sitting posture. The StSt motion was identified by measuring the ground reaction forces recorded via instrumented shoes worn by the participant. An insole with force-sensitive resistors embedded in the toe and heel was used in the instrumented shoe. Surface electromyography (sEMG) measured the GM muscle activity during STSt. The surface-mount EMG sensor was placed as shown in Fig. 6.9 a) using adhesive tape to ensure tight surface contact. The skin was initially cleaned with rubbing alcohol and let dry before the attachment of the sensor to ensure a clean contact surface. The LPVAcs were operated in an open-loop without using sensor feedback in this exosuit test to investigate the usability of the LPVAc in driving an STSt-assist exosuit.

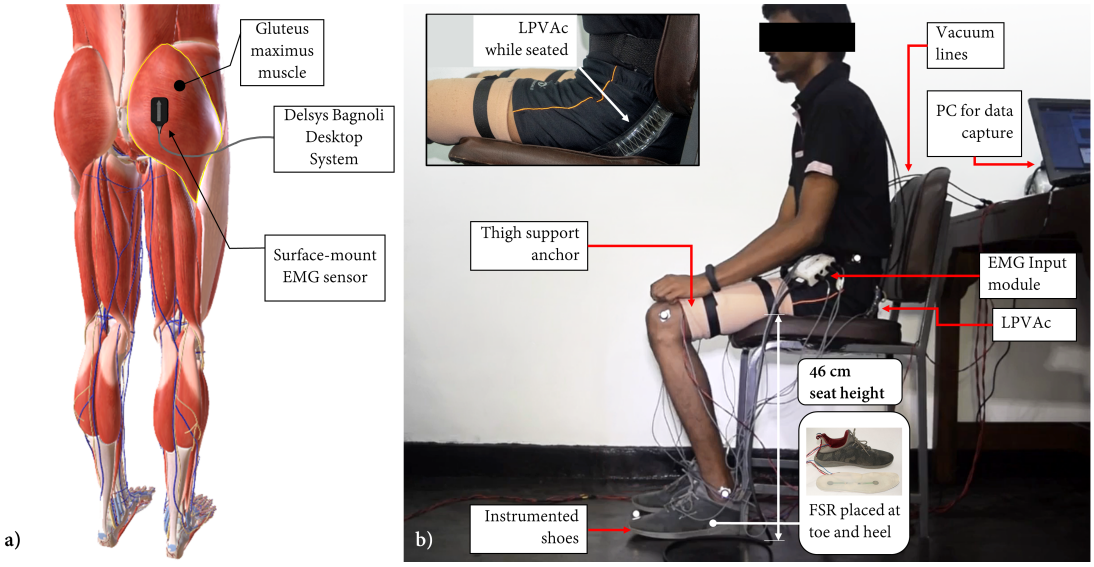

Fig. 6.9: The test setup used for EMG data capture. a) The positioning of the surface-mount EMG sensor on the GM muscle. b) The seated setup used for the StSt. The inset demonstrates the LPVAc's unobtrusiveness when seated.

6.2.5 EMG analysis

Surface EMG data (sEMG) were obtained from the GM muscles of both legs, and only the data from the dominant leg was analyzed. The sEMG data were collected using a Bagnoli desktop EMG system (Delsys, Inc., USA). Initially, the collected data were captured and analyzed using the EMGworks software (Delsys, Inc., USA). The sEMG data was captured at 4 kHz, and the raw data stream was smoothed to get the RMS value using a 250-sample frame. This smoothening generated a 16 Hz output signal, which was then post-processed in MATLAB. For each muscle, the mean of ten sit-to-stand repetitions in the powered suit and without suit testing was averaged and normalized as a percentage of the MVC reading.

The mean values of the RMS'd sEMG obtained for each of the two tests (without the suit and with the suit assisted by the LPVAc) were then DC offset by subtracting the minimum from itself. The STSt time was normalized to the StSt duration measured between the highest gradients measured by the ground response force sensors at the toe and heel. Fig. 6.10 presents the observed EMG reduction during this evaluation.

The percentage reduction in the area under the GM muscle activity curves in Fig. 6.10 was computed to assess the efficiency of the exosuit-provided help. The acquired data show a mean decrease of 45 % in muscle activation during STSt. This reduction is analogous to the findings in [14]. The variation in muscle activity decrease can be ascribed to the participants' varied BMI (see Table 6.2). As a result, it can be inferred that the prototype soft exosuit powered by the proposed LPVAc can significantly reduce the amount of muscular activity required during STSt.

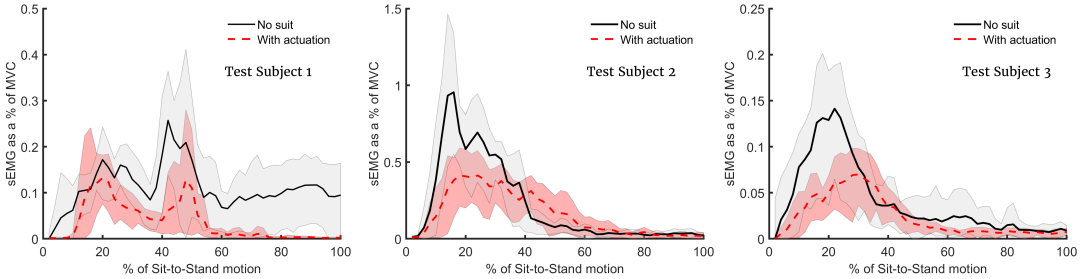

Fig. 6.10: The decrease in sEMG of GM muscles seen in three test participants. The shaded region represents the range of maximum and minimum values recorded at each point of the STSt motion during a total of 10 repetitions.

6.3 Summary

This section presented the proposed ThinVAc and LPVAc in exosuit applications. The ThinVAc and LPVAc were incorporated into wearable application use; an assist device for knee extension and a sit-to-stand-transition assist exosuit, respectively. The positive results of these device evaluations show promise in applying the proposed soft actuators in soft wearable assistive exosuits.

CHAPTER 7

CONCLUSIONS AND FUTURE WORK

7.1 Conclusions

The thesis presents the development, performance evaluation, case studies, modeling, and application of soft linear contractile vacuum actuators. The primary objectives of this research included the development of soft linear actuators, their modeling, and control for use with soft wearable assist exosuits. These objectives were met by the work presented in this thesis.

This thesis proposes two main categories of novel, vacuum-driven, soft contractile linear actuators. The primary novelty lies in developing vacuum-driven thin and low-profile actuators for soft robotic applications. The proposed actuators use inextensible yet flexible, thin-film materials to create enclosed volumes. The cross-sectional shape is maintained throughout the actuation using springs that act like collapsible skeletal structures. Upon evacuation of the enclosed air volume, the actuator collapses guided along the spring. This spring's presence limits the structure's collapse to the longitudinal axis.

This thesis presents two soft actuator designs with thin and low-profile cross-sections named ThinVAc and LPVAc. The ThinVAc uses a thin-film skin (LDPE or TPU) enclosing a small diameter (6 mm OD) stainless steel spring. The LPVAc uses an LDPE skin enclosing a specially designed, obround-shaped low-profile ($30\,mm \times 10\,mm$) spring (made from GI and MS). The ThinVAc monofilament is combined to create multi-filament actuators to scale the force. THE LPVAc force is also scaled using differently proportioned low-profile springs. These actuators' performance characteristics of contraction and blocked force are experimentally evaluated. The ThinVAc and the LPVAc present good contraction and blocked force properties suitable for assistive soft exosuit applications. The successful case studies demonstrate the applicability of these actuators in soft robotic applications.

An integrated sensing solution for the LPVAc is developed based on inductive sensing. The performance of this sensor is also characterized. This sensor is used with a controller to evaluate the closed-loop controllability of the actuator. The LPVAc is controlled in a closed loop to evaluate the ability of the actuator to follow a given square wave signal. The LPVAc can successfully follow a square wave signal with minimal error at 0.25 Hz.

Existing models require external sensory feedback to describe the contractile and blocked force performance of vacuum-driven contractile soft actuators. Hence, numerical models are developed to describe the actuators' contraction and blocked force performance and predict the blocked force when the monofilament structures are scaled to multi-filament structures. Multi-parameter regression models were developed to describe the contraction performance of the LDPE and TPU ThinVAc, monofilaments. These models enable the designer to use applied absolute pressure and the load to determine the contraction ratio of the ThinVAc with minimal RMSE. Linear regression models were calculated to represent the blocked force behavior of the LDPE-ThinVAc monofilaments. The blocked-force characteristics of the multi-filament LDPE-ThinVAc

was predicted using a multiplicative model using the observed scalability of monofilament results. Similarly, a normalized model was developed to predict the blocked-force performance of the TPU-ThinVAc multi-filaments. Both blocked force models for the multi-filament structures exhibit low RMSE.

These soft actuators are then incorporated into wearable application use. The ThinVAc is tested in a device that can be used for assisting knee extension during knee rehabilitation. The LPVAc is incorporated for a sit-to-stand-transition assist exosuit. The positive results of these device evaluations show promise in applying the proposed soft actuators in soft wearable assistive exosuits.

This thesis presents actuators that use negative pressure (vacuum) for actuation. Using a vacuum for driving soft actuators has several associated limitations. The maximum applicable differential pressure restricts the highest applied blocked force, typically confined to a single atmosphere. Another limitation is the risk of suction of the ambient environment into the actuator upon damage to the structure. All the experiments in this research used desktop vacuum sources, including a single-stage vacuum pump, a vacuum chamber, and the associated flow control valves. Such a system is acceptable in a clinical setting, such as knee rehabilitation assistance. Using a desktop system poses problems when considering wearable exosuits that require portability and discrete use. The presence of vibrations from the vacuum pump operation, the bulk of the vacuum chamber, and the rigid control valves can hamper the user. The proposed soft actuators use flexible thin-walled pouches to create the actuation volume. The failure of this skin will deteriorate the performance of the actuator. Hence there will be a need to replace the actuators during use, but this replacement is low-cost and straightforward, as only another thin-film pouch is required. The developed position feedback method of the LPVAc uses inductive sensing. This measurement can be affected by the presence of high magnetic fields near the actuator.

7.2 Future directions

Future work for further developing the presented work can include the following aspects. Other potential thin-film materials can be tested, and other air-tight volume-creation methods can be explored. Different materials and fabrication techniques can also be considered for the springs. The same concepts of the ThinVAc can be further miniaturized for integration at the fabric level.

In this work, a desktop system was used as the vacuum source. Hence, there is a need to develop lightweight, wearable vacuum sources and vacuum control systems to integrate wearable systems more effectively.

The assist devices presented here were tested on lower limb models and healthy volunteers. Therefore, the developed assist devices can be used in clinical trials to evaluate the benefits in actual patients.

CHAPTER 8

LIST OF PUBLICATIONS

Journal Articles:

[1] A. L. Kulasekera, R. B. Arumathanthri, D. S. Chathuranga, R. C. Gopura, and T. D. Lalitharathne, "A Thin-walled Vacuum Actuator and development of multi-filament structures for Soft Robotic Applications," *Sensors and Actuators A: Physical*, vol. 332, p. 113 088, Dec. 2021, ISSN: 09244247. DOI: 10.1016/j.sna.2021.113088.

[2] A. L. Kulasekera, R. B. Arumathanthri, D. S. Chathuranga, R. A. R. C. Gopura, and T. D. Lalitharatne, "A Low-Profile Vacuum Actuator (LPVAc) With Integrated Inductive Displacement Sensing for a Novel Sit-to-Stand Assist Exosuit," *IEEE Access*, vol. 9, pp. 117 067–117 079, 2021, ISSN: 21693536. DOI: 10.1109/access.2021.3106319.

Conference Articles:

[1] A. L. Kulasekera, R. B. Arumathanthri, D. S. Chathuranga, T. D. Lalitharatne, and R. C. Gopura, "A Low-Profile Vacuum Actuator: Towards a Sit-to-Stand Assist Exosuit," in *2020 3rd IEEE International Conference on Soft Robotics, RoboSoft 2020*, IEEE, May 2020, pp. 110–115, ISBN: 9781728165707. DOI: 10.1109/RoboSoft48309.2020.9115999.

[2] R. B. Arumathanthri, A. L. Kulasekera, and D. S. Chathuranga, "An Induction Type Displacement Sensor used in a Novel Soft Robotic Muscle Actuator," in *Proceedings of International Conference on Image Processing and Robotics, ICIPRoB 2020*, IEEE, Mar. 2020, pp. 1–6, ISBN: 9781728165417. DOI: 10.1109/ICIP48927.2020.9367333.

[3] A. L. Kulasekera, R. B. Arumathanthri, D. S. Chathuranga, R. A. R. C. Gopura, and T. D. Lalitharatne, "Development and preliminary evaluation of a soft-exosuit for sit-to-stand assistance," in *11th Multidisciplinary International Student Workshop*, Tokyo, Japan, 2019.

[4] L. S. Weerasooriya, B. Chathuranga, O. I. Somaratna, A. L. Kulasekera, R. B. Arumathanthri, and D. S. Chathuranga, "A novel contractile vacuum actuator and multi-actuator development for knee extension assist," IEEE, Apr. 2021. DOI: 10.1109/robosoft51838.2021.9479255.

[5] A. Osorio, A. Kulasekera, Y. Sugahara, D. Matsuura, and Y. Takeda, "A novel scalable SMA actuator using thermally conductive fluid : Its concept and basic characterization," in *37th Annual Meeting of the Robotics Society of Japan*, Waseda Univ., Tokyo, 2019, pp. 2–3.

[6] C. Premarathna, A. Kulasekera, D. Chathuranga, and T. Lalitharatne, "A Novel Fabrication Method for Rapid Prototyping of Soft Structures with Embedded Pneumatic Channels," in *MERCon 2019 - Proceedings, 5th International Multi-disciplinary Moratuwa Engineering Research Conference*, 2019, pp. 430–435, ISBN: 9781728136325. DOI: 10.1109/MERCon.2019.8818891.

REFERENCES

[1] P. Polygerinos, N. Correll, S. A. Morin, B. Mosadegh, C. D. Onal, K. Petersen, M. Cianchetti, M. T. Tolley, and R. F. Shepherd, "Soft Robotics: Review of Fluid-Driven Intrinsically Soft Devices; Manufacturing, Sensing, Control, and Applications in Human-Robot Interaction," *Advanced Engineering Materials*, vol. 19, no. 12, p. 1700016, May 2017. [Online]. Available: https://doi.org/10.1002/adem.201700016

[2] N. Kastor, V. Vikas, E. Cohen, and R. D. White, "A definition of soft materials for use in the design of robots," *Soft Robotics*, vol. 4, no. 3, pp. 181–182, September 2017. [Online]. Available: https://doi.org/10.1089/soro.2017.29012.nka

[3] D. Chiaradia, M. Xiloyannis, M. Solazzi, L. Masia, and A. Frisoli, "Comparison of a soft exosuit and a rigid exoskeleton in an assistive task," in *Biosystems and Biorobotics*, M. C. Carrozza, S. Micera, and J. L. Pons, Eds., vol. 22. Pisa, Italy: Springer Nature Switzerland, 2019, pp. 415–419. [Online]. Available: http://link.springer.com/10.1007/978-3-030-01887-0{_}80

[4] S. Bao, S. Yin, H. Chen, and W. Chen, "A wearable multimode system with soft sensors for lower limb activity evaluation and rehabilitation," in *2018 IEEE International Instrumentation and Measurement Technology Conference (I2MTC)*. IEEE, May 2018. [Online]. Available: https://doi.org/10.1109/i2mtc.2018.8409880

[5] J. Walker, T. Zidek, C. Harbel, S. Yoon, F. S. Strickland, S. Kumar, and M. Shin, "Soft robotics: A review of recent developments of pneumatic soft actuators," *Actuators*, vol. 9, no. 1, p. 3, January 2020. [Online]. Available: https://doi.org/10.3390/act9010003

[6] N. El-Atab, R. B. Mishra, F. Al-Modaf, L. Joharji, A. A. Alsharif, H. Alamoudi, M. Diaz, N. Qaiser, and M. M. Hussain, "Soft actuators for soft robotic applications: A review," *Advanced Intelligent Systems*, vol. 2, no. 10, p. 2000128, aug 2020. [Online]. Available: https://doi.org/10.1002%2Faisy.202000128

[7] V. Bartenbach, K. Schmidt, M. Naef, D. Wyss, and R. Riener, "Concept of a soft exosuit for the support of leg function in rehabilitation," in *IEEE International Conference on Rehabilitation Robotics*, vol. 2015-September. IEEE, aug 2015, pp. 125–130. [Online]. Available: http://ieeexplore.ieee.org/document/7281187/

[8] H. Herr, "Exoskeletons and orthoses: Classification, design challenges and future directions," *Journal of NeuroEngineering and Rehabilitation*, vol. 6, no. 1, p. 21, dec 2009. [Online]. Available: https://jneuroengrehab.biomedcentral.com/articles/10.1186/1743-0003-6-21

[9] B. Chen, H. Ma, L. Y. Qin, F. Gao, K. M. Chan, S. W. Law, L. Qin, and W. H. Liao, "Recent developments and challenges of lower extremity exoskeletons," *Journal of Orthopaedic Translation*, vol. 5, pp. 26–37, apr 2016. [Online]. Available: https://linkinghub.elsevier.com/retrieve/pii/S2214031X15000716

[10] S. Rossi, A. Colazza, M. Petrarca, E. Castelli, P. Cappa, and H. I. Krebs, "Feasibility Study of a Wearable Exoskeleton for Children: Is the Gait Altered by Adding Masses on Lower Limbs?" *PLoS ONE*, vol. 8, no. 9, p. e73139, sep 2013. [Online]. Available: https://dx.plos.org/10.1371/journal.pone.0073139

[11] A. Schiele, "Ergonomics of exoskeletons: Objective performance metrics," *Proceedings - 3rd Joint EuroHaptics Conference and Symposium on Haptic Interfaces for Virtual Environment and Teleoperator Systems, World Haptics 2009*, pp. 103–108, 2009. [Online]. Available: http://ieeexplore.ieee.org/document/4810871/

[12] M. Cianchetti, C. Laschi, A. Menciassi, and P. Dario, "Biomedical applications of soft robotics," *Nature Reviews Materials*, vol. 3, no. 6, pp. 143–153, jun 2018. [Online]. Available: http://www.nature.com/articles/s41578-018-0022-y

[13] M. Wehner, B. Quinlivan, P. M. Aubin, E. Martinez-Villalpando, M. Baumann, L. Stirling, K. Holt, R. Wood, and C. Walsh, "A lightweight soft exosuit for gait assistance," in *Proceedings - IEEE International Conference on Robotics and Automation*. IEEE, may 2013, pp. 3362–3369. [Online]. Available: http://ieeexplore.ieee.org/document/6631046/

[14] K. Schmidt, J. E. Duarte, M. Grimmer, A. Sancho-Puchades, H. Wei, C. S. Easthope, and R. Riener, "The myosuit: Bi-articular anti-gravity exosuit that reduces hip extensor activity in sitting transfers," *Frontiers in Neurorobotics*, vol. 11, no. OCT, pp. 1–16, oct 2017. [Online]. Available: http://journal.frontiersin.org/article/10.3389/fnbot.2017.00057/full

[15] W. Awantha, A. Wanasinghe, A. Kavindya, A. Kulasekera, and D. Chathuranga, "A Novel Soft Glove for Hand Tremor Suppression: Evaluation of Layer Jamming Actuator Placement," in *2020 3rd IEEE International Conference on Soft Robotics (RoboSoft)*. IEEE, may 2020, pp. 440–445. [Online]. Available: https://ieeexplore.ieee.org/document/9115994/

[16] S. Kurumaya, H. Nabae, G. Endo, and K. Suzumori, "Design of thin McKibben muscle and multifilament structure," *Sensors and Actuators, A: Physical*, vol. 261, pp. 66–74, jul 2017. [Online]. Available: https://linkinghub.elsevier.com/retrieve/pii/S0924424716308792http://dx.doi.org/10.1016/j.sna.2017.04.047

[17] C. Premarathna, A. Kulasekera, D. Chathuranga, and T. Lalitharatne, "A novel fabrication method for rapid prototyping of soft structures with embedded pneumatic channels," in *2019 Moratuwa Engineering Research Conference (MERCon)*. IEEE, July 2019. [Online]. Available: https://doi.org/10.1109/mercon.2019.8818891

[18] A. Osorio, A. Kulasekera, Y. Sugahara, D. Matsuura, and Y. Takeda, "A novel scalable SMA actuator using thermally conductive fluid : Its concept and basic characterization," in *37th Annual Meeting of the Robotics Society of Japan*, Waseda Univ., Tokyo, 2019, pp. 2–3.

[19] C. Laschi, B. Mazzolai, and M. Cianchetti, "Soft robotics: Technologies and systems pushing the boundaries of robot abilities," *Science Robotics*, vol. 1, no. 1, pp. 1–11, 2016.

[20] M. Manti, V. Cacucciolo, and M. Cianchetti, "Stiffening in soft robotics: A review of the state of the art," *IEEE Robotics and Automation Magazine*, vol. 23, no. 3, pp. 93–106, 2016.

[21] G. Agarwal, N. Besuchet, B. Audergon, and J. Paik, "Stretchable Materials for Robust Soft Actuators towards Assistive Wearable Devices," *Scientific Reports*, vol. 6, no. September, pp. 1–8, 2016.

[22] H.-T. Lin, G. G. Leisk, and B. Trimmer, "GoQBot: a caterpillar-inspired soft-bodied rolling robot," *Bioinspiration and Biomimetics*, vol. 6, no. 2, p. 026007, Apr. 2011. [Online]. Available: https://doi.org/10.1088/1748-3182/6/2/026007

[23] C. Laschi, M. Cianchetti, B. Mazzolai, L. Margheri, M. Follador, and P. Dario, "Soft robot arm inspired by the octopus," *Advanced Robotics*, vol. 26, no. 7, pp. 709–727, 2012.

[24] F. Carpi, S. Bauer, and D. De Rossi, "Stretching dielectric elastomer performance," *Science*, vol. 330, no. 6012, pp. 1759–1761, 2010.

[25] R. F. Shepherd, A. A. Stokes, J. Freake, J. Barber, P. W. Snyder, A. D. Mazzeo, L. Cademartiri, S. A. Morin, and G. M. Whitesides, "Using explosions to power a soft robot," *Angewandte Chemie - International Edition*, vol. 52, no. 10, pp. 2892–2896, 2013.

[26] F. Ilievski, A. D. Mazzeo, R. F. Shepherd, X. Chen, and G. M. Whitesides, "Soft robotics for chemists," *Angewandte Chemie - International Edition*, vol. 50, no. 8, pp. 1890–1895, 2011.

[27] P. Polygerinos, K. C. Galloway, S. Sanan, M. Herman, and C. J. Walsh, "EMG controlled soft robotic glove for assistance during activities of daily living," in *2015 IEEE International Conference on Rehabilitation Robotics (ICORR)*. IEEE, August 2015. [Online]. Available: https://doi.org/10.1109/icorr.2015.7281175

[28] Y.-L. Park, J. Santos, K. G. Galloway, E. C. Goldfield, and R. J. Wood, "A soft wearable robotic device for active knee motions using flat pneumatic artificial muscles," in *2014 IEEE International Conference on Robotics and Automation (ICRA)*. IEEE, May 2014. [Online]. Available: https://doi.org/10.1109/icra.2014.6907562

[29] F. Iida and C. Laschi, "Soft robotics: Challenges and perspectives," *Procedia Computer Science*, vol. 7, pp. 99–102, 2011.

[30] R. Pfeifer, M. Lungarella, and F. Iida, "The challenges ahead for bio-inspired 'soft' robotics," *Communications of the ACM*, vol. 55, no. 11, pp. 76–87, 2012.

[31] S. Kim, C. Laschi, and B. Trimmer, "Soft robotics: A bioinspired evolution in robotics," *Trends in Biotechnology*, vol. 31, no. 5, pp. 287–294, 2013.

[32] P. Polygerinos, Z. Wang, J. T. Overvelde, K. C. Galloway, R. J. Wood, K. Bertoldi, and C. J. Walsh, "Modeling of Soft Fiber-Reinforced Bending Actuators," *IEEE Transactions on Robotics*, vol. 31, no. 3, pp. 778–789, 2015.

[33] M. Memarian, R. Gorbet, and D. Kulic, "Modelling and experimental analysis of a novel design for soft pneumatic artificial muscles," *IEEE International Conference on Intelligent Robots and Systems*, vol. 2015-December, pp. 1718–1724, 2015.

[34] C. P. Chou and B. Hannaford, "Measurement and modeling of McKibben pneumatic artificial muscles," *IEEE Transactions on Robotics and Automation*, vol. 12, no. 1, pp. 90–102, 1996.

[35] B. Tondu and P. Lopez, "Modeling and Control of McKibben Artificial Muscle Robot Actuators," *IEEE Control Systems*, vol. 20, no. 2, pp. 15–38, apr 2000. [Online]. Available: https://ieeexplore.ieee.org/document/833638/

[36] B. Tondu, "Modelling of the McKibben artificial muscle: A review," *Journal of Intelligent Material Systems and Structures*, vol. 23, no. 3, pp. 225–253, 2012.

[37] A. A. M. Faudzi, N. H. I. Mat Lazim, and K. Suzumori, "Modeling and force control of thin soft McKibben actuator," *International Journal of Automation Technology*, vol. 10, no. 4, pp. 487–493, 2016.

[38] N. Saga, T. Nakamura, and K. Yaegashi, "Mathematical model of pneumatic artificial muscle reinforced by straight fibers," *Journal of Intelligent Material Systems and Structures*, vol. 18, no. 2, pp. 175–180, 2007.

[39] T. Nakamura and H. Shinohara, "Position and force control based on mathematical models of pneumatic artificial muscles reinforced by straight glass fibers," in *Proceedings - IEEE International Conference on Robotics and Automation*. IEEE, apr 2007, pp. 4361–4366. [Online]. Available: http://ieeexplore.ieee.org/document/4209769/

[40] P. Polygerinos, Z. Wang, K. C. Galloway, R. J. Wood, and C. J. Walsh, "Soft robotic glove for combined assistance and at-home rehabilitation," *Robotics and Autonomous Systems*, vol. 73, pp. 135–143, 2015.

[41] E. T. Roche, R. Wohlfarth, J. T. Overvelde, N. V. Vasilyev, F. A. Pigula, D. J. Mooney, K. Bertoldi, and C. J. Walsh, "A bioinspired soft actuated material," *Advanced Materials*, vol. 26, no. 8, pp. 1200–1206, 2014.

[42] F. Connolly, P. Polygerinos, C. J. Walsh, and K. Bertoldi, "Mechanical programming of soft actuators by varying fiber angle," *Soft Robotics*, vol. 2, no. 1, pp. 26–32, 2015.

[43] J. Wirekoh and Y. L. Park, "Design of flat pneumatic artificial muscles," *Smart Materials and Structures*, vol. 26, no. 3, p. 035009, mar 2017. [Online]. Available: https://iopscience.iop.org/article/10.1088/1361-665X/aa5496

[44] F. Daerden and D. Lefeber, "The concept and design of pleated pneumatic artificial muscles," *International Journal of Fluid Power*, vol. 2, no. 3, pp. 41–50, jan 2001. [Online]. Available: http://www.tandfonline.com/doi/abs/10.1080/14399776.2001.10781119

[45] B. Mosadegh, P. Polygerinos, C. Keplinger, S. Wennstedt, R. F. Shepherd, U. Gupta, J. Shim, K. Bertoldi, C. J. Walsh, and G. M. Whitesides, "Pneumatic networks for soft robotics that actuate rapidly," *Advanced Functional Materials*, vol. 24, no. 15, pp. 2163–2170, 2014.

[46] S. Sanan, P. S. Lynn, and S. T. Griffith, "Pneumatic torsional actuators for inflatable robots," *Journal of Mechanisms and Robotics*, vol. 6, no. 3, p. 31003, 2014.

[47] R. Niiyama, X. Sun, C. Sung, B. An, D. Rus, and S. Kim, "Pouch motors: Printable soft actuators integrated with computational design," *Soft Robotics*, vol. 2, no. 2, pp. 59–70, 2015.

[48] A. J. Veale, S. Q. Xie, and I. A. Anderson, "Modeling the Peano fluidic muscle and the effects of its material properties on its static and dynamic behavior," *Smart Materials and Structures*, vol. 25, no. 6, pp. 1–16, 2016.

[49] N. Kellaris, V. G. Venkata, G. M. Smith, S. K. Mitchell, and C. Keplinger, "Peano-HASEL actuators: Muscle-mimetic, electrohydraulic transducers that linearly contract on activation," *Science Robotics*, vol. 3, no. 14, pp. 1–11, 2018.

[50] M. De Volder and D. Reynaerts, "Pneumatic and hydraulic microactuators: A review," *Journal of Micromechanics and Microengineering*, vol. 20, no. 4, 2010.

[51] A. V. Coccaro, "Pneumatic Jack," United States, United States, 2013. [Online]. Available: https://patents.google.com/patent/US20130187107A1/en

[52] B. Gorissen, D. Reynaerts, S. Konishi, K. Yoshida, J. W. Kim, and M. De Volder, "Elastic Inflatable Actuators for Soft Robotic Applications," *Advanced Materials*, vol. 29, no. 43, pp. 1–14, 2017.

[53] B. Gorissen, T. Chishiro, S. Shimomura, D. Reynaerts, M. De Volder, and S. Konishi, "Flexible pneumatic twisting actuators and their application to tilting micromirrors," *Sensors and Actuators, A: Physical*, vol. 216, pp. 426–431, 2014.

[54] S. Hirai, P. Cusin, H. Tanigawa, T. Masui, S. Konishi, and S. Kawamura, "Qualitative synthesis of deformable cylindrical actuators through constraint topology," *IEEE International Conference on Intelligent Robots and Systems*, vol. 1, pp. 197–202, 2000.

[55] S. Hirai, T. Masui, and S. Kawamura, "Prototyping pneumatic group actuators composed of multiple single-motion elastic tubes," *Proceedings - IEEE International Conference on Robotics and Automation*, vol. 4, no. c, pp. 3807–3812, 2001.

[56] C. Moraes, Y. Sun, and C. A. Simmons, "Solving the shrinkage-induced PDMS alignment registration issue in multilayer soft lithography," *Journal of Micromechanics and Microengineering*, vol. 19, no. 6, p. 65015, 2009.

[57] Y. C. Su, L. Lin, and A. P. Pisano, "A water-powered osmotic microactuator," *Journal of Microelectromechanical Systems*, vol. 11, no. 6, pp. 736–742, 2002.

[58] R. V. Martinez, C. R. Fish, X. Chen, and G. M. Whitesides, "Elastomeric origami: Programmable paper-elastomer composites as pneumatic actuators," *Advanced Functional Materials*, vol. 22, no. 7, pp. 1376–1384, 2012.

[59] X. Gong, K. Yang, J. Xie, Y. Wang, P. Kulkarni, A. S. Hobbs, and A. D. Mazzeo, "Rotary Actuators Based on Pneumatically Driven Elastomeric Structures," *Advanced Materials*, vol. 28, no. 34, pp. 7533–7538, 2016.

[60] M. C. Birch, R. D. Quinn, G. Hahm, S. M. Phillips, B. Drennan, A. Fife, H. Verma, and R. D. Beer, "Design of a cricket microrobot," in *Proceedings - IEEE International Conference on Robotics and Automation*, vol. 2, 2000, pp. 1109–1114.

[61] T. Chishiro, T. Ono, and S. Konishi, "Pantograph mechanism for conversion from swelling into contraction motion of pneumatic balloon actuator," in *Proceedings of the IEEE International Conference on Micro Electro Mechanical Systems (MEMS)*, 2013, pp. 532–535.

[62] K. Takemura, S. Yokota, and K. Edamura, "A micro artificial muscle actuator using electro-conjugate fluid," in *Proceedings - IEEE International Conference on Robotics and Automation*, vol. 2005, 2005, pp. 532–537.

[63] B. Verrelst, R. Van Ham, B. Vanderborght, F. Daerden, D. Lefeber, and J. Vermeulen, "The pneumatic biped "lucy" actuated with pleated pneumatic artificial muscles," *Autonomous Robots*, vol. 18, no. 2, pp. 201–213, 2005.

[64] F. Daerden and D. Lefeber, "Pneumatic artificial muscles: Actuators for robotics and automation," *European Journal of Mechanical and Environmental Engineering*, vol. 47, no. 1, pp. 11–21, 2002.

[65] B. Tondu, "What is an artificial muscle? A systemic approach," *Actuators*, vol. 4, no. 4, pp. 336–352, 2015.

[66] O. Erin, N. Pol, L. Valle, and Y. L. Park, "Design of a bio-inspired pneumatic artificial muscle with self-contained sensing," *Proceedings of the Annual International Conference of the IEEE Engineering in Medicine and Biology Society, EMBS*, vol. 2016-October, pp. 2115–2119, 2016.

[67] I. Gaiser, R. Wiegand, O. Ivlev, a. Andres, H. Breitwieser, S. Schulz, and G. Bretthauer, "Smart Actuation and Sensing Systems - Recent Advances and Future Challenges," *Smart Actuation and Sensing Systems - Recent Advances and Future Challenges*, no. February, pp. 567–608, 2012.

[68] J. E. Takosoglu, P. A. Laski, S. Blasiak, G. Bracha, and D. Pietrala, "Determining the Static Characteristics of Pneumatic Muscles," *Measurement and Control (United Kingdom)*, vol. 49, no. 2, pp. 62–71, 2016.

[69] D. Yang, M. S. Verma, J. H. So, B. Mosadegh, C. Keplinger, B. Lee, F. Khashai, E. Lossner, Z. Suo, and G. M. Whitesides, "Buckling Pneumatic Linear Actuators Inspired by Muscle," *Advanced Materials Technologies*, vol. 1, no. 3, p. 1600055, jun 2016. [Online]. Available: http://doi.wiley.com/10.1002/admt.201600055

[70] M. S. Verma, A. Ainla, D. Yang, D. Harburg, and G. M. Whitesides, "A Soft Tube-Climbing Robot," *Soft Robotics*, vol. 5, no. 2, pp. 133–137, 2018.

[71] G. Agarwal, M. A. Robertson, H. Sonar, and J. Paik, "Design and Computational Modeling of a Modular, Compliant Robotic Assembly for Human Lumbar Unit and Spinal Cord Assistance," *Scientific Reports*, vol. 7, no. 1, pp. 1–11, 2017.

[72] S. Li, D. M. Vogt, D. Rus, and R. J. Wood, "Fluid-driven origami-inspired artificial muscles," *Proceedings of the National Academy of Sciences*, vol. 114, no. 50, pp. 13 132–13 137, dec 2017. [Online]. Available: http://www.pnas.org/lookup/doi/10.1073/pnas.1713450114

[73] J.-G. Lee and H. Rodrigue, "Origami-Based Vacuum Pneumatic Artificial Muscles with Large Contraction Ratios," *Soft Robotics*, vol. 00, no. 00, p. soro.2018.0063, 2018. [Online]. Available: https://www.liebertpub.com/doi/10.1089/soro.2018.0063

[74] J. Miller and N. Wicks, "Vacuum-Actuated Bending for Grasping," *Robotics*, vol. 7, no. 4, p. 73, 2018. [Online]. Available: http://www.mdpi.com/2218-6581/7/4/73

[75] S. D. Katugampala, K. M. S. Arachchi, S. Asanka, R. B. Arumathanthri, A. L. Kulasekera, and N. D. Jayaweera, "Design and Characterization of a Novel Vacuum Bending Actuator and a Bimorph: for Preliminary Use in a Continuum Robot Arm," in *2019 IEEE International Conference on Cybernetics and Intelligent Systems (CIS) and IEEE Conference on Robotics, Automation and Mechatronics (RAM)*. Bangkok, Thailand: IEEE, nov 2019, pp. 263–268. [Online]. Available: https://ieeexplore.ieee.org/document/9095543/

[76] H. Al-Fahaam, S. Davis, and S. Nefti-Meziani, "The design and mathematical modelling of novel extensor bending pneumatic artificial muscles (EBPAMs) for soft exoskeletons," *Robotics and Autonomous Systems*, vol. 99, pp. 63–74, 2018.

[77] N. Tsagarakis and D. G. Caldwell, "Improved modelling and assessment of pneumatic muscle actuators," *Proceedings - IEEE International Conference on Robotics and Automation*, vol. 4, pp. 3641–3646, 2000.

[78] D. G. Caldwell, N. Tsagarakis, and G. A. Medrano-Cerda, "Bio-mimetic actuators: Polymeric Pseudo Muscular Actuators and pneumatic Muscle Actuators for biological emulation," *Mechatronics*, vol. 10, no. 4, pp. 499–530, 2000.

[79] J. P. King, L. E. Valle, N. Pol, and Y. L. Park, "Design, modeling, and control of pneumatic artificial muscles with integrated soft sensing," *Proceedings - IEEE International Conference on Robotics and Automation*, pp. 4985–4990, 2017.

[80] D. Trivedi, C. D. Rahn, W. M. Kier, and I. D. Walker, "Soft robotics: Biological inspiration, state of the art, and future research," *Applied Bionics and Biomechanics*, vol. 5, no. 3, pp. 99–117, 2008.

[81] Z. Jiao, C. Ji, J. Zou, H. Yang, and M. Pan, "Vacuum-Powered Soft Pneumatic Twisting Actuators to Empower New Capabilities for Soft Robots," *Advanced Materials Technologies*, vol. 4, no. 1, p. 1800429, jan 2019. [Online]. Available: http://doi.wiley.com/10.1002/admt.201800429https://onlinelibrary.wiley.com/doi/10.1002/admt.201800429

[82] M. Yu, W. Yang, Y. Yu, X. Cheng, and Z. Jiao, "A Crawling Soft Robot Driven by Pneumatic Foldable Actuators Based on Miura-Ori," *Actuators*, vol. 9, no. 2, p. 26, 2020.

[83] J. Zou, Y. Lin, C. Ji, and H. Yang, "A Reconfigurable Omnidirectional Soft Robot Based on Caterpillar Locomotion," *Soft Robotics*, vol. 5, no. 2, pp. 164–174, 2018.

[84] M. A. Robertson, H. Sadeghi, J. M. Florez, and J. Paik, "Soft Pneumatic Actuator Fascicles for High Force and Reliability," *Soft Robotics*, vol. 4, no. 1, pp. 23–32, 2017. [Online]. Available: http://online.liebertpub.com/doi/10.1089/soro.2016.0029

[85] A. Sadeghi, A. Mondini, and B. Mazzolai, "A Vacuum Powered Soft Textile-Based Clutch," *Actuators*, vol. 8, no. 2, p. 47, jun 2019. [Online]. Available: https://www.mdpi.com/2076-0825/8/2/47

[86] N. S. Usevitch, A. M. Okamura, and E. W. Hawkes, "APAM: Antagonistic Pneumatic Artificial Muscle," in *2018 IEEE International Conference on Robotics and Automation (ICRA)*, vol. Accepted. Brisbane, Australia: IEEE, may 2018, pp. 1539–1546. [Online]. Available: https://ieeexplore.ieee.org/document/8460881/

[87] S. Terryn, G. Mathijssen, J. Brancart, D. Lefeber, G. V. Assche, and B. Vanderborght, "Development of a self-healing soft pneumatic actuator: A first concept," *Bioinspiration and Biomimetics*, vol. 10, no. 4, 2015.

[88] W. Felt, S. Lu, and C. D. Remy, "Modeling and Design of 'Smart Braid' Inductance Sensors for Fiber-Reinforced Elastomeric Enclosures," *IEEE Sensors Journal*, vol. 18, no. 7, pp. 2827–2835, apr 2018. [Online]. Available: http://ieeexplore.ieee.org/document/8281451/

[89] D. Yang, B. Mosadegh, A. Ainla, B. Lee, F. Khashai, Z. Suo, K. Bertoldi, and G. M. Whitesides, "Buckling of Elastomeric Beams Enables Actuation of Soft Machines," *Advanced Materials*, vol. 27, no. 41, pp. 6323–6327, nov 2015. [Online]. Available: https://onlinelibrary.wiley.com/doi/10.1002/adma.201503188

[90] H. M. Herr and R. D. Kornbluh, "New horizons for orthotic and prosthetic technology: artificial muscle for ambulation," in *Proc. SPIE 5385, Smart Structures and Materials 2004: Electroactive Polymer Actuators and Devices (EAPAD)*, Y. Bar-Cohen, Ed., jul 2004, p. 1. [Online]. Available: http://proceedings.spiedigitallibrary.org/proceeding.aspx?doi=10.1117/12.544510

[91] R. Arumathanthri, B. Abeygoonawardana, I. Kumarasinghe, D. Chathuranga, T. D. Lalitharatne, and A. Kulasekera, "A Soft Robotic Gripper with Sensory Feedback Fabricated by Latex using Coagulant Dipping Process," in *2018 IEEE International Conference on Robotics and Biomimetics (ROBIO)*. IEEE, dec 2018, pp. 2082–2087. [Online]. Available: https://ieeexplore.ieee.org/document/8665091/

[92] M. C. Yuen, R. Kramer-Bottiglio, and J. Paik, "Strain sensor-embedded soft pneumatic actuators for extension and bending feedback," in *2018 IEEE International Conference on Soft Robotics (RoboSoft)*. IEEE, apr 2018, pp. 202–207. [Online]. Available: https://ieeexplore.ieee.org/document/8404920/

[93] A. Hildebrandt, O. Sawodny, R. Neumann, and A. Hartmann, "Cascaded control concept of a robot with two degrees of freedom driven by four artificial pneumatic muscle actuators," in *Proceedings of the 2005, American Control Conference, 2005.* IEEE, pp. 680–685. [Online]. Available: http://ieeexplore.ieee.org/document/1470036/

[94] N. Farrow and N. Correll, "A soft pneumatic actuator that can sense grasp and touch," in *2015 IEEE/RSJ International Conference on Intelligent Robots and Systems (IROS)*. IEEE, sep 2015, pp. 2317–2323. [Online]. Available: http://ieeexplore.ieee.org/document/7353689/

[95] Yong-Lae Park, Bor-Rong Chen, and R. J. Wood, "Design and Fabrication of Soft Artificial Skin Using Embedded Microchannels and Liquid Conductors," *IEEE Sensors Journal*, vol. 12, no. 8, pp. 2711–2718, aug 2012. [Online]. Available: http://ieeexplore.ieee.org/document/6203551/

[96] W. Felt, K. Y. Chin, and C. D. Remy, "Contraction Sensing with Smart Braid McKibben Muscles," *IEEE/ASME Transactions on Mechatronics*, vol. 21, no. 3, pp. 1201–1209, 2016.

[97] W. Felt, M. J. Telleria, T. F. Allen, G. Hein, J. B. Pompa, K. Albert, and C. D. Remy, "An inductance-based sensing system for bellows-driven continuum joints in soft robots," *Autonomous Robots*, vol. 43, no. 2, pp. 435–448, 2019. [Online]. Available: https://doi.org/10.1007/s10514-018-9769-7

[98] C. Dohle, F. Müller, and K. Stephan, "Technical Developments for Rehabilitation of Mobility," *Neurology International Open*, vol. 01, no. 03, pp. E211–E216, 2017.

[99] A. S. Niyetkaliyev, S. Hussain, M. H. Ghayesh, and G. Alici, "Review on Design and Control Aspects of Robotic Shoulder Rehabilitation Orthoses," *IEEE Transactions on Human-Machine Systems*, vol. 47, no. 6, pp. 1134–1145, 2017.

[100] A. J. Young and D. P. Ferris, "State of the art and future directions for lower limb robotic exoskeletons," *IEEE Transactions on Neural Systems and Rehabilitation Engineering*, vol. 25, no. 2, pp. 171–182, feb 2017. [Online]. Available: http://ieeexplore.ieee.org/document/7393837/

[101] T. Kermavnar, V. Power, A. De Eyto, and L. W. O'Sullivan, "Computerized Cuff Pressure Algometry as Guidance for Circumferential Tissue Compression for Wearable Soft Robotic Applications: A Systematic Review," *Soft Robotics*, vol. 5, no. 1, pp. 1–16, 2018.

[102] A. T. Asbeck, S. M. De Rossi, K. G. Holt, and C. J. Walsh, "A biologically inspired soft exosuit for walking assistance," *International Journal of Robotics Research*, vol. 34, no. 6, pp. 744–762, may 2015. [Online]. Available: http://journals.sagepub.com/doi/10.1177/0278364914562476

[103] A. T. Asbeck, R. J. Dyer, A. F. Larusson, and C. J. Walsh, "Biologically-inspired soft exosuit," *IEEE International Conference on Rehabilitation Robotics*, 2013.

[104] A. T. Asbeck, S. M. De Rossi, I. Galiana, Y. Ding, and C. J. Walsh, "Stronger, smarter, softer: Next-generation wearable robots," *IEEE Robotics and Automation Magazine*, vol. 21, no. 4, pp. 22–33, 2014.

[105] J. Bae, S. M. M. De Rossi, K. O'Donnell, K. L. Hendron, L. N. Awad, T. R. Teles Dos Santos, V. L. De Araujo, Y. Ding, K. G. Holt, T. D. Ellis, and C. J. Walsh, "A soft exosuit for patients with stroke: Feasibility study with a mobile off-board actuation unit," *IEEE International Conference on Rehabilitation Robotics*, vol. 2015-September, pp. 131–138, 2015.

[106] F. A. Panizzolo, I. Galiana, A. T. Asbeck, C. Siviy, K. Schmidt, K. G. Holt, and C. J. Walsh, "A biologically-inspired multi-joint soft exosuit that can reduce the energy cost of loaded walking," *Journal of NeuroEngineering and Rehabilitation*, vol. 13, no. 1, p. 43, dec 2016. [Online]. Available: http://dx.doi.org/10.1186/s12984-016-0150-9https://jneuroengrehab.biomedcentral.com/articles/10.1186/s12984-016-0150-9

[107] G. Lee, J. Kim, F. A. Panizzolo, Y. M. Zhou, L. M. Baker, I. Galiana, P. Malcolm, and C. J. Walsh, "Reducing the metabolic cost of running with a tethered soft exosuit," *Science Robotics*, vol. 2, no. 6, p. eaan6708, may 2017. [Online]. Available: http://robotics.sciencemag.org/lookup/doi/10.1126/scirobotics.aan6708https://robotics.sciencemag.org/lookup/doi/10.1126/scirobotics.aan6708

[108] L. N. Awad, J. Bae, K. ODonnell, S. M. De Rossi, K. Hendron, L. H. Sloot, P. Kudzia, S. Allen, K. G. Holt, T. D. Ellis, and C. J. Walsh, "A soft robotic exosuit improves walking in patients after stroke," *Science Translational Medicine*, vol. 9, no. 400, p. eaai9084, 2017.

[109] L. N. Awad, J. Bae, P. Kudzia, A. Long, K. Hendron, K. G. Holt, K. ODonnell, T. D. Ellis, and C. J. Walsh, "Reducing Circumduction and Hip Hiking During Hemiparetic Walking Through Targeted Assistance of the Paretic Limb Using a Soft Robotic Exosuit," *American journal of physical medicine & rehabilitation*, vol. 96, no. 10, pp. S157–S164, 2017.

[110] Y. Ding, I. Galiana, A. T. Asbeck, S. M. M. De Rossi, J. Bae, T. R. T. Santos, V. L. De Araujo, S. Lee, K. G. Holt, and C. Walsh, "Biomechanical and physiological evaluation of multi-joint assistance with soft exosuits," *IEEE Transactions on Neural Systems and Rehabilitation Engineering*, vol. 25, no. 2, pp. 119–130, 2017.

[111] J. Bae, L. N. Awad, A. Long, K. O'Donnell, K. Hendron, K. G. Holt, T. D. Ellis, and C. J. Walsh, "Biomechanical mechanisms underlying exosuit-induced improvements in walking economy after stroke," *Journal of Experimental Biology*, vol. 221, no. 5, p. jeb.168815, 2018.

[112] D. J. Newman, K. Bethke, C. Carr, J. Hoffman, and G. Trotti, "Astronaut bio-suit system to enable planetary exploration," in *International Astronautical Federation - 55th International Astronautical Congress 2004*, vol. 12. Reston, Virigina: American Institute of Aeronautics and Astronautics, oct 2004, pp. 7708–7718. [Online]. Available: http://arc.aiaa.org/doi/10.2514/6.IAC-04-U.1.03

[113] K. Ohashi, Y. Akiyama, S. Okamoto, and Y. Yamada, "Development of a string-driven walking assist device powered by upper body muscles," *2017 IEEE International Conference on Systems, Man, and Cybernetics, SMC 2017*, vol. 2017-January, pp. 1411–1416, 2017.

[114] D. Sasaki, T. Noritsugu, and M. Takaiwa, "Development of pneumatic lower limb power assist wear driven with wearable air supply system," *IEEE International Conference on Intelligent Robots and Systems*, pp. 4440–4445, 2013.

[115] S. Jin, N. Iwamoto, K. Hashimoto, and M. Yamamoto, "Experimental Evaluation of Energy Efficiency for a Soft Wearable Robotic Suit," *IEEE Transactions on Neural Systems and Rehabilitation Engineering*, vol. 25, no. 8, pp. 1192–1201, 2017.

[116] S. Jin, S. Guo, K. Hashimoto, and M. Yamamoto, "Effects of a soft wearable robotic suit on metabolic cost and gait characteristics in healthy young subjects," *International Conference on Control, Automation and Systems*, vol. 2017-October, no. Iccas, pp. 680–684, 2017.

[117] S. Lessard, P. Pansodtee, A. Robbins, L. B. Baltaxe-Admony, J. M. Trombadore, M. Teodorescu, A. Agogino, and S. Kurniawan, "CRUX: A compliant robotic upper-extremity exosuit for lightweight, portable, multi-joint muscular augmentation," *IEEE International Conference on Rehabilitation Robotics*, vol. 3, pp. 1633–1638, 2017.

[118] A. Schiele and F. C. van der Helm, "Influence of attachment pressure and kinematic configuration on pHRI with wearable robots," *Applied Bionics and Biomechanics*, vol. 6, no. 2, pp. 157–173, 2009.

[119] N. Aliman, R. Ramli, and S. M. M. Haris, "Design and development of lower limb exoskeletons: A survey," *Robotics and Autonomous Systems*, vol. 95, pp. 102–116, 2017.

[120] B. Weinberg, J. Nikitczuk, S. Patel, B. Patritti, C. Mavroidis, P. Bonato, and P. Canavan, "Design, Control and Human Testing of an Active Knee Rehabilitation Orthotic Device," in *Proceedings 2007 IEEE International Conference on Robotics and Automation*. IEEE, apr 2007, pp. 4126–4133. [Online]. Available: http://ieeexplore.ieee.org/document/4209731/

[121] S. Sridar, P. H. Nguyen, M. Zhu, Q. P. Lam, and P. Polygerinos, "Development of a soft-inflatable exosuit for knee rehabilitation," in *2017 IEEE/RSJ International Conference on Intelligent Robots and Systems (IROS)*, vol. 2017-Septe. IEEE, sep 2017, pp. 3722–3727. [Online]. Available: http://ieeexplore.ieee.org/document/8206220/

[122] T. L. Floyd, *Electronic devices (conventional current version)*, 10th ed. Upper Saddle River, NJ: Pearson, Jan. 2018.

[123] Texas Instruments, "LDC1612, LDC1614 Multi-Channel 28-Bit Inductance to Digital Converter (LDC) for Inductive Sensing," p. 67, 2018.

[124] A. N. Chaudhury and D. Datta, "Analysis of prismatic springs of non-circular coil shape and non-prismatic springs of circular coil shape by analytical and finite element methods," *Journal of Computational Design and Engineering*, vol. 4, no. 3, pp. 178–191, jul 2017. [Online]. Available: https://academic.oup.com/jcde/article/4/3/178/5715409http://dx.doi.org/10.1016/j.jcde.2017.02.001

[125] S. R. Krishnan and C. S. Seelamantula, "On the selection of optimum Savitzky-Golay filters," *IEEE Transactions on Signal Processing*, vol. 61, no. 2, pp. 380–391, 2013.

[126] M. J. Mendoza, S. D. Gollob, D. Lavado, B. H. B. Koo, S. Cruz, E. T. Roche, and E. A. Vela, "A vacuum-powered artificial muscle designed for infant rehabilitation," *Micromachines*, vol. 12, no. 8, p. 971, August 2021. [Online]. Available: https://doi.org/10.3390/mi12080971

[127] Y. L. Park, B. R. Chen, N. O. Pérez-Arancibia, D. Young, L. Stirling, R. J. Wood, E. C. Goldfield, and R. Nagpal, "Design and control of a bio-inspired soft wearable robotic device for ankle-foot rehabilitation," *Bioinspiration and Biomimetics*, vol. 9, no. 1, p. 016007, jan 2014. [Online]. Available: https://iopscience.iop.org/article/10.1088/1748-3182/9/1/016007

[128] K. L. Bennell, M. A. Hunt, T. V. Wrigley, B.-W. Lim, and R. S. Hinman, "Muscle and Exercise in the Prevention and Management of Knee Osteoarthritis: an Internal Medicine Specialist's Guide," *Medical Clinics of North America*, vol. 93, no. 1, pp. 161–177, jan 2009. [Online]. Available: https://linkinghub.elsevier.com/retrieve/pii/S0025712508001259

[129] N. C. Clark, "(vii) the role of physiotherapy in rehabilitation of soft tissue injuries of the knee," *Orthopaedics and Trauma*, vol. 29, no. 1, pp. 48–56, February 2015. [Online]. Available: https://doi.org/10.1016/j.mporth.2014.11.008

[130] M. Cross, E. Smith, D. Hoy, S. Nolte, I. Ackerman, M. Fransen, L. Bridgett, S. Williams, F. Guillemin, C. L. Hill, L. L. Laslett, G. Jones, F. Cicuttini, R. Osborne, T. Vos, R. Buchbinder, A. Woolf, and L. March, "The global burden of hip and knee osteoarthritis: Estimates from the Global Burden of Disease 2010 study," *Annals of the Rheumatic Diseases*, vol. 73, no. 7, pp. 1323–1330, jul 2014. [Online]. Available: https://ard.bmj.com/lookup/doi/10.1136/annrheumdis-2013-204763

[131] H. D. Atkinson, J. M. Laver, and E. Sharp, "(vi) physiotherapy and rehabilitation following soft-tissue surgery of the knee," *Orthopaedics and Trauma*, vol. 24, no. 2, pp. 129–138, April 2010. [Online]. Available: https://doi.org/10.1016/j.mporth.2010.03.006

[132] M. G. Mohamed Thariq, H. P. Munasinghe, and J. D. Abeysekara, "Designing chairs with mounted desktop for university students: Ergonomics and comfort," *International Journal of Industrial Ergonomics*, vol. 40, no. 1, pp. 8–18, 2010.

[133] J. D. Abeysekera and H. Shahnavaz, "Body size data of Sri Lankan workers and their variability with other populations in the world: its impact on the use of imported goods." *Journal of human ergology*, vol. 16, no. 2, pp. 193–208, 1987.

[134] W. Brie, "Consideration of Function & Functional Decline," in *Current Diagnosis and Treatment: Geriatrics, Second Edition*, 2nd ed., B. A. Williams, A. Chang, C. Ahalt, H. Chen, R. Conant, C. S. Landefeld, C. Ritchie, and M. Yukawa, Eds. New York, NY: McGraw-Hill Education, 2014, pp. 3–4.

[135] E. T. Yümin, T. T. Şimşek, M. Sertel, A. Öztürk, and M. Yümin, "The effect of functional mobility and balance on health-related quality of life (HRQoL) among elderly people living at home and those living in nursing home," *Archives of Gerontology and Geriatrics*, vol. 52, no. 3, pp. 180–184, 2011.

[136] M. Roebroeck, C. Doorenbosch, J. Harlaar, R. Jacobs, and G. Lankhorst, "Biomechanics and muscular activity during sit-to-stand transfer," *Clinical Biomechanics*, vol. 9, no. 4, pp. 235–244, jul 1994. [Online]. Available: https://linkinghub.elsevier.com/retrieve/pii/0268003394900043

[137] K. Boren, C. Conrey, J. Le Coguic, L. Paprocki, M. Voight, and T. K. Robinson, "Electromyographic analysis of gluteus medius and gluteus maximus during rehabilitation exercises." *International journal of sports physical therapy*, vol. 6, no. 3, pp. 206–23, 2011. [Online]. Available: http://www.ncbi.nlm.nih.gov/pubmed/22034614{%}0Ahttp://www.pubmedcentral.nih.gov/articlerender.fcgi?artid=PMC3201064

[138] S. Kurumaya, K. Suzumori, H. Nabae, and S. Wakimoto, "Musculoskeletal lower-limb robot driven by multifilament muscles," *ROBOMECH Journal*, vol. 3, no. 1, Sep. 2016. [Online]. Available: https://doi.org/10.1186/s40648-016-0061-3

[139] R. A. Gopura, D. S. Bandara, K. Kiguchi, and G. K. Mann, "Developments in hardware systems of active upper-limb exoskeleton robots: A review," *Robotics and Autonomous Systems*, vol. 75, pp. 203–220, 2016. [Online]. Available: http://dx.doi.org/10.1016/j.robot.2015.10.001

[140] T. Yan, M. Cempini, C. M. Oddo, and N. Vitiello, "Review of assistive strategies in powered lower-limb orthoses and exoskeletons," *Robotics and Autonomous Systems*, vol. 64, pp. 120–136, 2015. [Online]. Available: http://dx.doi.org/10.1016/j.robot.2014.09.032

APPENDIX A

PLANE AND MOTION NOTATIONS USED IN ANATOMY

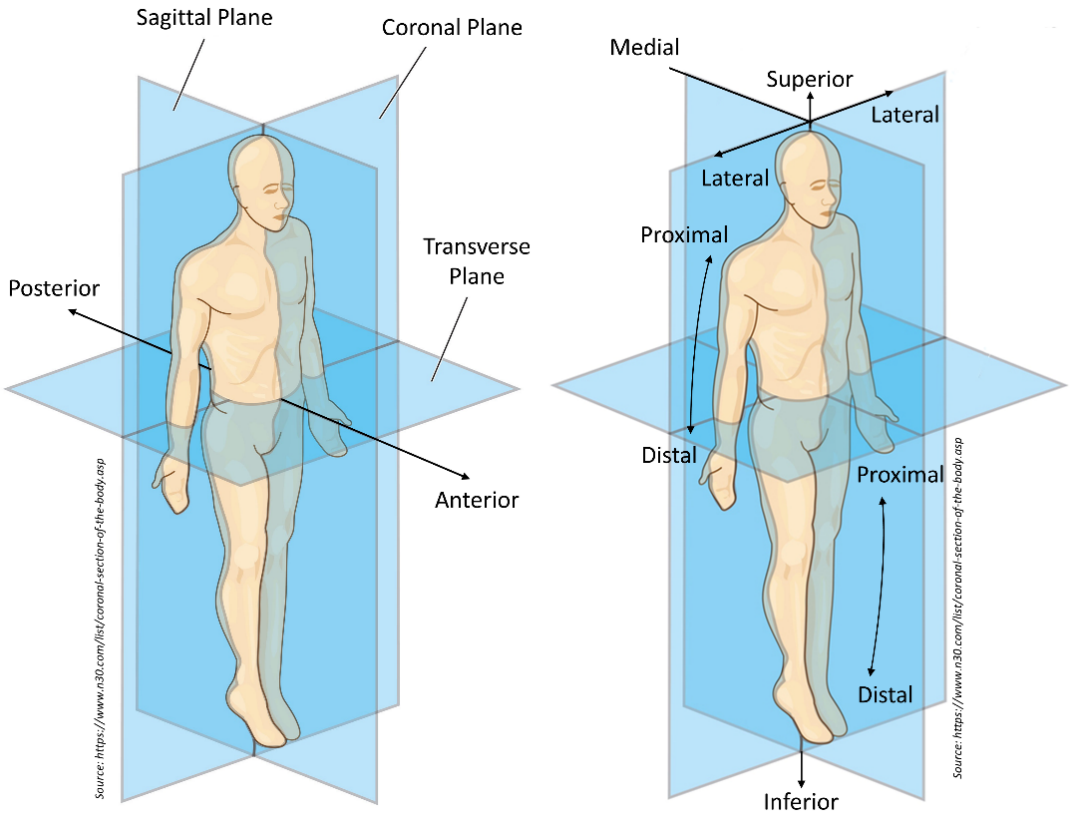

Fig. A.1: Body plane notions used in anatomy [*image source: Shutterstock.com*].

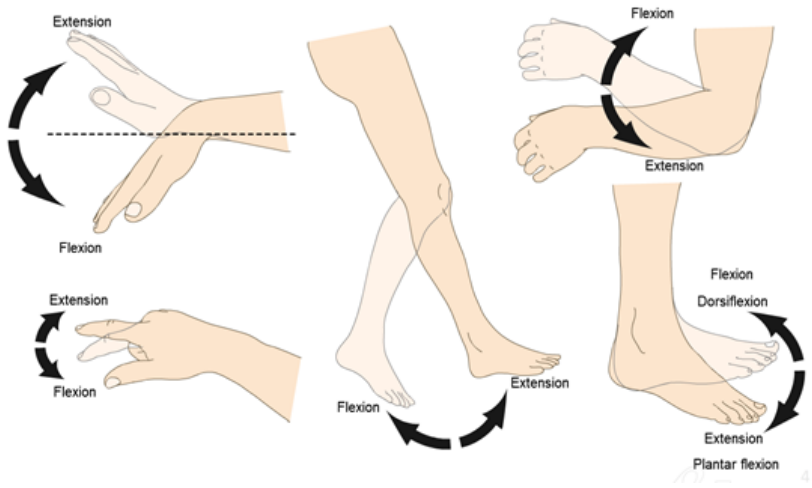

Fig. A.2: Limb motion definitions [*source: www.imaios.com/en/e-anatomy*]

APPENDIX B

MUSCLE RECRUITMENT IN LOWER LIMB MOTIONS

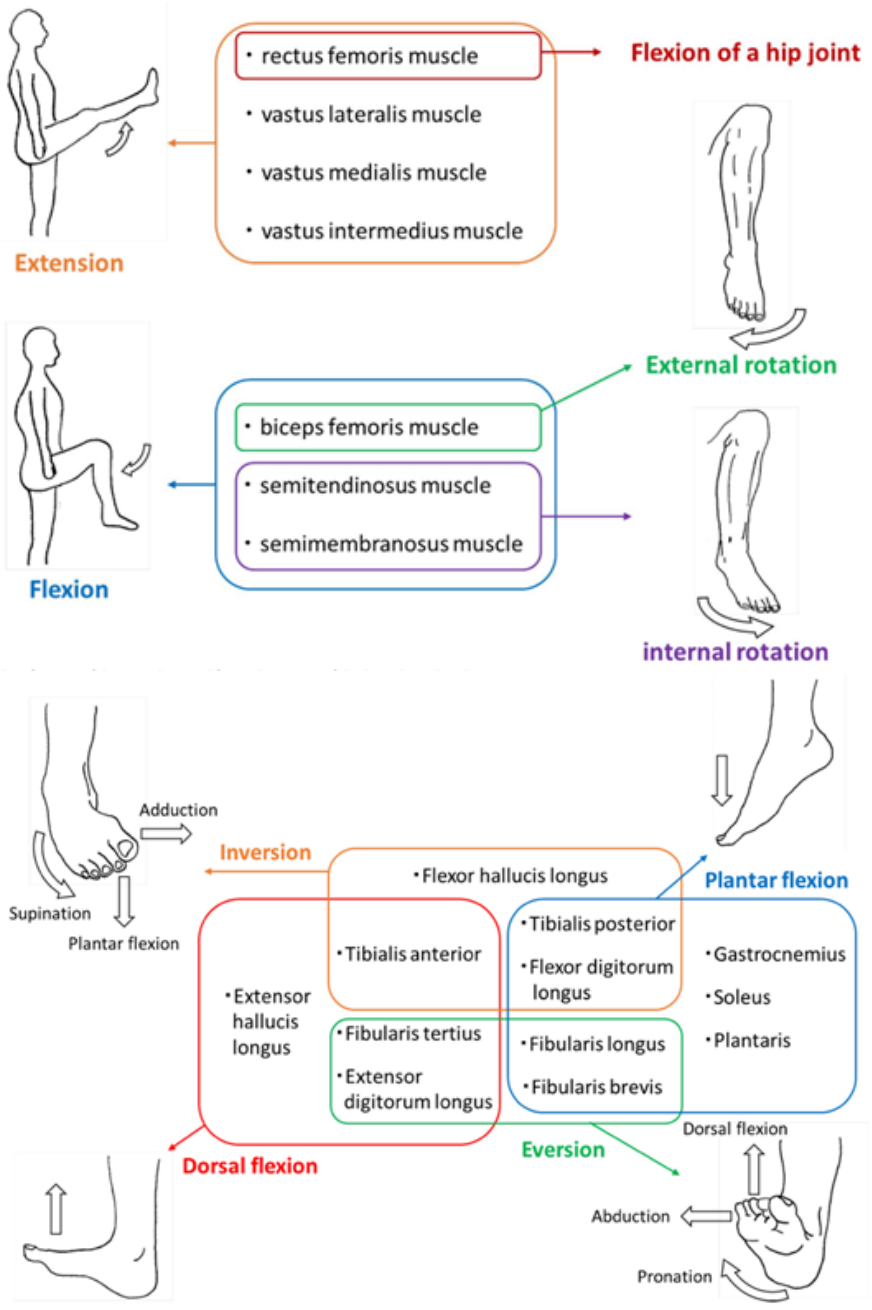

Fig. B.1: Classification of the muscles used for lower limb motions [138].

APPENDIX C

TYPES OF LOWER LIMB ORTHOSES

Wearable lower-limb assistive devices can be broadly divided into orthoses and prostheses. A prosthesis is an artificial substitute one can wear, replacing a missing limb. An *orthosis* is an orthopedic apparatus that can be used to support and correct deformities/abnormalities or improve movable parts' functionality by providing assistance or force augmentation [139]. Within orthoses, there is a distinction between devices where the device joints are made to coincide with the biological joints of the user and those which are only concerned with the particular motion of a selected user limb. The former is the devices commonly known as exoskeleton devices [139].

Exoskeleton devices are defined as active mechanical devices that are essentially anthropomorphic, worn by the user, fitting closely to the body, and working in tandem with the user's motions. The term' active orthosis', has been used to define a device to increase the ambulatory ability of a person suffering from a lower limb pathology [8]. As orthoses are not limited by a requirement to follow the joints of a user, they are the best-suited approach for soft assistive devices.

Fig. C.1 shows how commonly used lower limb orthotic devices, active orthoses, and exoskeletons are classified by the biological joint/joint group they seek to assist. In terms of orthoses, they are identified as multi-joint devices, trunk–hip–knee– ankle–foot orthoses (THKAFO), hip–knee–ankle–foot orthoses (HKAFO), trunk–hip–knee orthoses (THKO), hip–knee orthoses (HKO), knee–ankle–foot orthoses (KAFO), ankle-foot orthoses (AFO), or as single-joint devices, hip orthoses (HO), knee orthoses (KO), ankle orthoses (AO) [140].

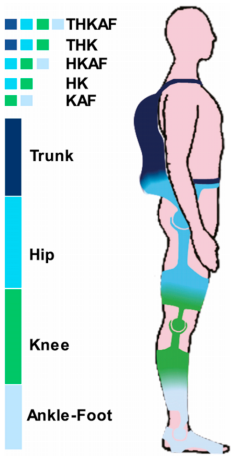

Fig. C.1: Types of lower limb orthoses [140].

APPENDIX D

REGRESSION MODELS USED FOR LDPE-THINVAC

ThinVAc Contraction Model 1: Single parameter regression model for contraction

A numerical analysis based on the experimental data was utilized to develop a contraction model of the ThinVAc. The displacement characteristics of the monofilament ThinVAc were evaluated using an isotonic experiment. The experiment results were grouped by actuator length (50 mm, 100 mm, and 200 mm) and four pressure levels applied (20, 40, 60, 80 kPa). A linear regression fit using the least squares method was initially obtained for each group based on the following model. The contraction of the ThinVAc presents linear behavior with the applied load for each actuator in isobaric conditions, as shown in Fig. D.1. These provide relationships per actuator, with a total of 12 functions (shown in Table D.1)) describing the contraction of three different length actuators at four different pressure levels each.

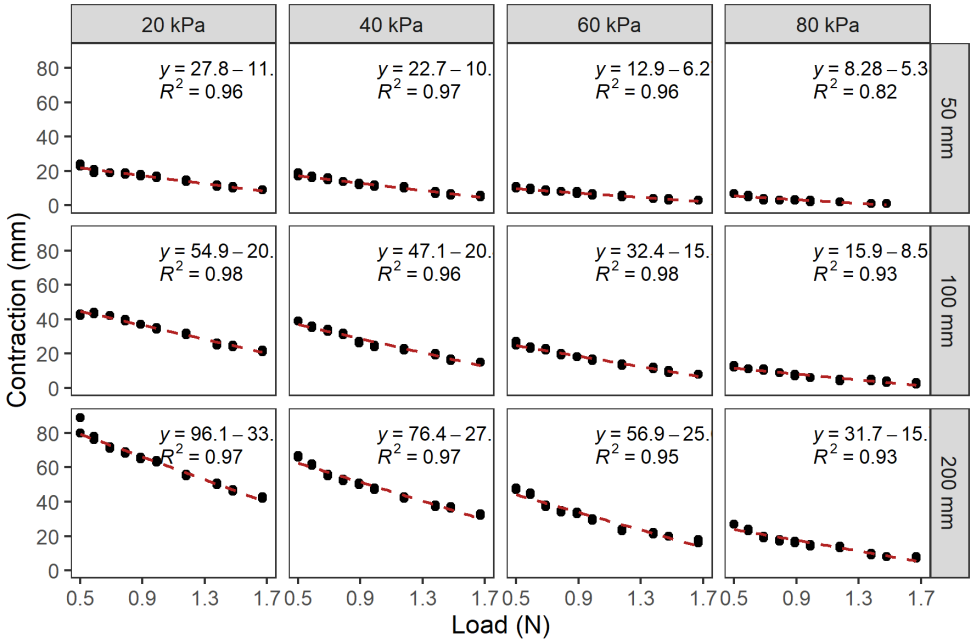

Fig. D.1: Combined graph of the single parameter regression model I for each actuator at each pressure. The dashed line shows the estimation. The fit is above 0.9 for all combinations.

ThinVAc Contraction Model 2: Single regression model for contraction ratio

The ThinVAc were fabricated at three lengths for initial assessment, 50 mm, 100 mm, and 200 mm. Their behavior can further be analyzed based on the contraction as a ratio

TABLE D.1: Linear regression fit: ThinVAc length and pressure level (model I).

LDPE ThinVAc	Pressure (kPa) abs.	Contraction (mm) Load (N) + const. mx + c	R^2	RMSE (mm)	RMSE ($\Delta L/L$)
50 mm	20	- 11.6 x + 27.8	0.962	0.86	0.0172
	40	- 10.7 x + 22.7	0.972	0.89	0.0178
	60	- 6.27 x + 12.9	0.957	0.8	0.016
	80	- 5.38 x + 8.28	0.824	1.04	0.0208
100 mm	20	- 20.3 x + 54.7	0.981	1.34	0.0134
	40	- 20.4 x + 47	0.964	1.79	0.0179
	60	- 15.3 x + 32.3	0.977	1.14	0.0114
	80	- 8.55 x + 15.8	0.935	1.03	0.0103
200 mm	20	- 33.2 x + 95.9	0.973	2.16	0.0108
	40	- 27.6 x + 76.2	0.967	2.06	0.0103
	60	- 25.6 x + 56.7	0.947	2.22	0.0111
	80	- 15.7 x + 31.6	0.928	1.81	0.0091

to their initial size. Hence, the isobaric characteristics of the actuators were evaluated with respect to their contraction ratio. The regression model eq. D.1 was calculated for each pressure. Here L is the driven load in N. Following Fig. D.2 shows a linear behavior of the contraction ratio with applied load. The shown pressures are absolute values.

$$CR = aL + b \tag{D.1}$$

In the 20 – 40 kPa (abs.) range, the regression fit between the applied load and the contraction ratio is reported $R^2 \quad 0.9$. The overall regression fit is above 0.8. Hence, the contraction ratio shows significant linear behavior with the attached load.

A comparison of the RMSE performance for the linear regression models 1, 2, and eq. 5.2, are shown in Table D.2. The linear fit considering model 2 delivers the best error performance at the expense of a moderate number (04) of model equations. The multiple linear regression fit considering eq. 5.2 delivers almost the same error performance using a single model equation. Therefore, for effective prediction of the contraction behavior of the LDPE-ThinVAc monofilament, the multi-parameter regression model can be recommended.

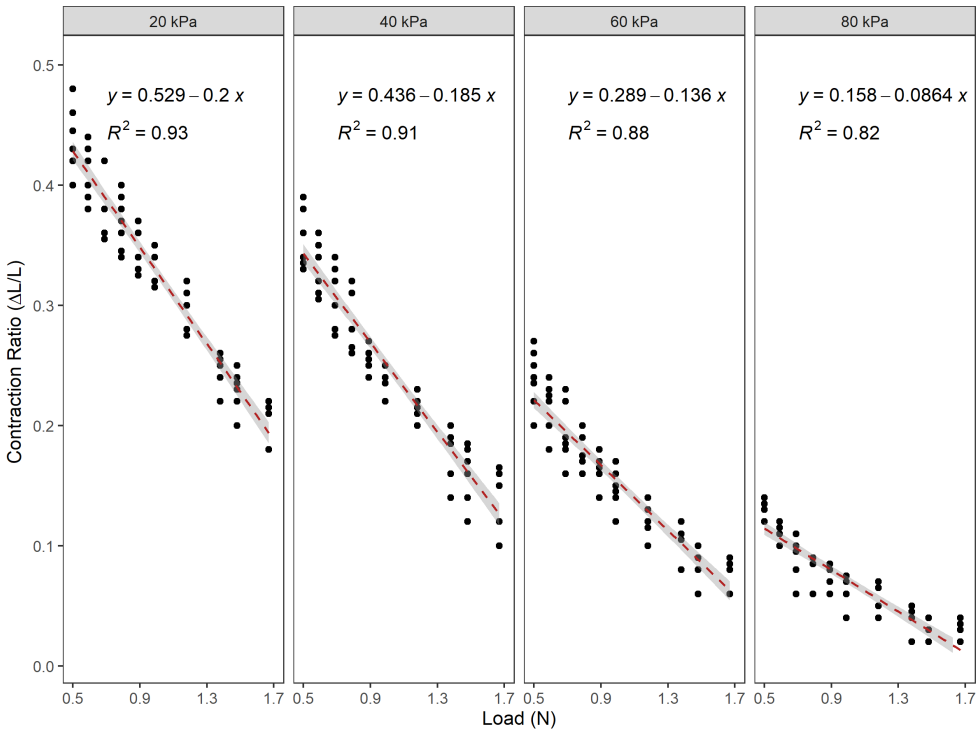

Fig. D.2: Contraction ratio of the ThinVAc with varied vacuum pressure (absolute). The dashed line shows the prediction from the single parameter regression fit model. The standard error for each regression fit is shown in gray.

TABLE D.2: Isobaric comparison of RMSE for contraction and contraction ratio linear regression models.

		20 kPa	40 kPa	60 kPa	80 kPa	Over the complete pressure range
50 mm	model I	0.0172	0.0178	0.016	0.0208	0.0248
	model 2	0.0237	0.0224	0.024	0.0229	0.0293
	Eq. 4	0.0348	0.0268	0.0262	0.0244	0.0287
100 mm	model I	0.0134	0.0179	0.0114	0.0103	0.0437
	model 2	0.0196	0.0239	0.0201	0.0093	0.0262
	Eq. 4	0.026	0.0338	0.0174	0.0277	0.0269
200 mm	model I	0.0108	0.0103	0.0111	0.0091	0.0636
	model 2	0.0209	0.0195	0.011	0.0122	0.0208
	Eq. 4	0.01924	0.01137	0.01506	0.03222	0.021

Note: All RMSE values have been converted to a ratio of respective actuator length for comparison.